Hydro-, morpho- and sediment-dynamic processes in the subaqueous Mekong Delta, Southern Vietnam

Dissertation

zur Erlangung des Doktorgrades

der Mathematisch-Naturwissenschaftlichen Fakultät

der Christian-Albrechts Universität

Kiel

vorgelegt von

Daniel Unverricht

Kiel, 2014

Referent: Prof. Dr. Karl Stattegger

Koreferent: Prof. Dr. Sebastian Krastel-Gudegast

Tag der mündlichen Prüfung: 03.Juni 2014

Zum Druck genehmigt: 30.06.2014

gez. Prof. Dr. Wolfgang J. Duschl, Dekan

Ich versichere an Eides statt, dass:

1) Ich bis zum heutigen Tage weder an der Christian-Albrechts-Universität zu Kiel noch an einer anderen Hochschule ein Promotionsverfahren endgültig nicht bestanden habe oder mich in einem entsprechenden Verfahren befinde oder befunden habe.
2) Ich die Inanspruchnahme fremder Hilfen aufgeführt habe, sowie, dass ich die wörtlich oder inhaltlich aus anderen Quellen entnommenen Stellen als solche gekennzeichnet habe.
3) Die Arbeit unter Einhaltung der Regeln guter wissenschaftlicher Praxis der Deutschen Forschungsgemeinschaft entstanden ist.

Kiel, Unterschrift:

Abstract

Various sediment- and hydrodynamic factors including tides (meso-tidal system), waves, coastal currents and seasonal-driven river discharge influence the coastal zone of southern Vietnam. In particular, the Mekong River Delta (MRD) that belongs to Asian Mega-deltas, represents these land-ocean interactions in many variations. The locally prevailing processes and the amount of sediment, supplied by the Mekong distributaries, characterize the morphology and sediment distribution of the subaqueous delta. In contrast, delta morphology and sedimentary pattern reflect these impacts. This study investigates the hydro-, morpho- and sediment-dynamic processes of the subaqueous MRD to figure out their interactions.

Three cruises in 2006, 2007 and 2008 were carried out in the subaqueous MRD extending from the Bassac River, the main distributary of the MRD, to the coast N of Ca Mau Cape in the Gulf of Thailand. All cruises were performed during the inter-monsoon season (March to May) where wave and wind influences have low effects to sedimentation processes compared to the summer monsoon (May to early October) and winter monsoon season (October to early March). This study presents data of suspended matter (turbidity meter, water samples, LISST-instrument), seismic profiles (Boomer and C-Boom-system), grab and sediment core sampling and point and current-measurements (using Acoustic Doppler Current Profiler) that provide information of current velocities and directions. Data of different tide gauge stations in the MRD were included to compare the mixed semidiurnal–diurnal tidal cycle and related own relevant measurements (e.g. suspended matter, sediment transport direction).

Various factors including tides (meso-tidal system), waves, coastal currents, monsoon-driven river discharge and human impact (agriculture, fishing, sand mining, tourism) influence the MRD. The present study aims to document the seafloor relief, sediment distribution and sediment accumulation rates to interpret modern sediment transport directions and main sedimentation processes in the subaqueous Mekong Delta.

The major results of this investigation include the detection of two delta fronts 200 km apart, one at the mouth of the Bassac River (the biggest branch of the Mekong Delta) and the other around Ca Mau Cape (most south-western end of the Mekong Delta). The sediment accumulation rates vary greatly according to the location in the subaqueous delta and have reached up to 10 cm/yr for the last century. A cluster analysis of surface sediment samples revealed two different sediment types within the delta including well-sorted sandy sediment and poorly sorted, silty sediment. In addition, a third end member with medium to coarse sand

characterize the distant parts of the delta at the transition to the open shelf. The increase of organic matter and carbonate content to the bottom set area and other sedimentary features such as shell fragments, foraminifera and concretions of palaeo-soils that do not occur in delta sediments, supports grain size-based classification.

Beginning in front of the Bassac River mouth, sedimentary pattern indicates clockwise sediment transport alongshore in western direction to a broad topset area and the delta front around Ca Mau Cape. Our results clearly show the large lateral variability of the subaqueous Mekong Delta that is further complicated by strong monsoon-driven seasonality. River, tidal and wave forcing vary at local and seasonal scales with sedimentary response to localized short term depositional patterns that are often not preserved in long term geological records.

Land-ocean interactions in the coastal zone are severely influenced by tidal processes. In regions of high sediment discharge like the Mekong River Delta in southern Vietnam, these processes are even more significant.

Cruise results show significant areas of suspended sediment concentrations (SSCs) greater than 25 µl/l in the Mekong River branches and its subaqueous delta during the inter-monsoon season. 20 % of all measured SSCs in the subaqueous Mekong Delta exceed 100 µl/l. Highest concentrations occur close to the seabed. SSCs decrease at the transition to the open shelf. The shelf region contains only low suspension loads, especially on the south-eastern shelf (99 % of all samples < 25 µl/l). However, in the southern shelf region around Ca Mau Cape the suspension load is also higher (> 25 µl/l) close to the seabed in water depths of 20 to 25 m.

Two surveys lasting 25 hours each were performed on mooring stations in 12 m (Mooring 1) and 26 m (Mooring 2) water depth and located 3.2 km apart on the subaqueous delta slope. Similar patterns of SSC over time show that concentrations of suspension load correlate with the tidal current velocities. High tidal current velocities of up to 0.6 m/s near the sea bottom generate increasing SSCs of more than 25µl/l in the water column. Additionally a significant trend of decreasing SSC from the near-seabed to the upper part of the water column can be observed. In terms of sediment transport the ebb phase dominates the tidal cycle by its higher tidal current velocities but the flood phase has the longer duration. The switch of the tidal current direction from ebb to flood phase occurs rapidly against which the change from flood to ebb phase requires up to 3 hours. This leads to an asymmetry of the tidal ellipses and may cause a net-sediment transport from the shelf into the subaqueous Mekong delta.

In the subaqueous Mekong Delta and adjacent shelf, seven transects show similar patterns of SSCs dependent to the tidal phase. A hypopycnal sediment plume from the subaqueous Mekong Delta into the shelf region was not observed. Our results imply that resuspension by tidal currents dominates the sediment transport in the subaqueous Mekong Delta and adjacent shelf regions during the inter-monsoon season.

Mega-deltas like the Mekong River delta differ in shape and sedimentary pattern in dependence on the interplay of river, tide and wave forces. Specific hydro- and morphodynamic conditions in the subaqueous part of the Mekong River Delta generate a sand-ridge-system combined with erosional channels, which is unique in subaqueous delta formations. This large-scale morphological feature extends along the delta front, in particular, the delta slope and subaqueous delta platform of the Mekong River Delta. A system consisting of two sand ridges and two erosional channels (termed sand-ridge-channel-system (SRCS)) covers at least an area of 1971 km^2 and extends in minimum 128 km along the coast. Three different areas west of the Bassac river mouth, the largest and western-most Mekong distributary, were distinguished according to their morphology. The eastern area, where the channel-ridge formation begins, stretches along the delta slope and inner shelf platform southwest of the Bassac river mouth with slightly concave and erosional features. The central area covers the southern part of the subaqueous delta platform with a pronounced sand-ridge and erosional channel morphology. Hydroacoustic cross-sections of the SRCS reveal an asymmetric shape including steeper ridge flanks facing into offshore direction. The channel troughs incise up to 18.2 m b.s.l. and 10.5 m from the ridge top at the shallow subaqueous delta platform, respectively. At the western part of the central area, the sand ridges pinch out while the two channels merge into one and form a giant scour of up to 33 m water depth within the subaqueous delta platform of generally less than 7.7 m water depth. In the western area, the channel gets shallower and vanishes along the south-western most subaqueous delta platform around Ca Mau Cape.

Headland retreat and sediment transport from erosive areas of the Mekong river delta coast are the source to form the sand-ridges and coastal subparallel tidal currents maintain and stabilize them. In contrast, tide and wind-driven currents cut the erosional channels, which act as fine sediment conveyor to the distal part of the delta front that is 200 km apart of the next main distributary. The SRCS represents a new morphological feature in the subaqueous deltaic environment and is a relevant indicator of delta instability and coastal erosion in subaqueous deltas.

Zusammenfassung

Einflüsse sediment- und hydrodynamischer Faktoren wie Tide, Wellen, küstennahe Strömungen und sich verändernde Flusseinträge infolge jahreszeitlich bedingter Wettervariationen (Monsun) sind in den Küstenzonen zu beobachten. Besonders das Mekong-Delta in Südvietnam, das zu Asiens großen Deltas zählt, repräsentiert diese Interaktionen zwischen Land und Meer in vielfacher Weise. Der Flusseintrag aus den Mekongarmen und die lokal domierenden Prozesse bestimmen die Deltamorphologie und die örtliche Sedimentverteilung im subaquatischen Delta. Im Gegensatz gibt die Deltaform und die Sedimentverteilung Einsichten über die Einflussfaktoren wieder. Diese Arbeit beschäftigt sich mit den hydro-, morpho- und sedimentdynamischen Prozessen im subaquatischen Mekongdelta und versucht einen Beitrag zum Verständnis ihrer Interaktionen zu leisten.

In den Jahren 2006, 2007 und 2008 wurden Forschungsausfahrten in das subaquatische Deltagebiet zwischen dem Bassac Fluß, dem größten Hauptarm im Mekongdelta, und dem östlich gelegenen Golf von Thailand durchgeführt. Alle Ausfahrten fanden während der Intermonsunzeit statt (März bis Mai), in der vergleichweise zur Sommer- und Wintermonsunzeit (Mai bis anfang Oktober bzw. Oktober bis März) Wind- und Wellenenergie geringen Einfluss auf die Sedimentationsprozesse haben. Diese Studie verarbeitet Daten von Sedimentschwebstoffen (Trübemesser, Wasserproben, LISST-Instrument), hydroakustischen Profilen (Boomer und C-Boom-System), Backgreiferproben und Schwerelotkernen. Des Weiteren wurden Strömungsgeschwindigkeiten und -richtungen mit Hilfe eines ADCPs (Acoustic Doppler Current Profiler) entlang von Profilen und an speziellen Ankerstationen über die gesamte Wassersäule aufgenommen. Die tideabhängigen Wasserstandsveränderungen entlang der Küste des Mekongdeltas wurden von geeigneten Messstationen hinzugezogen, um die Tidephasen mit den eigenen Untersuchungen zu korrelieren.

Das Mekong-Delta wird von vielfältigen Faktoren wie Tide (meso-tidales System), Windwellen, küstennahe Strömungen, monsungesteuerter Ausfluss der Flüsse und menschlichen Eingriffen (Agrikultur, Fischerei, Sandausbaggerungen, Tourismus) geprägt. Deshalb soll die rezente Untersuchung darauf zielen, die Meeresbodenmorphologie, Sedimentverteilung und Sedimentakkumulationsraten zu erfassen, um somit die gegenwärtige Sedimenttransportrichtung und die dominierenden Sedimentationsprozesse im subaquatischen Mekong-Delta zu interpretieren.

Im Mekong-Delta sind zwei Deltafronten herausgebildet. Eine befindet sich direkt vor dem Bassac-Fluss und den Hauptflussmündungen des Mekong-Flusses während die Zweite sich 200 km am Kap Ca Mau, dem südwestlichen Ende des Mekong-Deltas, erstreckt. Die Sedimentakkumulationsraten des subaquatischen Mekong-Deltas sind stark ortsabhängig und erreichen für das letzte Jahrhundert bis zu 10 cm/a. Eine Klusteranalyse der Oberflächensedimente ergab zwei Sedimenttypen, die das subaquatische Mekong-Delta repräsentieren. Der erste Typ besteht aus gut sortierten Sanden während der zweite Typ ein breites Korngrößenspektrum dominierend in der Siltfraktion aufweist und schlecht sortiert ist. Ein drittes Kluster, bestehend aus mittleren und groben Sanden, charakterisiert den distalen Deltabereich im Übergang zum offenen Schelf. Die auf der Korngrößenverteilung basierende Klassifikation wird sowohl durch einen anwachsenden Anteil an organischen Material und erhöhtem Karbonatanteil am auslaufenden Deltahang in seewärtiger Richtung als auch vorkommende Muschelbruchstücke, Foraminiferen und Konkretionen von Paläoböden, die nicht in Deltasedimenten vorkommen, unterstützt.

Die Sedimentmuster seewärts des Bassac-Flusses zeigen einen Sedimenttransport im Uhrzeigersinn und in westlicher Richtung entlang der Küste bis zu einem breiten flachen Gebiet der Deltafront von Kap Ca Mau. Die subaquatischen Deltasedimente zeigen eine sehr hohe laterale Variabilität auf, die durch die stark lokal und monsungesteuerte saisonal variirende Wirkung aus Flussfracht, Tide und Wellen resultiert. Häufig werden diese Sedimente nicht in langfristigen geologischen Aufzeichnungen erhalten.

Tideprozesse beeinflussen die Interaktion zwischen Land und Meer. Besonders in Regionen mit einem hohen Sedimentausfluss wie im Mekongdelta in Südvietnam sind diese Prozesse weitaus stärker von Bedeutung.

Während der Forschungsausfahrten in der Intermonsunzeit sind erhöhte Sedimentkonzentration größer 25µl/l in Bereichen der Hauptflussarme des Mekongs und des subaquatischen Gebietes beobachtet worden. Im Besonderen überstiegen 20 % aller Messungen im subaquatischen Delta eine Sedimentkonzentration von 100 µl/l, wobei die höhsten Werte nahe des Meeresbodens gemessen wurden. Im Übergang zum offenen Schelf nehmen die Sedimentkonzentrationen ab und speziell in der südöstlichen Schelfregion sind 99 Prozent aller Messungen unterhalb von 25 µl/l. Eine Ausnahme zeigt das südliche Schelfgebiet um das Kap Ca Mau, wo bodennah in Wassertiefen von 20 bis 25 m eine erhöhte Sedimentschwebfracht (>25 µl/l) auftritt.

Es wurden zwei Untersuchungen von jeweils 25 Stunden an Ankerstationen in Wassertiefen von 12 m (Ankerstation 1) und 26 m (Ankerstation 2) durchgeführt, um jeweils über eine Tidephase die Sedimentkonzentrationen der Wassersäule und die Strömungsgeschwindigkeiten bzw. -richtungen in unterschiedlichen Wassertiefe zu ermitteln. Die Stationen befinden sich am subaquatischen Deltahang und 3.2 km voneinander entfernt. Beide Untersuchungen zeigen über die Zeit ähnliche Sedimentverteilungen, die mit den Tidesströmungen korrelieren. Es werden erhöhte Sedimentkonzentrationen (>25µl/l) bei hohen Tideströmungen von bis zu 0.6 m/s gemessen. Zusätzlich ist ein abnehmender Trend der Sedimentkonzentration vom bodennahen Bereich hin zu der Meeresoberfläche zu beobachten. Bezüglich des Sedimenttransportes hat die Ebbphase höhere Strömungsgeschwindigkeiten gegenüber der Flutphase, die jedoch länger andauert. Des Weiteren ist der Wechsel von Ebb- zur Flutphase sehr schnell während der Übergang von Flut zu Ebbe bis zu 3 Stunden andauern kann. Die erzeugte Asymmetrie der Tideellipse, kann infolge der höheren Tideströmungen der Ebbphase einen Netzsedimenttransport vom Schelf in das subaquatische Mekong-Delta verursachen.

Sieben Transekte zeigen in Abhängigkeit zur Tidephase im subaquatischen Mekong-Delta und dem angrenzenden Schelf ähnliche Schwebfrachtverteilungen. Ein hypopyknischer Plume vom subaquatischen Mekong-Delta in den offenen Schelf ist nicht beobachtet worden. Aus den Untersuchungsergebnissen ist zu folgern, dass während der Intermonsunzeit der Sedimenttransport aufgrund der Resuspension durch Tideströmungen erfolgt.

Der lokale Einfluss von Tide, Wellen und Flüssen prägt die Morphologie und Sedimentverbreitung in großen Deltas wie dem Mekong-Delta. Spezifische hydro- und morphodynamische Bedingungen bilden im Mekong-Delta ein Sandrücken-System in Verbindung mit erosiven Rinnen, dass einzigartig in subaquatischen Deltagebieten ist. Es erstreckt sich großräumig entlang der Deltafront, im Besonderen am Deltahang und der subaquatischen Deltaplattform. Bestehung aus zwei Sandrücken und zwei erosiven Rinnen nimmt es mindestens eine Fläche von 1971 km² ein und verläuft 128 km entlang der Küste. In Abhängigkeit von der Morphologie werden drei Einheiten westlich der Mündung des Bassac-Flusses, dem größten und westlichsten Flussarm des Mekong-Deltas, unterschieden. Der östliche Bereich des Sandrücken-Rinnen-System beginnt südwestlich der Bassac-Flussmündung. Dort erstreckt es sich am Deltahang und der inneren Schelfplattform und ist morphologisch durch konkave und erosive Merkmale am Meeresboden gekennzeichnet. Den zentralen Bereich des Sandrücken-Rinnen-Systems nimmt die südliche subaquatische Deltaplattform ein, auf der die Sandrücken und erosiven Rinnen deutlich ausgeprägt sind. Anhand hydroakustischer

Querschnitte durch das Sandrücken-Rinnen-System ist seine asymmetrische Form gut erkennbar, wobei die steileren Flanken in seewärtige Richtung zeigen. Die Rinnen schneiden sich bis zu 18 m Wassertiefe und bis zu 10.5 m, gemessen vom Rückenkamm, in die subaquatische Deltaplattform ein. Im westlichen Bereich des zentralen Gebietes laufen die Sandrücken aus und die Rinnen vereinigen sich in Form einer großen Kolkung von bis zu 33 m Wassertiefe in der subaquatischen Deltaplattform, die im Umfeld der Kolkung Wassertiefen kleiner als 7.7 m aufweist. In dem westlichen Gebiet des Sandrücken-Rinnen-Systems wird die einzelne Rinne stetig flacher bis sie in der südwestlichen subaquatischen Deltaplattform um das Kap Ca Mau verschwindet.

Rückschreitende Erosion an Landzungen und weitere erosiven Küstengebiete des Mekongdeltas sind Nährgebiete für die Sandrücken während Tideströmungen, subparallel zur Küste, sie unterhalten und stabilisieren. Im Gegensatz formen auch Tide- und windinduzierte Strömungen die Rinnen, die sich tief in die subaquatische Deltaplatform einschneiden und als Sedimentförderband zu der distalen Deltafront um das Kap Ca Mau dienen, das 200 km von der nächsten Haupflussmündung entfernt liegt. Das Sandrücken-Rinnen-System repräsentiert eine neue morphologisches Besonderheit in einer Deltaumgebung und ist ein Indikator für Instabilitäten und Küstenerosion in subaquatischen Deltas.

Table of Contents

Chapter I

General Introduction

The necessity of understanding human influences within natural environments is important without a doubt, because it turns natural condition into different and hence unnatural directions. For examples, simultaneously, humans have stepped up sediment transport by global rivers due to soil erosion by 2.3 ± 0.6 billion t yr^{-1} and have decreased the sediment flux into the ocean by 1.4 (± 0.3) billion t yr^{-1} due to reservoir retention (Syvitski et al., 2005b). Both processes change the natural equilibrium against each other and it becomes hard to distinguish between the impacts of these particular processes. Therefore, it is important to understand and reconstruct most of the physical environmental conditions.

The population in the Mekong River delta amounts to 20 million people (Ericson et al., 2006). Although its delta plain covers an area of 49,500 km^2, the Mekong River delta has one of the highest population densities (412 person per km^2) in Vietnam (Käkönen, 2008). The local economy is prevailed by agriculture and aqua farming. In 2005, two to three rice harvests supply 19.2 million tons (Sakamoto et al., 2007) and the freshwater fishery in 2006 produced 1.2 million tons per year, a total of 2.6 billion US$ per year (MRC, 2010). The importance for the global and inner-South-Asian economy and food production is immense, because many people life in dependence on the agro- and aquaculture of the Mekong River delta. The food production depends on the stability of many influence factors like nutrient and sediment supply, water quality and saline intrusion into croplands, coastline retreat or progradation. The knowledge of the factor processes is crucial to estimate future developments in food production.

The more than 500 km long coast of the Mekong River delta is prevailed by boundary condition between land-ocean interaction and influenced by various sediment- and hydro-dynamic factors including tides, waves, coastal currents and seasonal driven river discharge (Syvitski and Saito, 2007). In mega-deltas like the Mekong River Delta both the local energetic environment and the supply of sediment regulate subaerial and subaqueous coastal morphology. In reverse, delta morphology and sedimentary pattern reflect these impacts. For example, Tamura et al. (2012) present shoreline changes of centennial scale, whereas delta front bars/islands are developed. In landward direction, bay head deltas evolve and are secondarily filled by muddy sediment due to the lower energetic environment behind the delta front bars and islands.

However, little is known about the prevailing hydro- and sediment-dynamic influence factors of the subaqueous Mekong delta and only sparse data of morphodynamic processes exist. The investigations of this thesis aim directly at closing these gaps of knowledge.

The work is integrated into the German-Vietnamese marine research project "*Land-ocean-atmospheric interactions in the coastal zone of Southern Vietnam"* supported by the DFG (DFG_STA401/10). In more detail it has the following objectives:

Hydrodynamic conditions including tidal amplitudes and currents:

Wind and tide driven currents and wave action are crucial parameters in the coastal environment. Interpretation of coastal hydrodynamic processes cannot be done without a quantification of their influences. This study will access the tidal influence as factor to the hydrodynamic processes, because wind and wave action were diminished during the data acquisition.

Morphodynamic processes of the subaqueous Mekong delta:

Different models of delta shapes exist in dependence on their driving influence factors (Orton and Reading, 1993; Walsh and Nittrouer, 2009). In mega-deltas like the Mekong-River Delta, the driving influence factors changes and alter morpho dynamic parameters. Consequently, the delta morphology varies in shape. This study surveys the subaqueous delta shape and morpho dynamic conditions are reconstructed.

Sedimentdynamic processes of the subaqueous Mekong delta:

Understanding sediment delivery from source to sink is one of the crucial challenges of sedimentologists of the 21st century. Although many models (Postma et al,. 2008, Xue et al., 2012a) and investigations (Harris et al., 2004; Duc et al., 2007) already exist about sediment transport, erosion and accumulation in subaqueous river deltas, they show that each deltaic environment is unique (Bhattacharya and Giosan, 2003). Results of hydro and morphodynamic factors are used to identify the depositional conditions in the subaqueous Mekong delta. Particularly, this study will focus on the spatial suspended sediment distribution from the Mekong-River mouth region to the open shelf.

Chapter II

Methods

Two cruises in 2007 and 2008 were carried out to survey the multifaceted hydro-, morpho- and sediment dynamic processes in the subaqueous Mekong delta. Two fisher boats were equipped with several scientific tools to investigate all the objectives of the project (Fig. 1). The first boat responsible for seismic surveys has used two different boomer systems.

The second boat covered sediment sampling (surface and suspended sediment, sediment coring), water column features (particle size distribution, suspended sediment concentration, variation of salinity and temperature) and hydro dynamic properties (current velocity and direction). Therefore, a crane was mounted for short gravity cores and measurements in Laser in situ Scattering and Transmissiometry (LISST). Furthermore, frame-mounted CTD, turbidity meter and niskin bottle for water sampling were applied. Surface sediment samples were taken by a grab-sampler and current properties was measured using an acoustic Doppler current profiler (ADCP).

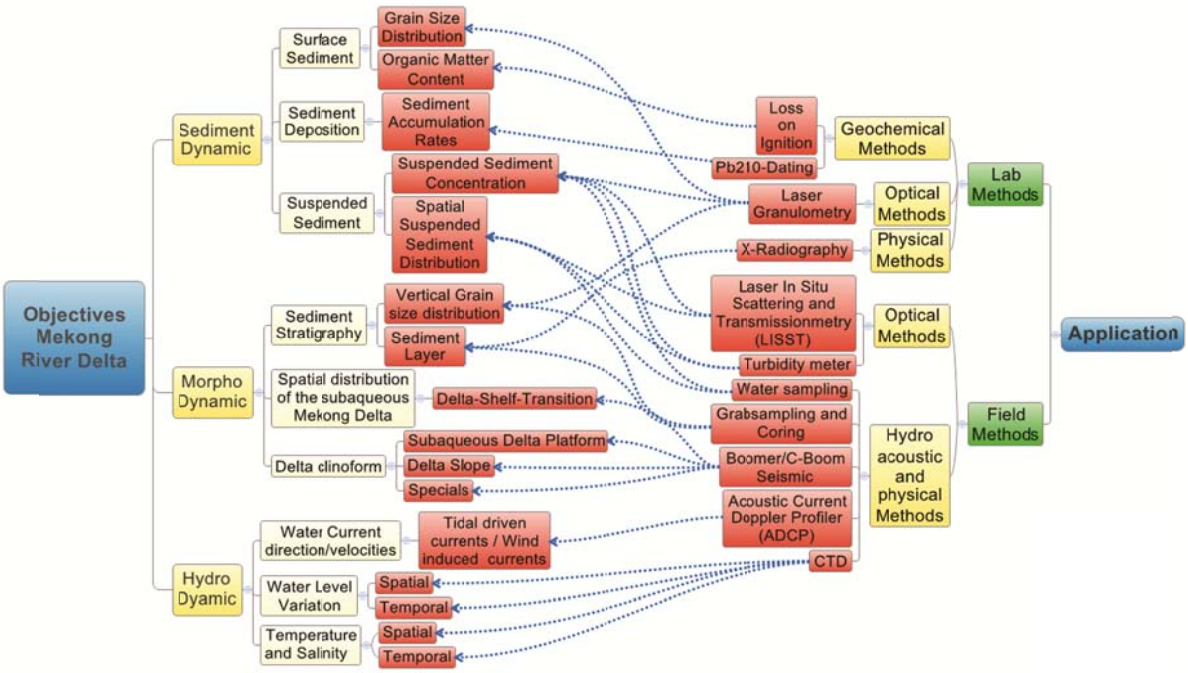

Fig. 1 Objectives and methods during the field campaigns in 2007 and 2008

In the lab, sediment cores were splitted, described, subsampled and X-radiograph-negatives were taken, respectively. Sediment samples are separated for loss on ignition and laser granulometry method. Water samples are filtered to estimate suspended sediment concentration. The following chapter describes the methodology of the main applications (geochemical, physical, especially optical and hydro acoustic methods).

1 Geochemical Methods

1.1 Loss on Ignition-Method

The loss on ignition method (LOI) is used to estimate the amount of organic matter and carbonate mineral content in sediments (Dean, 1974; Heiri et al., 2001; Santisteban et al., 2004). Heating sediments at 550°C and 950°C cause the combustion of organic matter (LOI_{550}) and carbonate (LOI_{950}) to carbon dioxide, respectively. The amount of the weight loss is simply estimated by weighing using the following procedure (after Heiri et al., 2001):

1. Weighing of sample cup and sample cup plus wet sediment sample
2. Sediment drying at 50 °C for 24 hours (between all following heating and weighing steps sediment were put into a desiccator to avoid higher moisture in the sample due to high humidity)
3. Homogenizing of the sediment sample in a mortar
4. Weighing crucible (high temperature (>1000°C) resistant) and additionally crucible plus sediments using a micro balance (accuracy = 0.00001 g)
5. Heating the sediment into a muffle furnace at 105 °C for 24 hours
6. Weighing sediment including crucible (LOI_{105}) using the micro balance
7. Heating the sediment into a muffle furnace at 550 °C for 6 hours
8. Weighing the sediment including crucible (LOI_{550}) using the micro balance
9. Heating the sediment into a muffle furnace at 950°C for 2 hours
10. Weighing the sediment (LOI_{950}) using the micro balance

Afterwards, the weight loss of organic matter und carbonate was calculated by the following equations:

$$LOI_{550} = ((DW_{105} – DW_{550})/DW_{105})*100 \text{ (for organic matter content)}$$

And

$$LOI_{950} = ((DW_{550} – DW_{950})/DW_{105})*100 \text{ (for carbonate content)}$$

Whereas

LOI_{XXX} = Loss on ignition at XXX °C

DW_{XXX} = dry weight at XXX °C

A factor of 1.36 was applied to determine the carbonate content (CO_3^{2-}) assuming:

$$M_{CO_3^{2-}} \div M_{CO_2} = 60\ g*mol^{-1} \div 44\ g*mol^{-1} = 1.36$$

$$CC = 1.36 * LOI_{950}$$

$M_{CO_3^{2-}}$ = molecular weight of CO_3^{2-}

M_{CO_2} = molecular weight of CO_2

CC = Carbonate Content

LOI_{950} = Loss on Ignition by 950°C in wt(%)

1.2 ^{210}Pb-dating

Dating of sediment accumulation in shallow marine environments is very important, but to find an appropriate method is a challenge in itself. In the early 70s of the last century the radionuclide Lead 210 (^{210}Pb) became very useful to estimate the sediment accumulation at shelf environments (Nittrouer et al., 1979). The half-life of ^{210}Pb amounts to 22.3 years (Appleby and Oldfield, 1978) and thus allows an appropriate dating for at least the past century.

^{210}Pb is a daughter-nuclide of the radioisotope Uran 238 (^{238}U). Particularly, in nature it results from the radioactive decay of the radionuclide Radium (^{226}Ra) in rocks and soils, which decays to the gas Radon, especially to the isotope Radon 222 (^{222}Rn). If ^{222}Rn emanate into the atmosphere it decays via four daughters, each with half-lives of milliseconds until 27 minutes, to ^{210}Pb. Hence, half-lives of the daughters are negligible in terms of geological time-scales.

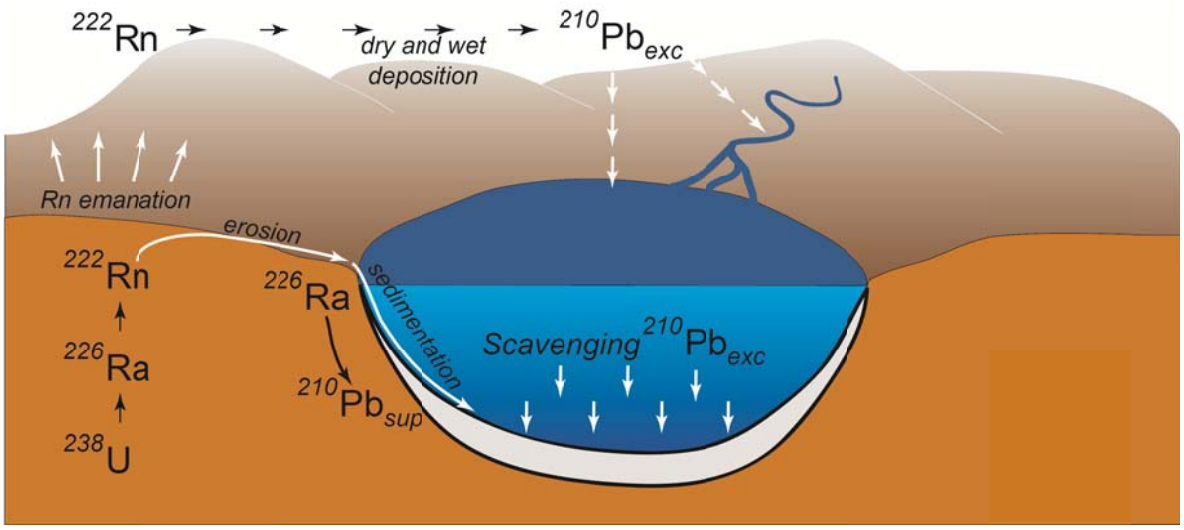

Fig. 2 Principle of ^{210}Pb-dating method (modified after Pittauerová et al. 2011)

One source produces ^{210}Pb in situ due to the decay of particulate ^{226}Ra (Fig. 2) within the studied sediment column, which is not emanated to the atmosphere. ^{210}Pb of this origin is referred to supported ^{210}Pb ($^{210}Pb_{sup}$).

A second source is ^{210}Pb diffused into the atmosphere (Fig. 2). This portion of ^{210}Pb settles out of the atmosphere (dry deposition), is scavenged by rain (wet deposition) or by aerosols and dust particles. Finally, it ends up into soils, the sea or other water bodies and will be sequestered by the respective recently deposited sediments, in particular organic matter. ^{210}Pb coming over these kinds of pathways into the system is called unsupported or excess ^{210}Pb ($^{210}Pb_{exc}$). The relation of the total ^{210}Pb at a certain sediment depth to its sources is described by the following equation:

$$^{210}Pb_{tot} = {}^{210}Pb_{exc} + {}^{210}Pb_{sup}$$

The activity of $^{210}Pb_{excess}$ decreases in sediment cores with increasing depth due to the radioactive decay until it reaches the background activity of $^{210}Pb_{supported}$. The effect of radioactive decay over time can be used to estimate the sediment accumulation rate (SAR) of the local environment.

Particular models are evolved to determine sediment accumulation rates in sediment. In the study environment dominates sediment mixing and hence, the following equation was chosen to estimate the SAR:

$$SAR = \lambda \times z \times [\ln\{A_0/A(z)\}]^{-1}$$

Whereas:

$\lambda = {}^{210}Pb$ decay constant (0.03114 yr^{-1})

z = core depth [cm]

A_0 = specific activity of the excess ^{210}Pb at a particular reference horizon or the surface

A(z) = specific activity of the excess ^{210}Pb at depth z below the reference horizon

(McKee et al., 1983)

2 Optical Methods

Concentrations of suspended particles and sizes of sediment grains can be measured with different optical methods. In addition, laser granulometry can subdivide suspended particles and sedimentary grains into different size classes. These methods will be explained in the following chapter.

2.1 Grain size analysis via laser granulometry

2.1.1 Sediment pretreatment

Organic and calcareous material of marine sediments can influence enormously the grain size distribution via laser granulometry. Therefore, pretreatments to remove these component parts of the sample are inevitable.

In dependence of the sedimentological composition, samples by a weight between 150 mg (very clayey) and 750 mg (very sandy) were given into a 50 ml centrifuge tube by adding 20 ml deionised water. First, samples were treated in a water bath with 10 ml of 10% solution of hydrochloric acid (HCL) by 60°C temperature. It occurs that huge components of calcareous skeletons of foraminifera and shell fragments cannot be removed completely with that treatment. After four hours, samples were rinsed and centrifuged to remove the residual

HCl-solution. Before each centrifuge procedure was applied, 500 µl of magnesium sulphate (Mg_2SO_4) were added to accelerate the particle settling. After the rinsing procedure, the centrifuge tube was filled up with 20 ml deionised water to keep the sediment wet.

The removal of organic matter was achieved by adding 10 ml 35% solution of hydrogen oxygen (H_2O_2) to the sample. The sediment was treated for at least 24 hours and by a temperature of 60°C. Lignin fibres of plant fragments cannot be removed with that method. If this procedure is finished, the sample is prepared for laser granulometry by adding sodium pyrophosphate ($Na_4P_2O_7$) that supports the dispersion of sediment grains.

2.1.2 Laser granulometry

A Malvern Mastersizer 2000 and a Beckman Coulter LS 13320 were applied for grain size analysis via laser granulometry. Based on laser diffraction, laser light scattered forward through a grain. In dependence on its size, the laser beam diffract in a particularly angle. The rule of thumb is as smaller the grain as higher the diffraction angle.

The Malvern Mastersizer 2000 is working with two light sources, one red laser beam of 632.8 nm wavelength and a blue LED of 470 nm wave length. Principles of Frauenhofer-diffraction and Mie-theory (are applied to distinguish grain sizes of 50 classes in a range between 0.02 µm and 2000 µm.

The Beckman Coulter LS 13 320 has also different light sources, one single laser beam of 780 nm wavelength and multi-wavelength system PIDS (Polarisation Intensity Differential System) working wave length of 450 (blue), 600 (orange) and 900 (near-infrared, invisible) nm.

Each sediment sample was measured twelve times for 60 second. Measurement results were post processed to remove outliers and subsequently averaged including 2σ-standard deviation. Afterwards, the grain size distribution was statistically analysed using the software script GRADISTAT (Blott and Pye, 2001).

2.2 Laser In Situ Scattering and Transmissiometry (LISST)

Analysis of suspended particle distribution in the water column was achieved using the Laser In Situ Scattering and Transmissiometry (LISST). The methodology is described by (Agrawal, and Pottsmith, 2000) and application examples are published by (Mikkelsen and Pejrup 2000, 2001; Mikkelsen, 2002a, 2002b; Mikkelsen et al., 2005; Bowers et al., 2009). Mounted on a steal frame the LISST were lowered horizontal through water column with the speed of

approximately 0.25 m/s by record frequency of one second. Hence, the vertical data resolution in the water column amounts ca. 4 measurements per meter.

The data postprocessing in Microsoft Excel removed all data with a transmission lower than 0.3, which indicates potential multiple scattering of the laser beam due to higher amounts of particles. Supported by a FORTRAN-script of Thanh Cong Nguyen, data were converted for spatial visualisation into the Ocean Data View-format (Schlitzer 2011).

2.3 Turbidity meter

Suspended sediment concentration is estimated using a Seapoint turbidity meter. Thereby, light is emitted at a wavelength of 880 nm using a Light Emitting Diode (LED). Scattered light at an angle between 15 and 150 degree from particles in the water column are detected by a silicon photodiode (Seapoint Sensors, Inc, 2013). The sensor measures the scattered light in Formazin Turbidity Units (FTUs). Water samples have been taken to correlate FTUs with the suspended sediment concentration (SSC) due to the proportionality between the amount of scattered light and the turbidity or suspended particle concentration in water.

During the cruises in 2007 and 2008 the turbidity meter was used in the river mouth and subaqueous regions of the Mekong River delta. Deployed at a frame in combination with a water sampler it was vertically lowered in the water column. Water samples were taken approximately one meter above the sea bed and filled into water bottles. In the sediment laboratory of the University of Kiel turbid water was filtered using glass fibre filters of 0.7 µm pore density (Whatman GF Cat No 1822-047) by a vacuum of 300 mbar. Filters were dried at 100 °C and weighted with a micro balance of 0.00001 g accuracy. The correlation of weight results SSC and FTUs can be seen at Fig. 2 (Chapter V).

3 Hydro-acoustic Methods

The overview about stratigraphic information and local hydro-dynamic conditions can be achieved by using hydro-acoustic methods. Therefore, two different Boomer-systems and an Acoustic Doppler Current Profiler (ADCP) were applied in the subaqueous Mekong Delta.

3.1 Boomer / C-Boom

Boomer is a single channel hydro-acoustic system that resolves the sediment strata in high resolution. In principle, an electromechanical transducer produces a single broadband acoustic pressure pulse. Reflected sound energy from sediment layers can be received by hydrophones which transfer the signal to a digital recorder.

Reflection of the sound energy occurs along the boundary of two certain sediment layers, which differ in acoustic impedance. Impedance is defined as density of the medium (sediment) multiplied with the sound velocity of the corresponding layer.

Two different boomer systems were used during the cruise in 2007 and 2008. Mounted on a catamaran, the transducer was towed behind the ship with a distance of 25 m and parallel to the streamer that is composed of eight (2007) and one (2008) of hydrophones, respectively.

In 2007, the EG&G Uniboom-system was applied, whereas the transducer produces a broad bandwidth frequency ranging between 0.3 and 11 kHz. Depending on the acoustic impedance of the sediment penetration depths reached 20 to 100 m. During the surveys the ship runs around 4 knots with an acoustic pulse frequency of 4 Hz. NWC-Software was used for digital recording of the seismic traces and its postprocessing. Seismic interpretation was performed using Kingdom Suite Software. During the cruise in 2008 the low-voltage C-Boom-system was deployed working with a similar bandwidth but a dominant frequency of 1.76 kHz.

3.2 Acoustic Doppler Current Profiler

The Acoustic Doppler Current Profiler (ADCP) measures include the entire water column vertical and horizontal water velocities and their direction using the Doppler Effect. The Doppler effect results from a change of an observed sound pitch due to relative motion (Gordon, 1996; Simpson, 2001). Increasing sound pitches indicate an approaching object while decreasing pitches indicate removing objects. The change of the sound pitch (frequency) describes the Doppler Shift that is directly proportional to the object velocity. The Doppler Shift represents the difference between two frequencies of a sound wave caused by an object that moves to or away from the sound source at a certain angle (Gordon, 1996; Simpson, 2001). Doppler Shift

works only at radial motion of the object relative to the sound source. Fields of applications are described by van Maren and Hoekstra (2004), Hoitink and Hoekstra (2005), Kostaschuk et al. (2005), Grossmann et al. (2007) and detailed methodological descriptions are presented by (Gordon, 1996; Simpson, 2001; Mueller and Wagner, 2006).

During the cruises in 2007 and 2008 a broadband workhorse ADCP (RD-instruments) were used with a frequency of 1200 KHz. Data were recorded by Winriver software (RD-instruments) selecting profiling mode 1. One ensemble included 30 pings over a time of 0.2 seconds. The water column was divided into appropriate depth cells (bins). Data was exported for post-processing as ASCII-file and 300 single ensembles (1 min resolution) were combined to average the water direction and velocity. During the postprocessing procedure a FORTRAN-script written by Thanh Cong Nguyen removes headers and transforms the data set into a special data format which can read in Ocean data view (Schlitzer, 2011) or Grapher (Golden Software).

4 Physical Methods

4.1 X-Radiography

Fine sedimentation pattern imply hydro or sediment dynamic changes. To resolve this pattern x-radiography is applied. Therefore, plastic caps of 20 cm length, 6 cm width and 1 cm depth were pushed into the sediment of a splitted core section. The caps were retrieved and measured in the Radiology of the Medical Center “Prüner Gang” in Kiel, Germany. The digital x-radiograph-negatives could be directly used for the analysis of sediment stratigraphy.

Chapter III
Modern sedimentation and morphology of the subaqueous Mekong Delta, Southern Vietnam

Daniel Unverricht[1]*, Witold Szczuciński[2], Karl Stattegger[1], Robert Jagodziński[2],

Thuyen Xuan Le [3], Laval Liong Wee Kwong[4]

[1]*Institute of Geosciences – Department of Sedimentology, Christian-Albrechts-University of Kiel, Germany*

[2]*Institute of Geology, Adam Mickiewicz University, Poznań, Poland*

[3]*Institute of Resources Geography, VAST, Ho Chi Minh City,Vietnam*

[4] *Environment Laboratories, International Atomic Energy Agency, 4 Quai Antoine 1er, MC 98000, Monaco*

Published in Global and Planetary Change, reprinted with the permission from the publisher Elsevier

Abstract:

The Mekong River Delta is among the Asian mega-deltas and is influenced by various factors including tides (meso-tidal system), waves, coastal currents, monsoon-driven river discharge and human impact (agriculture, fishing, sand dredging, tourism). The present study aims to document the seafloor relief, sediment distribution and sediment accumulation rates to interpret modern sediment transport directions and main sedimentation processes in the subaqueous Mekong Delta. The major results of this investigation include the detection of two delta fronts 200 km apart, one at the mouth of the Bassac River (the biggest branch of the Mekong Delta) and the other around Cape Ca Mau (most south-western end of the Mekong Delta). Additionally, a large channel system runs in the subaqueous delta platform parallel to the shore and between the two fronts. The sediment accumulation rates vary greatly according to the location in the subaqueous delta and have reached up to 10 cm/yr for the last century. A cluster analysis of surface sediment samples revealed two different sediment types within the delta including a well-sorted sandy sediment and a poorly sorted, silty sediment. In addition, a third end member with medium to coarse sand characterized the distant parts of the delta at the

transition to the open shelf. The increase of organic matter and carbonate content to the bottom set area and other sedimentary features such as shell fragments, foraminifera and concretions of palaeo-soils that do not occur in delta sediments, supported grain size-based classification. Beginning in front of the Bassac River mouth, sedimentary pattern indicate clockwise sediment transport alongshore in the western direction to a broad topset area and the delta front around Cape Ca Mau. Our results clearly show the large lateral variability of the subaqueous Mekong Delta that is further complicated by strong monsoon-driven seasonality. River, tidal and wave forcing vary at local and seasonal scales with sedimentary response to localised short term depositional patterns that are often not preserved in long term geological records.

1 Introduction

The ongoing natural and human-driven global changes result in important variations in the sediment flux from land to ocean (Syvitski et al., 2005a), which are perceptible in the coastal zone and particularly in river deltas (Syvitski and Saito, 2007; Syvitski et al., 2009). The recent reduction of sediment input due to river damming and the resulting coastal erosion impacted the coastal zone (Milliman and Ren, 1995). Ranked among the 10 largest suppliers of sediments to the world's oceans (Milliman and Meade, 1983), and with estimated sediment discharge of 160 million tonnes per year (Milliman and Ren, 1995), the sediment discharge of Mekong River may diminish due to existing dams (Kummu et al., 2010; Wang et al., 2011). Large river systems complicate the comparison of the sediment flux estimates with the actual fluxes in the coastal zone because the final destination of the river sediments and the dominating sedimentary processes remain little understood.

A recent attempt to combine data from various river systems explored the driving processes on the dispersal and accumulation of riverine sediments in the coastal zone and defined the following important criteria: sediment discharge, shelf width, and wave and tidal conditions (Walsh and Nittrouer, 2009). Many more factors may affect the delta, however, including processes acting in the river catchment, the coastal zone and the marine realm (Vörösmarty et al., 2003; Kummu and Varis, 2007; Syvitski and Saito, 2007, Kummu et al., 2010; Yang et al., 2011). In many cases, lacks of good spatial and temporal data coverage limit these discussions. Similarly, in the Mekong River Delta, the sediment depocenter in a subaqueous part of the delta was only recently documented through several seismic profiles and 6 short sediment cores (Xue et al., 2010).

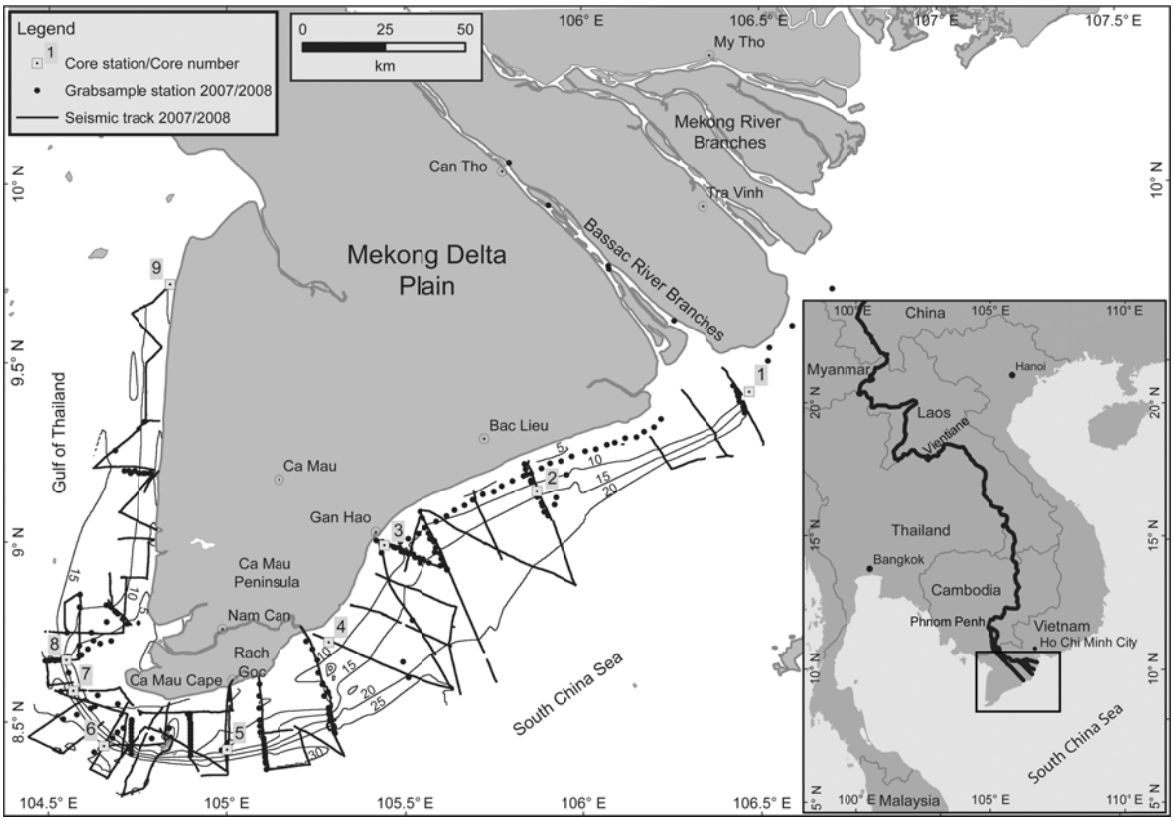

Fig. 1 The base map containing the investigated area with the subaqueous part of the Mekong Delta and adjacent continental shelf, with marked surveyed seismic lines, locations of surface sediment samples and sediment cores and the topographical features mentioned in the text. The presented bathymetry is based on own survey. The inset map shows the location of the Mekong River delta in South-east Asia.

The deltas also changed in the past, and understanding their developments proves valuable for predicting their future evolution. In the case of the Mekong River Delta, land-based borehole data and seismic surveys recorded the Holocene delta evolution from the initiation of delta progradation around 8.0 ka BP to the present (Nguyen et al., 2000; Ta et al., 2002b; Tamura et al., 2009; Xue et al., 2010; Proske et al., 2011; Hanebuth et al., 2012; Tamura et al., 2012b). During its development, the delta character changed from tide-dominated into a wave- and tide-dominated, and its shape and the orientation of the coastline changed through time (Ta et al., 2002a). The reconstruction of delta development is based on the character and structures of the sediments interpreted as a part of the subaqueous delta, but such data have not been gathered from the modern Mekong Delta, where the hydrodynamic conditions, the position of sediment within the delta and spatial and temporal relationships may be observed.

This study documents sea floor relief, sediments and sediment accumulation rates to interpret the modern sediment dispersal pattern, sedimentation processes and rates on the

subaqueous Mekong Delta. Additionally, future interpretations of the Mekong River Delta evolution will benefit from this data set.

2 Regional Setting

The Mekong River originates on the Tibetan Plateau and crosses China, Myanmar, Laos, Thailand, Cambodia and Vietnam, where it flows into the South China Sea (Fig. 1). Its delta plain stretches over an area of 49,500 km² between Phnom Penh in the Cambodian lowlands and the southeast Vietnamese coast (Le et al., 2007). Figure 1 depicts the main distributaries, the Bassac (Hau River) and the Mekong (Tien River), which split into the 2 branches of the Bassac and 6 of the Mekong before entering the sea. Strong seasonal climatic variations in the Mekong Delta are related to the phase of the East Asian Monsoon (Hordoir et al., 2006; Mitsuguchi et al., 2008; Xue et al., 2011). The north-eastern winter monsoon dominates from November to early March with high wind stress at the south-eastern exposed coast, and the south-western summer monsoon carries precipitation towards the Mekong Delta (ISPONRE, 2009; Mekong River Commission, 2005, 2009; Snidvongs and Teng, 2006). The annual average rainfall in southern Vietnam ranges between 1600 and 2000 mm. Wind speeds can reach 20-30 m/s under stormy conditions; however, mean annual wind velocities range between 1.5 and 3.5 m/s (Institute of Strategy and Policy on natural resources and environment (ISPONRE), 2009).

The distribution of the principal surface current system in the Southern South China Sea has been attributed to the East Asian Monsoon (Wendong et al., 1998). The maximum wind stress prevails along the south-eastern coast of the Indochina Peninsula in both monsoon seasons. In the Mekong River basin, 85% (475 billion m³) of the water discharge occurs during the wet season (May to October), and 15% (78.8 billion m³) in the dry season (November to April) (Snidvongs and Teng, 2006; Le et al., 2007). The Mekong River Commission provides a representative documentation of the water discharge and level for the upper Mekong Delta region. Data availability of the water discharge or tidal amplitudes is however problematic for the river mouth area of all the branches. The only existing sediment load data of 160 million t/yr (Milliman and Meade, 1983) was derived before many dams were constructed. Contemporary estimates of the sedimentary retention of the existing dams along the Mekong River calculate 35-45 million t/yr in sediment (Kummu et al., 2010).

Hydrodynamics and resulting sediment-dynamics formed the asymmetric shape of the delta plain. The incoming tidal waves of the dominant M2- and K1-constituents extend from northeast to southwest via the Strait of Luzon (Fang et al., 1999; Zu et al., 2008). These waves push water

masses into the coastal region and cause a meso-tidal regime in front of the Mekong Delta branches. The tidal range and regime vary along the southeast Vietnamese coast from a predominantly semi-diurnal tidal system with a mean range of 2.5-3.8 m in the east to a mixed-tide system with decreasing amplitudes towards the southwest (Nguyen et al., 2000). Diurnal tides predominate in the Gulf of Thailand with ranges of 0.5 to 1.0 m.

The sedimentary architecture of the delta plain is well investigated, especially in the region between the Mekong distributaries (Gagliano and McIntire, 1968; Nguyen et al., 2000; Proske et al., 2011; Ta et al., 2002b, 2005; Hanebuth et al., 2012; Tamura et al., 2009, 2012b). The study of the subaqueous part of the Mekong Delta is far less common. Annual net southwestward transport along a mesotidal beach and respective long-term shoreline changes were observed in the Tra Vinh province in the lower Mekong Delta plain by Tamura et al. (2010). There, interseasonal surveys were carried out in the intertidal area of the Mekong Delta coast. Wave heights of 1 m in maximum were observed for this region.

Gagliano and McIntire (1968) provided first sedimentary and bathymetric results of the subaqueous Mekong Delta. Several coastal normal transects showed the subaqueous clinoform reaching more than 20 km offshore in front of the main distributaries and around Ca Mau Peninsula. Recently, seismic profiles of a higher resolution and several sediment cores revealed a Holocene subaqueous delta with up to 20 m thick sediments and a heterogeneous of topset-foreset-bottomset architecture (Xue et al., 2010). In order to refer more intensively to wide spreaded shallow subaqueous regions this article add the term of the subaqueous delta platform as a morphological description of topset areas. Further, the term delta slope is used for the foreset region.

3 Materials and Methods

High-resolution seismic profiles have been recorded during two surveys (2007 and 2008) of the subaqueous Mekong Delta off Vietnam, from the Bassac River mouth to the Gulf of Thailand (Fig. 1). Using the cubic spline method, an approximated subaqueous delta shape was constructed by interpolating the seabed profiles, which were obtained from seismic surveys using the software The Kingdom Suite (Seismic Micro-Technology, U.K.). The two-way-travel-time (TWT) was converted into water depth and assigned a sound velocity of 1500 m/s, and bathymetry data were analysed in ArcGIS. However, an error of up to 1.8 m may exist between various profiles as the shown water depths could not be corrected for tides. There is no

correlation to the base level or a Vietnamese tidal gauge station applied due to unknown water level variation in the subaqueous Mekong delta region, which is necessary for such a water level correction.

The surface sediments (the upper 1 cm of the seabed) of 229 stations were analysed for grain size distribution. Before the analyses, the sediments were treated with 35% H_2O_2 and sieved using a 1 mm sieve. Then, samples were analysed using the Malvern Mastersizer 2000 based on laser diffraction. The obtained results are shown in volume percentages. The grain size statistics of the obtained results were calculated using GRADISTAT software (Blott and Pye, 2001), and the grain size data were also subjected to cluster analysis with the free statistical tool R. The Centroid method and the squared Euclidean distance were used to obtain the cluster centres.

In selected surface sediment samples, the proportional masses of organic matter and carbonates were estimated using the loss on ignition method (Heiri et al., 2001; Santisteban et al., 2004). The content of organic matter results from the weight loss on ignition by 550 °C. The carbonate content (CC) was assessed from the difference in weight loss on ignition between 950 °C and 550 °C, multiplied by a factor of 1.36.

The sedimentary structures and relative changes in grain size were documented in the sediment cores using digital X-radiography images obtained from 0.6 cm thin slabs of the split core surfaces. The sediment accumulation rate (SAR) over the last few decades was assessed through the analysis of ^{210}Pb and ^{137}Cs. The ^{210}Pb activities for Cores 5 and 7 were determined using alpha spectroscopy measurements of the granddaughter nuclide ^{210}Po in the Marine Environment Laboratories of the International Atomic Energy Agency in Monaco. For these analyses, sediment samples were homogenised, spiked with a yield determinator and dissolved by acid digestion, and the ^{210}Po isotope was autoplated on a silver planchet (Flynn, 1968). Cores 6, 8 and 9 were measured using gamma spectroscopy, which allows the simultaneous measurement of ^{210}Pb and ^{137}Cs. Core 6 was measured with a high purity coaxial germanium detector (Canberra GX2520) with its remote detector chamber option (RDC-6 inches) set for low energy background reduction in the Institute of Geology at Adam Mickiewicz University in Poznań (Poland). Cores 8 and 9 were investigated at the Leibniz-Laboratory for Radiometric Dating and Isotope Research in Kiel (Germany). Samples for the gamma analyses were dried, homogenised and measured on average for approximately 150 hours each.

The SAR was assessed from the decrease of excess ^{210}Pb activities with sediment depth, using the equation:

$SAR = \lambda \times z \times [\ln \{A_0 / A(z)\}]^{-1}$ (Robbins and Edgington, 1975; McKee et al., 1983)

where λ (= 0.0311 yr^{-1}) is the decay constant, z is the depth in the core (cm), A_0 is the specific activity of the excess ^{210}Pb at a particular reference horizon or the surface and $A(z)$ is the specific activity of the excess ^{210}Pb at depth z below the reference horizon. Excess (unsupported) ^{210}Pb activities were determined by subtracting the average supported activity of a given core from the total activity. If possible, the supported activities were calculated from the nearly uniform ^{210}Pb activity below the region of radioactive decay. In the case of Core 6, they were also confirmed by simultaneous measurements of ^{214}Pb, ^{214}Bi and ^{226}Ra using gamma spectrometry. The supported ^{210}Pb activity is 22.1±1.6 Bq/kg and correlates with the supported ^{210}Pb activity of 1.09-1.44 dpm/g (= 18.1–24 Bq/kg) in cores in the subaqueous Mekong delta region from Xue et al., (2010).

The SAR assessment was performed using the first occurrence of ^{137}Cs as a marker of the early 1950s, when it was first released on a large scale in the environment during atmospheric nuclear weapon tests (Robbins et al., 1978; Leslie and Hancock, 2008).

4 Results

4.1 Sea bed morphology

The subaqueous Mekong Delta area consists of 5 subareas distinguished by clinoform morphology (Fig. 2). With an approximately 27 km wide funnel-shaped river mouth, the Bassac dominates Area 1. The delta base is reached 28 km offshore in the south-eastern direction, and tidal and subtidal flats and shallow topsets, up to a depth of 6 m underwater, characterise the proximal littoral (Profile A-A' in Fig. 2). Southwest of the mouth of the Bassac River, the subaqueous delta platform spreads at least 10 km offshore. Distant from the coast, a sigmoidal delta slope rises to the southeast and reaches the delta base at a depth of 24 m underwater (Fig. 2). The slope lengths average 8 km by a mean slope angle $\alpha_{mean} = 0.05°$ ($\alpha_{max} = 0.2°$).

The width of the subaqueous delta platform in Area 2 decreases to 3.5 km in the offshore direction (Profile B-B', Fig. 2). The average slope angles reach inclinations of $\alpha_{mean} = 0.052°$ ($\alpha_{max} = 0.12°$). The most recent delta slope ends at a depth of approximately 15 m (Fig. 2).

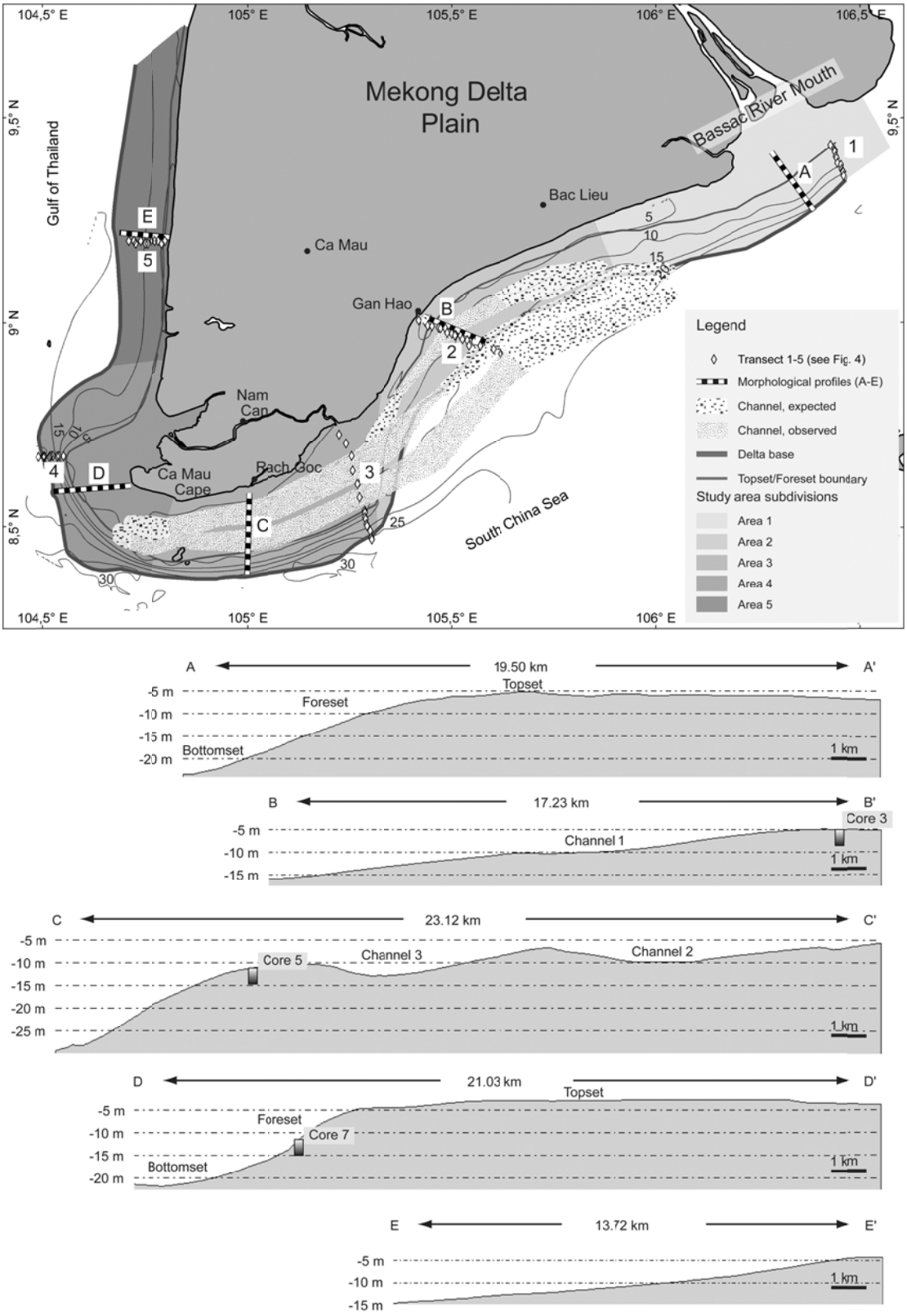

Fig. 2 Morphology of the subaqueous part of the Mekong River delta with the delta extension (delta base line), major morphological features (the break in the delta slope - topset / foreset boundary, channels), locations of morphological Profiles A to E presented below, sample transects 1-5 and the subdivision of the delta into 5 areas marked as discussed in the text. The location of sediment cores and major morphological features are marked on the morphological profiles.

Its significant undulated shape indicates the beginning of a multiple channel system (Fig. 2). One smaller and two larger channels are spread out in an alignment parallel to the coast (unpublished data). The channel linkage is located in the subaqueous delta platform and the delta slope close to Area 3 (Fig. 2), and its extension is more than 120 km.

The essential difference between the previous areas and Area 3 is the widespread subaqueous delta platform of 1100 km², including the channel system (Fig. 2). Channel 2 changes westwards from 13.5 m to 3 m water depth, and a deeper offshore channel (Channel 3) is levelling off from 17 m to 6 m water depth to the west. The southern flank of Channel 3 forms the transition to the delta slope (Fig. 2). Slope angles are relatively steep (α_{max} = 0.48°), with an average slope length of 5.7 km (min/max length = 3.4/8 km).

Around Cape Ca Mau (Area 4), a very shallow (less than 5 m) subaqueous delta platform is prograding 13.5 km offshore on average. The subaqueous Mekong Delta forms a further delta front here outside of the direct influence of distributaries (Fig. 2). It has an average slope gradient of α_{mean} = 0.054° (α_{max} = 0.43°).

Along the western and north-western coast (Area 5), the subaqueous delta platform regresses abruptly to the coast by an average width of 1.8 km, and the delta base is reached at a depth of 15 m with an average slope width of 11.8 km (Fig. 2).

4.2 Surface sediments

4.2.1 Spatial sedimentary distribution and Grain size end members

The surface sediments of the subaqueous Mekong Delta vary strongly in sorting and dominant grain size mode, but show a spatial pattern depending on the distance from the distributaries and their position in the delta clinoform. Near the Bassac River, fine sand prevails and silty sediment occurs in more distant regions (Figures 3C and 4). Fine sediment (silt and sandy silt) primarily covers Area 2, but there is a distinct occurrence of sand and silty sand along the recent delta slope close to Transect 2 (Fig. 3C and 4). Except for an occurrence of silty sand along Transect 3 (Fig. 3C and 4), the southern subaqueous delta area (Area 3) is dominated by sandy silt. Cape Ca Mau forms a junction between sandy silt and silty sediments. The northward continuing subaqueous delta exposed to the Gulf of Thailand consists of silt (Fig. 3C and 4).

Cluster analysis was performed to generalise the sedimentary pattern and evaluate the grain size end members for different depositional subenvironments. The cluster analysis used the

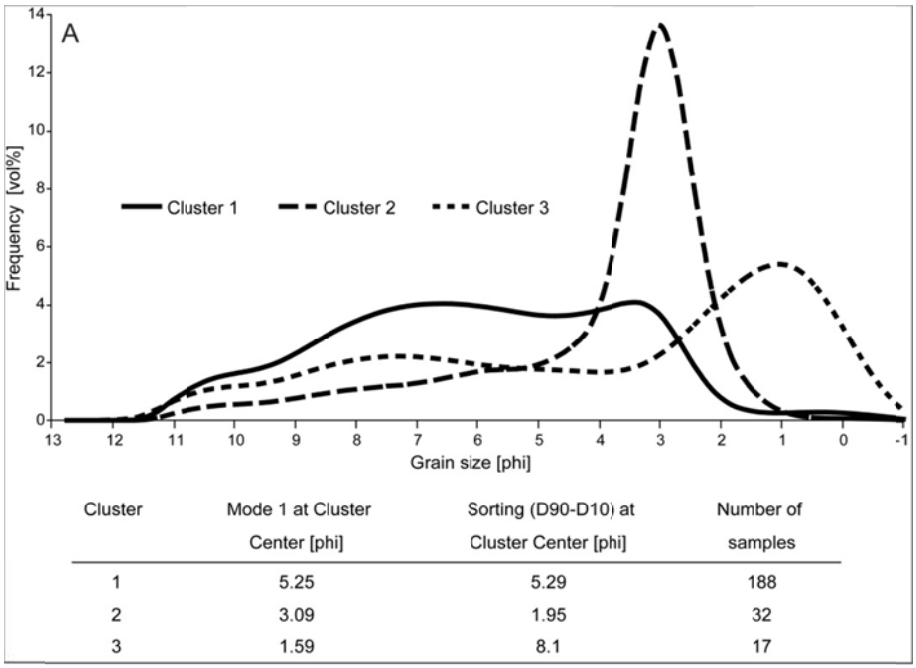

Cluster	Mode 1 at Cluster Center [phi]	Sorting (D90-D10) at Cluster Center [phi]	Number of samples
1	5.25	5.29	188
2	3.09	1.95	32
3	1.59	8.1	17

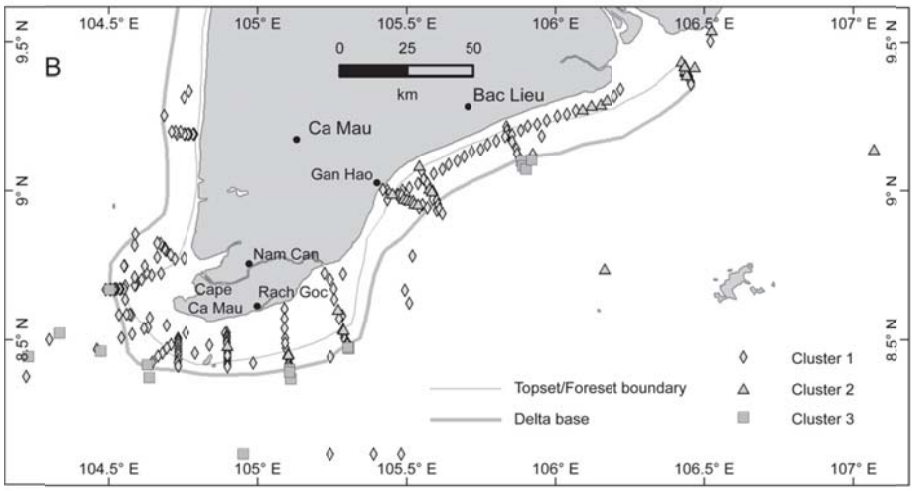

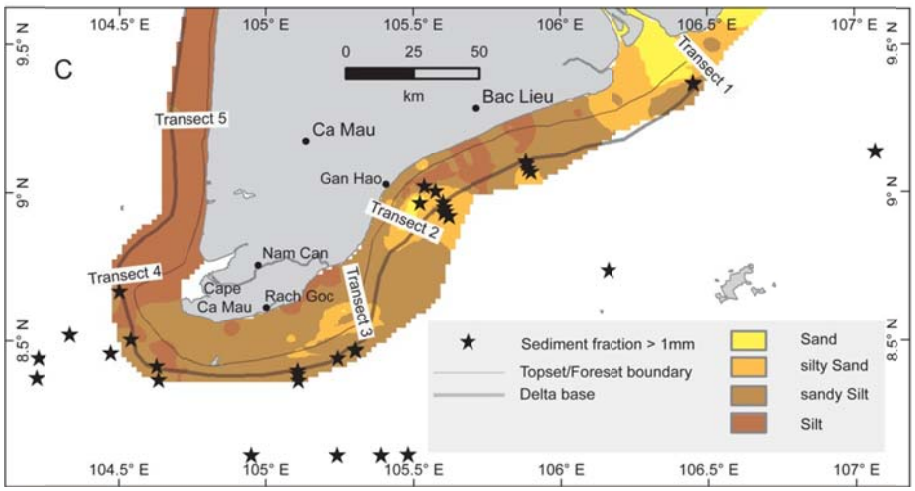

Fig. 3 A) Average grain size distributions of three sediment clusters and the numerical cluster centres (the first mode and D90-D10); B) spatial distribution of surface sediments grouped into particular clusters; C) the surface sediment map with marked surface sediments containing the fraction > 1 mm.

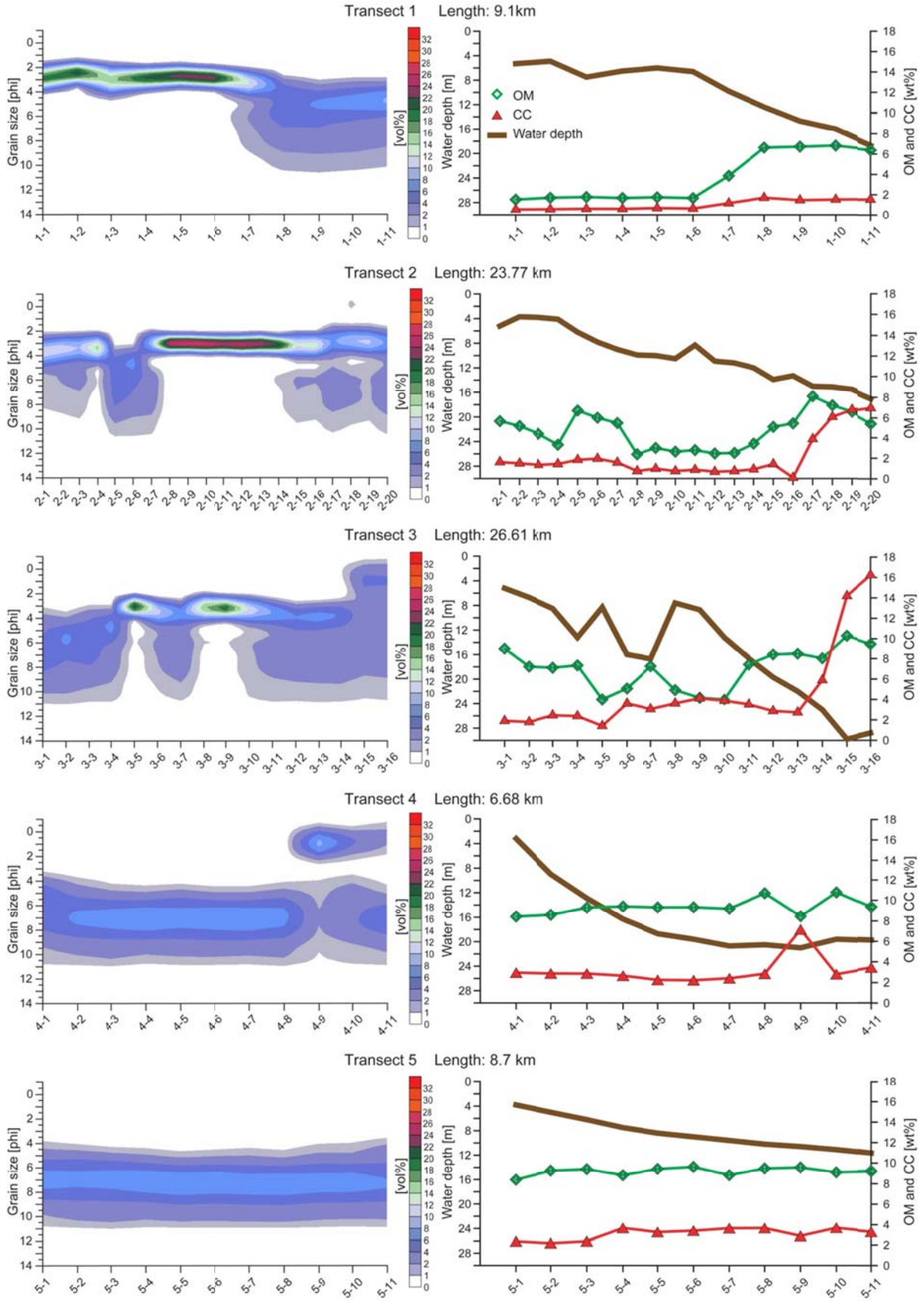

Fig. 4 Sediment properties along the five shore normal transects, grain size distribution (left hand), organic matter (OMC) and carbonate contents (CC), and seafloor morphology (right hand); see Fig. 2 for transect locations. The numbers on the x-axis refer to the sediment sampling sites along the transects.

grain size parameters as the primary mode (Mode 1) for the prevailing grain size class at certain locations and the difference between the ninth and first deciles (D90-D10) as a measure of sorting. Together, the two parameters represent a particular depositional environment.

The cluster analysis defines three clusters as grain-size end members in the subaqueous Mekong Delta and the transitional shelf region (Fig. 3A and 3B). Cluster 1 represents most of the subaqueous delta sediment and exhibits poor sorting, and the primary mode has its cluster centre in medium silt (Fig. 3A). However, uni- or bimodal grain size distributions occur as well with different positions, where modes mainly in fine sand and silt prevail.

The second cluster is also a part of the delta sediment, but its primary mode cluster centre is fine sand, exhibiting good sorting. The spatial distribution of Cluster 2 shows consistence with the special subaqueous delta regions (Fig. 3B). The tendencies of coarse to fine sediment from near to distant regions is typical for a river mouth area, due to sorting by diminishing water velocity (Transect 1 in Fig. 4). Alongshore tidal and wind induced currents cause the same succession in coast parallel direction (Fig. 5). The well-sorted sands of Cluster 2 dominate the subaqueous delta platform in front of the Bassac River mouth (Fig. 3B), where strong currents occur. The sandy spots of Cluster 2 punctuate the fine sediment close to Transect 2 (Fig. 3B and 3C). Additionally, the sandy sediment of Cluster 2 distributes along the southern flanks of Channel 2 and 3 (Fig. 4).

Very poor sorting by a primary mode of medium sand predominates in Cluster 3, representing its differences from Clusters 1 and 2 (Fig. 3A). The delta base marks the landward border of Cluster 3 because it extends between the delta base and the open shelf region (Fig. 3B). This distribution was also observed in the sediment fraction > 1 mm, except in the region close to Gan Hao (Fig. 3C). It represents a significant proxy for sediment interaction between the subaqueous delta and shelf sediment. This coarse fraction consists of shell fragments, foraminifera and concretions, the latter of which are likely residuals of lateritic palaeosoils outcropped on the inner shelf.

A more detailed resolution of grain size distributions along the coastal normal transects provides a miscellaneous pattern in a higher resolution. Supplementary data of percentages from organic matter (OMC) and carbonate content (CC) coincide mainly with that pattern. The subaqueous delta platform in front of the Bassac River mouth, shown by Transect 1 (Fig. 4), accommodates well sorted fine sands (mode ~2.85 Phi), low organic matter (< 1.74 wt (%)) and

carbonate content (< 0.66 wt (%)). With increasing water depths, OMC increases rapidly to more than 6.58 wt (%), and CC rises only slightly (< 1.67 wt (%)).

Transect 2 shows heterogeneous grain size features (Fig. 3C and 4), and is situated close to Gan Hao in Area 2. The shallow subaqueous delta platform consists predominately of very fine sand with low percentages of silt and clay. Fine silt prevails along the delta slope, where sand content decreases below 9.1 Vol (%), but sand predominates along the deeper delta slope, with sand content between 45-99 Vol (%). At the delta base, silt and clay content increase again, and the organic matter and carbonate concentration follow that trend, except near the delta base. A rapid increase of carbonate percentages (maximum = 6.97 wt (%)) indicates the transition to the open shelf, where shell fragments are common.

The southern area is shown by Transect 3 (Fig. 3C and 4), which crosses both channels in that area. The silty regions of the subaqueous delta platform and channel troughs have high percentages of organic matter (> 7.11 wt (%)), but the southern channel flanks correlate with decreased OM-content (< 5.08 wt (%)). The sand fraction dominates there with up to 90 Vol (%). Along the delta slope, silt prevails with increasing OM-content (Fig. 4). The highest carbonate content occurs with up to 16.2 wt (%) at the delta base, where shell fragments in the sediment fraction > 1 mm mark the transition to the open shelf.

Transect 4 extends along the delta front around Cape Ca Mau (Fig. 3), and silt and clay (content > 94 Vol (%)) dominate this area, including a high OM-content (Fig. 3C and 4). At the delta base, medium sand dominates, and the carbonate content increases up to 7.21 wt (%), due to the occurrence of the sediment fraction > 1 mm, where many concretions from palaeosoils, shell fragments and foraminifera occur.

Represented by Transect 5, the subaqueous delta in the Gulf of Thailand shows a pattern similar to Transect 4, with high organic matter content and predominant silt percentages. However, it exhibits a lower gradient of the delta slope. Samples likely did not reach the transition of prodelta and shelf because no coarser sediment was found in the surface samples. The comparison of the last sample of transect 5 (Fig. 2) with the location of the delta base confirms that assumption.

4.2.2 Sedimentary structures

X-radiograph negatives of the upper 20 centimetres from selected cores, which were taken along the transition of the subaqueous delta platform and slope (topset to foreset), reveal a

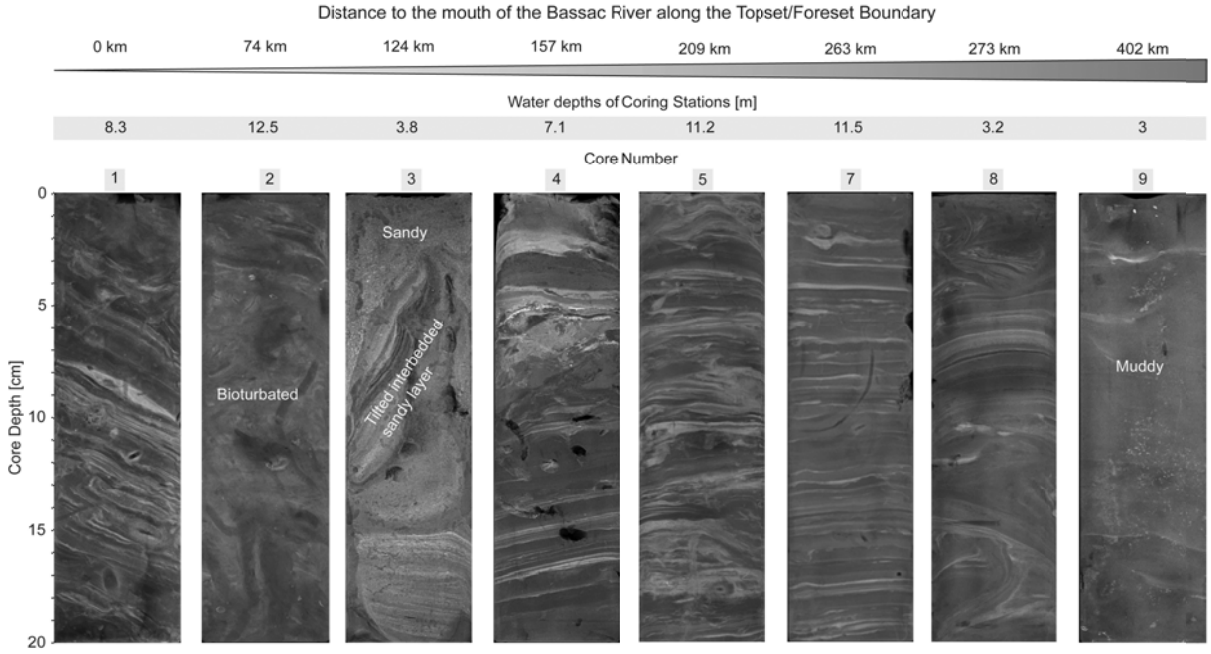

Fig. 5 X-radiograph negatives from the uppermost parts (20 cm) of eight sediment cores (see Fig. 1 for locations) aligned with increasing distance from the river mouth. The black parts in Core 4 are artefacts due to the sample preparation.

successive alternation of interbedded and interlaminated sands and silts (Fig. 5). Sand content is primarily decreasing with distance to the eastern main distributaries that coincide with the trend of surface sediment distribution. However, around the Gan Hao area (Fig. 1), sand dominates in the upper layers (Core 3 in Fig. 5), and X-radiograph negatives show anomalies in the sediment pattern (Core 4).

The most common sedimentary structure is lamination, which is observed in all the cores, although commonly it is disturbed. The common lamination shows changing conditions, which are probably caused due to tidal influence. Thin sandy (bright on the Fig. 5) and thicker silty laminae or layer mainly marks this lamination (darker on Fig. 5). They are horizontal (e.g. cores 5 and 7), wavy or inclined (core 1). The latter, reveals deformations and slight folding, possibly related to redeposition on the inclined sea floor. In cores dominated by mud, the thicker parts of sand laminae form loading structures, due to sinking of sand in unconsolidated mud (see for instance upper part of core 7). Some of the sandy laminae of wavy shape (e.g. core 7, Fig. 5) were likely formed as small ripple marks, and their shape is still preserved in places. Evident erosional surfaces are visible (e.g. cores 3, 4. 8), which suggest frequent redeposition of the sediments. In the core 3 are evident tilted laminations are evident (Fig. 5) which are not caused by coring, as shown in the lower horizontal layering in the core, but indicates redeposition of several centimetre in size intraclasts of sediments in form of mass movements along the delta slope. The complex sediment supply is shown by findings of shell fragments (e.g. core 4, depth 5 cm, Fig. 5), which are not representative of the delta sediment. However, it implies sediment

exchange with shelf sediment, for instance during storm surges. Although the location of core 2 is relatively close to the Bassac River mouth its X-radiographs negatives reveal features of bioturbation that indicates lower deposition. In contrast, even core 9, situated far away from areas of high sediment supply, consists of fine laminated silt and clay with little traces of bioturbation, which suggest relatively high accumulation rate.

4.2.3 Sediment accumulation rates

Estimations of sediment accumulation rates (SARs) based on measurements of ^{137}Cs and ^{210}Pb activity (Fig. 6) use three approaches (Table 1). The first approach assumes that sediments containing ^{137}Cs have to be deposited after the early 1950s when the first atmospheric nuclear weapon tests were done. The half-life of ^{210}Pb is 22.3 years, and no excess ^{210}Pb as a portion of the total ^{210}Pb resulting from atmospheric fallout, is expected to be detected in deposits older than a century. The second approach therefore uses the presence of excess ^{210}Pb as an indicator of sediments deposited within the last 100 years at maximum. The third approach is based on the constant initial concentration model presented in Chapter 3. All cores indicated very high SARs. The well preserved laminations revealed unsteady sedimentation, and the measured activities are often very low. The presented calculations must therefore be treated as minimum estimates of an order of magnitude.

Core 5 is composed of laminated sandy mud (Fig. 6). The ^{210}Pb activity profile reveals a steady decrease in the activities from a depth of 22 to 102 cm. Below, the ^{210}Pb activities are almost stable, but they are not reach the supported ^{210}Pb activities. The lower activity in the uppermost sample may be due to the dilution in the larger mass of temporary deposited sediments. Assuming supported ^{210}Pb activities of about 22.1 (Bq/kg), the SAR estimations reveal a rate of slightly above 4.0±2.1 cm/yr.

In Core 6, two sedimentary units are found (Fig. 6). The upper one comprises brown mud with high water content, below which there is a sharp unconformity at 200 cm core depth followed by an olive-grey and consolidated mud unit. In the lower unit, the ^{137}Cs activity is below the detection limit, and no excess ^{210}Pb activities were measured (the lower unit has higher supported ^{210}Pb activities than the upper). These sediments are at least older than 60 years. In the upper unit, the SAR is approximately 2.6±1.5 cm/yr, as calculated from the decrease in excess ^{210}Pb activities between 20 and 120 cm core depth. The upper 20 cm reveal relatively stable activities, at slightly lower rates than below, and it likely results from the

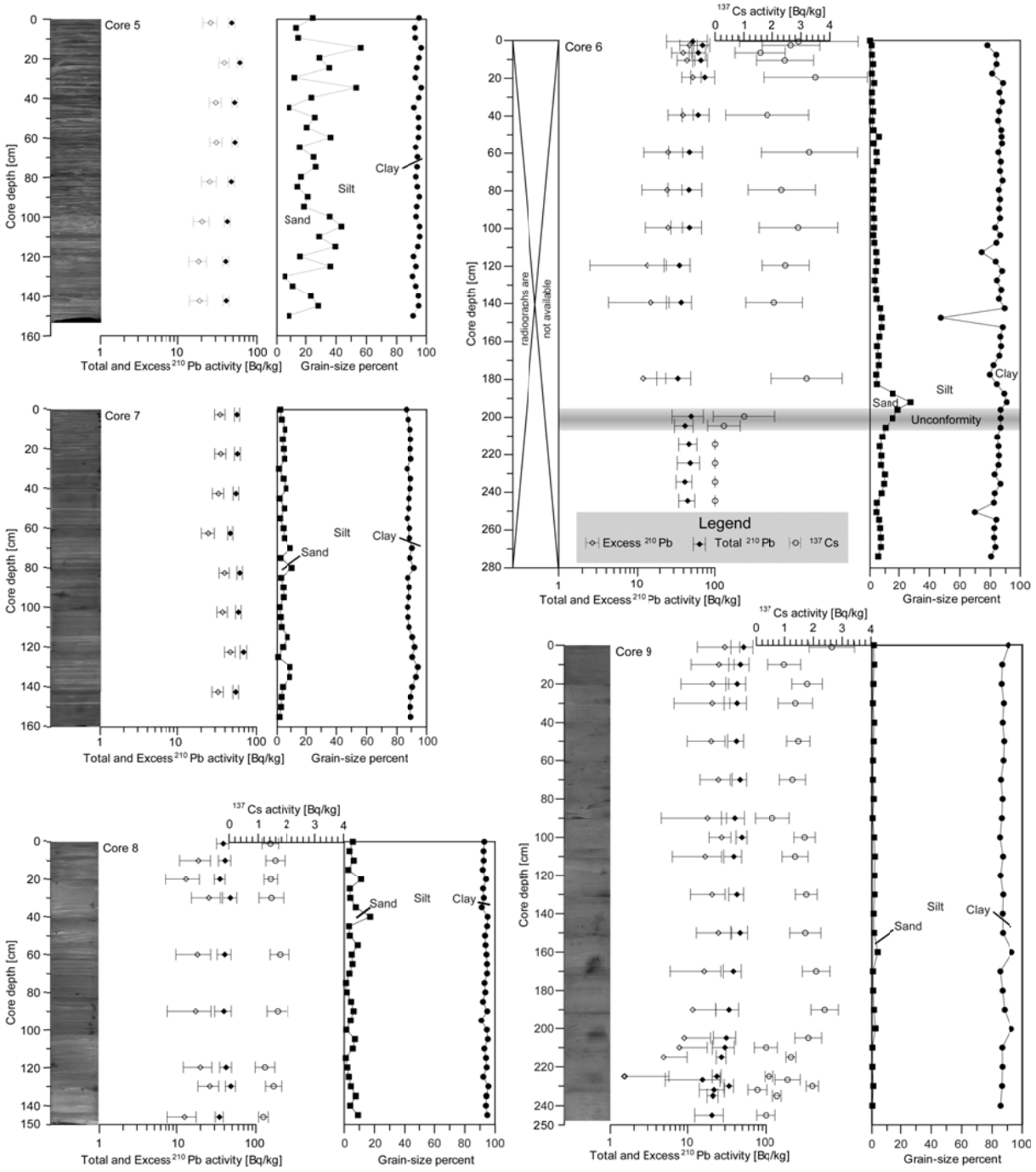

Fig. 6 X-radiographs, total and excess 210Pb activities, 137Cs activity and clay, silt and sand fraction percentages in the 5 cores (see Fig. 1 for locations). The 210Pb activities are presented in logarithmic scale with 2-σ error. Note, there is a clear unconformity at approximately 200 cm in Core 6 separating different sediment types.

dilution of temporarily deposited larger masses of sediment. The presence of ^{137}Cs in the complete upper unit suggests that the SAR could be even higher than 3.6 cm/yr.

The ^{210}Pb activity of Core 7 shows little changes. Applying supported ^{210}Pb activities from Core 6, the excess ^{210}Pb activities are found in the complete Core 7 and SAR amounts are at least 1.4 cm/yr. Very little or no change in the excess ^{210}Pb, typical for very high deposition

Table 1 Assessments of linear sediment accumulation rates (cm/yr) based on the 210Pb and 137Cs activity profiles (Fig. 6). Calculations are explained in the text.

Sediment Accumulation Rates [cm/yr]			
Core	Based on the Presence of ^{137}Cs	Based on the Presence of the Excess ^{210}Pb	Calculated from Decay of the Excess of ^{210}Pb
5	-	>1	4.0 ± 2.1
6	>3.6	>1	2.6 ± 1.5
7	-	>1.4	>10 ?
8	>2.5	>1.4	>10 ?
9	>3.9	>2.2	>10 ? (upper 1.5 m); 1.6 ± 0.4 (below 1.5 m)

rates and supported by the laminated sediments, suggests sediment accumulation at the rate in the order of ~10 cm/yr, or temporarily deposited during the last winter monsoon season.

Core 8 has a very similar ^{210}Pb activity profile and estimated SAR as Core 7 (Fig. 6; Table 1). The only difference is the lower average activity. However, the sedimentary differences between the cores may cause variations in supported activities, as exemplified by the upper and lower unit in Core 6, and the SAR may be so high that the excess ^{210}Pb is diluted by the large mass of deposited sediments. The presence of ^{137}Cs throughout the core supports the very high SAR and suggests that the SAR is at least 2.5 cm/yr.

The ^{210}Pb activity profile in Core 9 is generally characterised by three parts: the uppermost 150 cm of near-uniform activities, the zone of decreasing activities down to about 225 cm and the relatively stable (supported) activities underneath these zones. The supported activities are much smaller than in the previous cores. The uppermost part has to be deposited in a very short period at a rate of more than 10 cm/yr and likely reflects the temporary (seasonal) deposition or recent rapid increase in the SAR. The calculations based on the decay of excess ^{210}Pb between 150 and 215 cm revealed a SAR of about 1.6±0.4 cm/yr, and the presence of ^{137}Cs in the upper 230 cm of the sediment core suggested a SAR of at least 3.9 cm/yr.

5 Discussion

Modern delta morphology and sediment dynamics are shaped mainly by waves, tides and river impact, factors that also serve as the basis for delta classification schemes he following discussion focuses on the interpretation of sedimentary processes and controlling factors in different delta regions.

5.1 Subaqueous delta division and sedimentation pattern

The results of our investigations lead to the division of the subaqueous Mekong Delta into 5 areas, instead of 4 as proposed by Xue et al., (2010). It is based on the delta morphology, sediment types and their location relative to the Bassac River, a main distributary (Table 2). Two conspicuous regions exhibit broad topsets and steep foresets and are probably the areas of

Table 2 Summary of hydrodynamic factors, morphological features, sedimentary properties as well as sediment accumulation rates (SAR) of the subaqueous Mekong delta subareas.

Delta Regions (Fig. 2)	Tides	Waves (relative impact)		River Influence		Delta Shape	Sediment			Sedimentary Structures	SAR
Area	Amplitude in [m]	Summer	Winter	Summer	Winter		Grain Size	OM [%]	CC [%]		[cm y-1]
1	2.5 – 3.8 (semi-diurnal)	low	high	high	moderate	wide topset (> 12 km) ; steep foreset (< 0.2°)	silty sand to sandy silt	1.5 – 6.8	0.5 – 1.7	laminated sand and silt, crossbedding	unknown
2	2.5 – 3.8 (semi-diurnal)	low	high	low	low	narrow topset (< 3.5 km); gentle and wavy shaped foreset (< 0.12°)	sandy silt, sand (local)	2.4-8	0.7 – 7	laminated sand and mud; partly bioturbated	unknown
3	2.5 – 3.8 (semi-diurnal)	moderate	moderate	low	low	wide topset (> 15 km) including two channels; steep foreset (< 0.4°)	sandy silt, sand (local)	4 – 10.2	1.4 – 16.2	laminated sand and mud	> 1
4	1 – 2.5 (mixed-tide)	moderate	low	low	low	wide (> 10 km) and very shallow topset; steep foreset (< 0.43 °)	sandy silt to silt	8.3 -10.8	2.2 – 7.2	laminated mud	>1; seasonal deposition rate >10
5	0.5 - 1 (diurnal)	moderate	low	low	low	narrow (< 2 km) topset; gentle foreset (<0.1°)	silt	8.4 – 9.6	2.1 – 3.7	homogeneous mud; partly laminated	>1; seasonal deposition rate >10

the fastest delta progradation (Fig. 2, Table 2). The delta progradation takes place in two different directions (southeast and west) and in parts of the delta approximately 200 km apart: next to the river mouth and around the Ca Mau Peninsula tip (Subareas 1 and 4). These areas were already identified previously (Gagliano and McIntire, 1968; Xue et al., 2010). Our results show that the two areas differ significantly in sediment type. Fine sand dominates near the Bassac River mouth and silt and clay near Cam Mau Cape (Fig. 3C and 4). Additionally, our data set provide new information about heterogeneous sedimentary pattern due to the variable contribution of riverine and oceanographic factors (Fang et al., 1999; Nguyen et al., 2000; Zu et al., 2008).

Pronounced by narrow topsets and atypical well sorted sand along gentle, wavy foresets (Fig. 2 and 3C), Area 2 indicates in X-radiograph negatives either bioturbated laminated sand and silt or sandy beds and tilted layers (Cores 2 and 3 in Fig. 5). This area is interpreted as dominated by redeposition processes and sediment bypassing, particularly during the winter monsoon. Additionally, it is probably the area with the lowest sediment accumulation rate in the

subaqueous Mekong delta. This region is also a transition between two regions of a spacious subaqueous delta platform.

Broad topsets with two channels and steep foresets prevail in Area 3 (Fig. 2). This part of the subaqueous Mekong delta is characterised by a high sediment accumulation rate as proved by common horizontal lamination of the sediments (Fig. 5) as well as estimated accumulation rate of >1 cm/yr (core 5, Table 1). The sediments are generally finer than in the Area 2. However, their distribution is partly governed by sand deposits on the ridges between the channels and on their flanks while mud occurs in the channel troughs (transect 3, Fig. 4). The genesis and formation processes of the channels are not clear. However, tidal ellipses and resulting tidal currents run shore parallel in that region (Zu et al., 2008). In combination with strong wind-induced shore parallel currents during the winter monsoon season it can leads to higher shear stress near the seabed and increasing erosional condition. Seismic profiles provided by Xue et al. (2010) show erosional pattern in the channel region.

Both areas serve, however, as sedimentary conveyors between Areas 1 and 4. The latter is dominated by the combination of high sediment delivery (SARs > 1.4-10 cm/yr (Table 1, Fig. 6)) due to alongshore currents in that region and prevailing low hydrodynamic forces that provide sediment to this depocenter distant from a main river mouth like the Bassac. The presence of predominantly sandy silt and silt also gives the evidence of a low energetic environment supported by laminations with no bioturbation traces (core 7 and 8, Fig. 5).

Similar sedimentation conditions were found for the most distal region (Area 5) indicated also by very high sediment accumulation rates (>10 cm/yr, Table 1) and finer deposits (about 90% of silt and clay) with no bioturbation traces in X-radiograph negatives (core 9, Fig. 5). However, this region is far from another sediment source and no strong alongshore currents occur that can explain the high sediment accumulation rates.

Borehole data in the lower delta plain indicate facies changes around 3000 cal yr BP (Ta et al., 2002a) due to a shift from “tide-dominated” to “wave and tide-dominated” influences. In contrast, the nine short cores along the transect of more than 400 km in the subaqueous Mekong Delta (Fig. 5) show recent lateral alongshore facies changes (Fig. 3C, 4 and 5) under the varying influence of tidal amplitudes, annual alongshore currents and wave impact (Nguyen et al., 2000, Tamura et al., 2010; Xue et al., 2012a). However, all facies changes occur in the Mekong River Delta. This example should call attention to the

difficulty to interpret sediment facies of a Mega-Delta with many local differences in hydrodynamic conditions at the same time.

5.2 Controlling factors

The monsoon climate controls the sedimentation pattern off the Mekong River mouth and affects the sediment and freshwater discharge and the directions of their distribution (Xue et al., 2011). High precipitation during the summer monsoon season leads to flooding events and irregular water discharge. Moreover, the river outflow has water velocities up to 1 m/s (Wolanski et al., 1996), increasing channel and riverbank erosion (Le et al., 2007). Sediment is transported into the sea and temporarily deposited on tidal flats in nearby river mouth areas. Under summer monsoon conditions, the suspended sediment is also transported in the north-eastern direction due to south-easterly winds and the resulting surface currents.

As proven by the previous studies, sand and relict sand areas cover the adjacent continental shelf that otherwise lacks sediment (Anikiev et al., 2004; Jagodziński, 2005; Schimanski and Stattegger, 2005; Kubicki, 2008). The cluster analysis reveals differences in the delta (Clusters 1 and 2) and the shelf sediments (Cluster 3) concerning its spatial grain size distribution (Fig. 3A and 3B). Consisting of shell fragments, foraminifera and concretions from late Pleistocene soils, Cluster 3 reflects the presence of the sediment fraction > 1 mm that occurs on the shelf area, except along the foresets in the Gan Hao region (Fig. 3C). This fraction increases the carbonate content in surface samples close to the delta base and serves as a good proxy for the delta-shelf transition. Similar sedimentary features in bottomsets are described for the clinoform in the Gulf of Papua (Walsh et al., 2004) and the Atchafalaya Shelf (Neill and Allison, 2005).

Composed mostly of silt and clay, the suspended sediment may be temporarily deposited on the inner shelf and delivered by a suspension plume (Wolanski et al., 1996). The East Asian winter monsoon may cause reworking by wind-induced currents and sediment transport towards the southwest. The mechanism of temporal deposition of the fine-grained sediments on the inner shelf during the high sediment discharge season and the subsequent redeposition to the final depocenter that is usually located farther offshore in the mid-shelf mud belts and clinoforms is commonly reported from various settings (McKee et al., 1983; Crockett and Nittrouer, 2004; Nittrouer et al., 2009; Szczuciński et al., 2009; Walsh and Nittrouer, 2009). However, in the shelf region offshore the Mekong Delta branches prevail sandy sediment (Anikiev et al., 2004; Kubicki, 2008). Cluster 3 with its dominant mode in medium sand occurs close to the delta base and correlates with the shelf sediment (Fig. 3A). Furthermore, shell fragments and residuals of

lateritic palaeosoils distributed in junction to the shelf imply reworking of old sediment in that region and less sedimentation. It leads to the hypothesis that most of the Mekong sediment delivered into the subaqueous Delta is also finally deposited there. Xue et al. (2010) support this hypothesis with its estimation of the sediment capture from the subaerial and subaqueous Mekong Delta that is 80±18% of the annual sediment discharge, at least over the last 3000 years. Hence, the sediment transport to the outer shelf is limited. Tidal regime changes are considered to be the major factor controlling the delta development. The tides alternate from semi-diurnal over mixed to diurnal tides between the eastern Mekong River branches and the south-western Cape Ca Mau and adjacent Gulf of Thailand (Wolanski et al., 1996; Nguyen et al., 2000, Le et al., 2007). Moreover, the tidal range decreases from northeast to southwest. Small cotidal amplitudes of predominant tidal constituent were provided in the Gulf of Thailand and around Cape Ca Mau, yielding a decrease in the number of floods and ebbs per day and in the tidal current velocities (Fang et al., 1999, Zu et al., 2008). Such conditions privilege fine sediment deposition and are favourable for delta aggradation and progradation. In addition, the development of very shallow subaquatic delta topsets reduces wave impact over the shallow water area and the coast around Cape Ca Mau. In combination with the high sediment accumulation rates of 1.4 up to 10 cm/yr (Table 1) these factors support a fast accretion of the south-western Mekong Delta into the Gulf of Thailand.

5.3 The subaqueous Mekong Delta in classification schemes

Attempting to classify the character of the subaqueous Mekong Delta reveals its complexity. For instance, Walsh and Nittrouer (2009) suggested a hierarchical decision tree to predict the marine dispersal system at a river mouth using basic oceanographic and morphological characteristics, classifying the Mekong dispersal system as a "subaqueous delta clinoform," as in the case of the Amazon or Fly River. Accounting for the depocenter around Cape Ca Mau allows its classification as a "marine dispersal dominated" regime due to the distance to the next main distributary (more than 200 km) and low tidal range (Table 2).

Classifying the Mekong Delta using typical triangle classification scheme after Galloway (1975) with wave, tide and river dominated end members is even more difficult. Lobe switching relocate the main depocenter like in the case of the Yellow River (Wright et al., 1990, Saito et al., 2001). This may lead to different hydrodynamic condition and changes in the sediment delivery into the coastal ocean can occur. According to the predominant hydrodynamic factor, the deltaic lobe will deposit as river-, tide- or wave-dominated. For example, in the Danube delta the most northern Chilia branch with the highest discharge deposit recently as a river-dominated

lobe whereas the southerly Sf. Gheorghe arm build a wave-dominated lobe due to its stronger wave-exposed region (Bhattacharya and Giosan, 2003).

Similarities without consideration for temporal but spatial variation occur in the Mekong River delta between wave- and tide-dominated regions and between regions of different tidal amplitudes (Table 2). In consideration of seasonal variation (monsoon seasons) of prevailing hydrodynamic factors along a coastline of more than 400 km, the triangle classification scheme cannot be applied for the whole Mega-Delta like the Mekong River delta, but for spatial limited region.

6 Conclusion

The data presented in this paper shows that the subaqueous parts of a large delta are quite complex, especially regarding variations in morphological and sedimentary characteristics (Fig. 2 and 5, Table 2) and can be classified in different scales. Five regions, differed by their shape and sediments, of the studied subaqueous Mekong delta vary greatly in its sediment accumulation rates between 1 and >10 cm/yr (Table 1). The sedimentary patterns also changes within one area depended on their hydro- and morphodynamical regime (Fig. 3C, 4 and 5).

Nittrouer et al. (1984) described differences of the fine scale stratigraphy for the Changjiang (Yangtze) and the Huang He (Yellow) dispersal system based on the ratio of the mixing rate to accumulation rate due to the distance to the next major river mouth. As a result, the proximal deposits of the Yangtze River are physical stratified muds by a high accumulation rate while the distal deposits of the Huang He consist of homogenous mud due to the higher mixing rate and lower accumulation rate. In the Mekong River dispersal system occur physical stratified deposits proximal to the major river mouth of the Bassac (Fig. 5). However, in the distal region (nearly 200 km apart) around Ca Mau cape there are also physical stratified layers (Fig. 5) showing very high accumulation rates of at least 2.6 cm/yr (Table 1) and the area progrades with 24 m/yr (Xue et al., 2010) into the Gulf of Thailand. In between, there occur strong bioturbated sediments (core 2 in Fig. 5) as well as moderate sorted sandy deposits (Fig. 3C, 4 and core 3 in Fig. 5). It implies that in this transition region the ratio of mixing rate to accumulation rate must be changed. The most southerly region (Area 3) belongs to this transition region and has a wide spreaded subaqueous clinoform, physical stratified layers along the delta slope and high accumulation rates of 4 cm/yr (Table 1). However, there is also a shore parallel channel system of more than 120 km (Fig. 2). The channel troughs show erosional signatures (Xue et al., 2010) and represent silty sediments while the channel flanks consisting of well sorted fine sand

(transect 3, Fig. 4). We hypothesize, the difference of both is that the region in front of the Bassac River obtains its sediments directly from the major Mekong branches while the Ca Mau cape region receive either reworked deposits from the easterly lying subaqueous Mekong delta or also from the fluvial system as suspended sediment. Tamura et al. (2010) described mud and fine sand seasonal deposits in the tidal flats close to one of the major river mouth, which are reworked during the winter monsoon season due to wave impact and may transported to the southwest of Cape Ca Mau.

The cluster analysis of surface samples indicates two end members for the subaqueous delta and one for the delta shelf transition (Fig. 3A). In addition, the sediment class bigger than 1 mm including shell fragments and residuals of lateritic soils occurs only on the shelf and in a special region of area 2 (Fig. 3C). Vietnamese shelf sediments in front of the major rivers consist mainly of sand (Anikiev et al., 2004; Kubicki, 2008). It indicates a limited sedimentary exchange between the subaqueous delta and the shelf, and that most of the river delivered sediment is trapped in the subaerial and subaqueous Mekong delta.

The trial to classify a Mega–delta in the ternary river-wave-tide forcing system (after Galloway, 1975) occurs with difficulties due to the spatial changes of the hydrodynamic factors along a coast of more than 400 km. Each of our separated areas (Fig. 2) is influenced by different major hydrodynamic factors dependent on the season.

Human impacts accelerate coastal erosion together with relative sea level rise and delta subsidence, neither of which is reported in recent studies of the subaqueous Mekong Delta. Future investigations will therefore benefit from our results.

7 Acknowledgements

The work was supported by a research grant from the German Research Foundation (DFG_STA401/) and through scientific cooperation with the Vietnamese Academy of Science and Technology (VAST) and the Ministry of Science and Technology (MOST), Vietnam. Partners from the Institute of Resources Geography (VAST) in Ho Chi Minh City (Vietnam) provided significant help. Additionally, the authors thank the staff of the Leibniz-Laboratory at the Christian-Albrechts-University in Kiel and of the International Atomic Energy Agency in Monaco for their measurements of ^{210}Pb. The laboratory staffs at the Institute of Geography of Christian-Albrechts-University of Kiel (Germany) are acknowledged for access to the Malvern Particle Analyzer for grain size measurement and the Radiology Department (Prüner Gang) in

Kiel for measuring the X-radiographs. We thank two anonymous reviewers for constructive and critical comments.

Chapter IV

Suspended sediment dynamics during the inter-monsoon season in the subaqueous Mekong Delta and adjacent shelf, Southern Vietnam

Daniel Unverricht[1*], Thanh Cong Nguyen[1], Christoph Heinrich[1], Witold Szczuciński[2], Niko Lahajnar[3], Karl Stattegger[1]

[1] *Institute of Geosciences – Department of Sedimentology, Christian-Albrechts-University of Kiel, Germany*

[2] *Institute of Geology, Adam Mickiewicz University, Poznań, Poland*

[3] *Institute for Biogeochemistry and Marine Chemistry, University of Hamburg, Germany*

Published in the Journal of Asian Earth Sciences, reprinted with permission from the publisher Elsevier

Abstract

Land-ocean interactions in the coastal zone are severely influenced by tidal processes. In regions of high sediment discharge like the Mekong River Delta in southern Vietnam, these processes are even more significant. Three cruises in 2006, 2007 and 2008 were carried out to investigate the sediment suspension and their spatial distribution. Additionally, we investigated the influence of the tidal currents in relation to the suspended sediment. Therefore, all cruises took place during the inter-monsoon season between March and May where wave and wind influences are not dominant in contrast to the summer monsoon (May to early October) and winter monsoon season (November to early March).

Suspended sediment concentrations (SSCs) in the particle-size range between 2.5 and 500 μm were measured with an LISST-instrument (Laser In Situ Scattering and Transmissiometry). Current velocities and directions were recorded with an Acoustic Doppler Current Profiler (ADCP). Additionally, data of different tidal gauge stations in the Mekong River Delta were correlated and compared to the mixed semidiurnal-diurnal tidal cycle.

Our results show significant areas of SSCs greater than 25 µl/l in the Mekong River branches and its subaqueous delta during the inter-monsoon season. 20 % of all measured SSCs in the subaqueous Mekong Delta exceed 100 µl/l. Highest concentrations occur close to the seabed. SSCs decrease at the transition to the open shelf. The shelf region contains only low suspension loads, especially on the south-eastern shelf (99 % of all samples < 25 µl/l). However, in the southern shelf region around Ca Mau Cape the suspension load is also higher (> 25 µl/l) close to the seabed in water depths of 20 to 25 m.

Two surveys lasting 25 hours each were performed on mooring stations in 12 m (Mooring 1) and 26 m (Mooring 2) water depth and located 3.2 km apart on the subaqueous delta slope.

Similar patterns of SSC over time show that concentrations of suspension load correlate with the tidal current velocities. High tidal current velocities of up to 0.6 m/s near the sea bottom generate increasing SSCs of more than 25µl/l in the water column. Additionally a significant trend of decreasing SSC from the near-seabed to the upper part of the water column can be observed. In terms of sediment transport the ebb phase dominates the tidal cycle by its higher tidal current velocities but the flood phase has the longer duration. The switch of the tidal current direction from ebb to flood phase occurs rapidly against which the change from flood to ebb phase requires up to 3 hours. This leads to an asymmetry of the tidal ellipses and may cause a net-sediment transport from the shelf into the subaqueous Mekong delta.

In the subaqueous Mekong Delta and adjacent shelf, seven transects show similar patterns of SSCs dependent to the tidal phase. A hypopycnal sediment plume from the subaqueous Mekong Delta into the shelf region was not observed. Our results imply that resuspension by tidal currents dominates the sediment transport in the subaqueous Mekong Delta and adjacent shelf regions during the inter-monsoon season.

1 Introduction

Sediment delivery via rivers into the global oceans is one of the most important impacts in land-ocean interaction. The Sediment transport from the distributaries to the inner shelf passes many different stages (Wright and Nittrouer, 1995). In dependence on the prevailing environmental processes like waves, tides and wind induced currents the sediment will be net-transported in cross- or alongshore direction until its final deposition (Orton and Reading, 1993; Walsh and Nittrouer, 2009).

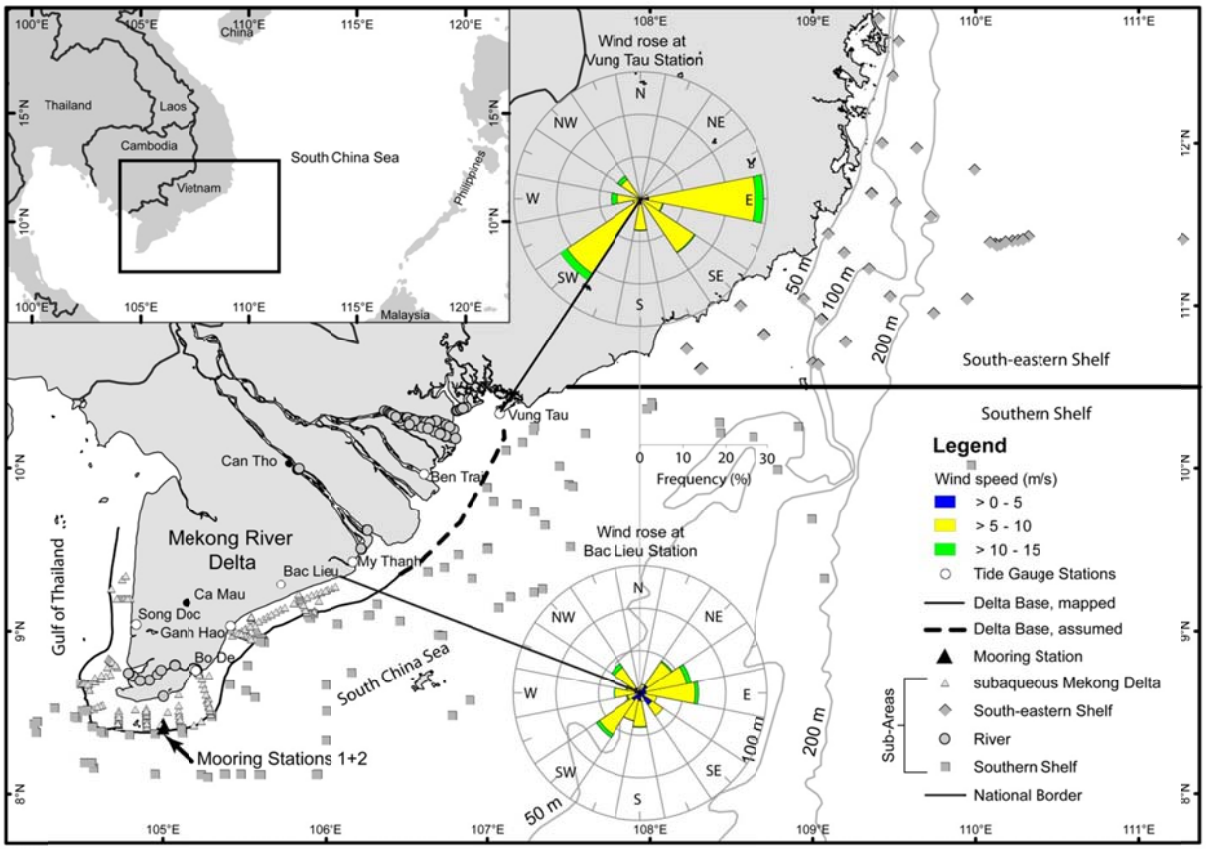

Fig. 1 Investigation area with positions of all LISST-stations within four sub-areas, moorings, and tide-gauge stations between 2006 and 2008. In addition, wind charts of the meteorological Station in Vung Tau and Bac Lieu include a data set of the daily mean from 1999 to 2008.

Asian Mega-Deltas show similar alongshore ranging clinoforms (Liu et al. 2009). The sediment discharge, transport and deposition in these deltas are strongly influenced by the monsoon seasons (Wright et al., 1990; van Maren and Hoekstra, 2004). The sedimentation in the subaqueous Mekong delta is also linked to wave impact and wind induced currents driven by the monsoon climate (Tamura et al. 2010). The Sediment pattern associated with the subaqueous delta morphology illustrates, that there are processes with regional dependency (Unverricht et al., 2013). However, many other factors influence sedimentation processes and shaping of subaqueous deltas (Vörösmarty et al., 2003, Syvitski and Saito, 2007).

Our cruises were carried out during the inter-monsoon season from March to May, where the monsoonal forces are low with less wind and wave activity. This situation gives an advantageous precondition to investigate possible influencing factors without monsoonal impact like tides. Tidal ranges of more than 3 m in the Mekong Delta region of the South China Sea affect the sediment transport and deposition due to its currents inside and outside the Mekong distributaries. Tidal induced sediment distributions can be observed also in other Asian Deltas like the Yellow and Yangtze River delta (Wright et al., 1990; Zhen Xia et al., 1998; Shi, 2010).

This article shows the spatial suspended sediment distribution during the inter-monsoon season in the subaqueous Mekong delta and its adjacent shelf. In addition, our investigations improve the understanding of tidal influences concerning sediment transport and deposition in the subaqueous delta region.

2 Study Area

The headwaters of the Mekong River are situated in the Tibetan Plateau. The river crosses six countries until it flows via 8 distributaries into the southern South China Sea. The delta plain covers an area of 49 500 km² between Phnom Penh in the Cambodian lowlands and the southeast Vietnamese coast (Le et al., 2007).

The complex character of the tidal regime is dominated by the M2- and K1-tidal-constituents which extend from northeast to southwest in the South China Sea (Fang et al., 1999; Zu et al., 2008). A pronounced meso-tidal regime prevails in the South China Sea, while in the Gulf of Thailand a micro-tidal system occurs. In the South China Sea it leads to tidal ranges of 2.5-3.8 m in a semi-diurnal to mixed-tidal system (Nguyen et al., 2000). However, the Gulf of Thailand has diurnal tides with tidal ranges between 0.5 and 1.0 m. Tidal ellipses of the dominant tidal constituents with its according currents extend in the subaqueous Mekong delta mainly in a shore-parallel direction (Hung and Dien, 2006, Zu et al., 2008).

The East Asian Monsoon causes strong seasonal climatic variations in the Mekong Delta (Hordoir et al., 2006; Mitsuguchi et al., 2008; Xue et al., 2011). In the winter monsoon season from November to early March winds are coming mainly from north-eastern direction and during the summer monsoon south-western winds prevail (Fig. 1). Annual wind speed recorded from 1999 to 2008 (Fig. 1) by the Southern Regional Hydro-Meteorological Centre (SRHMC,

Vietnam) ranges at Vung Tau station from 7 to 9 m/s and in Bac Lieu from 6 to 8 m/s (1st and 3rd quartile). Under stormy condition wind speeds can reach 20-30 m/s (Institute of Strategy and Policy on natural resources and environment (ISPONRE) 2009). The maximum wind stress prevails along the south-eastern coast of Vietnam in both monsoon seasons.

The wave climate differs significantly between the annual seasons and the Mekong delta subareas. In the river mouth region significant wave heights of more than 1 m can occur at the coastline in the whole year (Tamura et al., 2010). In Vin Tan (close to Bac Lieu), southwest of the Bassac distributary (Fig. 1) significant wave heights of 0.2-0.25 m (measured during 3.-5.10.2012) and up to 0.55 m (measured during 21.-28.01.2011) m respectively were measured 300 m far from the shoreline (Albers et al., 2011).

During the inter-monsoon season significant wave heights of 0.6 m are measured at the southern Mekong delta shoreline near the Bo De estuary (Nguyen, 2012; unpublished PhD-thesis).

The water discharge of the Mekong River varies significantly with the particularly monsoon season. Between May and October (wet season) occur 85% (475 billion m^3) of the annual water discharge while only 15% (78.8 billion m^3) are discharged in the dry season (November to April) (Snidvongs and Teng, 2006; Le et al., 2007).

The water current system is also attributed to the East Asian Monsoon (Wendong et al., 1998). During the winter-monsoon season the western coastal currents has a south-western and during the summer monsoon season a north-eastern direction.

Sediments of the subaqueous Mekong Delta consist of well sorted fine sand in the Bassac River mouth area and show a trend to fine silt along the distal delta slope(Unverricht et al., 2013). At the transition between the Bassac and Ca Mau Cape area the sediments start to become finer along a south-westward gradient. However, at distinct spots well sorted fine sand occurs along the delta slope (e.g., near Gan Hao) and also in the southern region at the southern flanks of two subaqueous erosional channels (Fig. 6 Section C and D)(Unverricht et al., 2013). Around Ca Mau Cape and in the Gulf of Thailand well sorted fine silt dominates the subaqueous Mekong delta.

3 Material and Methods

Data on the suspended sediment concentration (SSC) in the water column were collected on three cruises during the inter-monsoon season (March to May) in 2006, 2007 and 2008, along four different sub-areas: south-eastern and southern Vietnamese shelf, subaqueous Mekong delta and Mekong river branches (Fig. 1). Investigations on the shelf were mainly carried out in 2006 (13.04.2006 to 09.05.2006) while the waters of the subaqueous delta and the river branches were sampled during the campaigns in 2007 (08.03.2007 to 02.04.2007) and 2008 (22.03.2008 to 24.04.2008). All together SSCs were measured in 747 vertical profiles to document spatial and temporal (mooring stations) variations (Fig. 1).

The SSC was measured with a Laser In Situ Scattering and Transmissiometry (LISST, Sequoia Scientific, Inc.). The LISST 100X type C, operating with the laser diffraction technique, detects the volume particle concentration (VPC, in µl/l) of 32 size classes between 2.5 and 500 µm. Agrawal and Pottsmith (2000) introduce the principal of operation of the LISST instrument together with some examples of application.

Mikkelsen and Pejrup (2001) suggest the LISST as a suitable tool for investigating the spatial suspended sediment distribution and give first results of field data. In further studies the authors also point out some limitations of application (Mikkelsen and Pejrup, 2000, 2001; Mikkelsen, 2002a, 2002b; Mikkelsen et al., 2005).

The suspended load is measured by the LISST instrument as volume particle concentration (VPC). In this article the term volume particle concentration (VPC) is equate with the term of suspended sediment concentration (SSC).

The LISST was mounted at a winch wire and lowered slowly through the water column down to the seabed with a mean winch speed of 0.25 m/s. With a sampling interval of 2 seconds two measurements per meter water depth were achieved.

A better vertical subdivision of SSCs over the entire water column can be reached by using a depth ratio (D_{ratio}) of the “Sample Depth” and the “Bottom Depth” of a LISST- depth profile.

$$D_{ratio} = \frac{\text{Sample Depth}}{\text{Bottom Depth}}$$

If the value is smaller than 0.5 the samples originate from the upper water column and vice versa.

The LISST-data are presented as isosurface maps (Fig. 2) and profile sections (Fig. 6), which were prepared with the Ocean Data View software (Schlitzer, 2011), using the DIVA-gridding-algorithm. Additionally, data of different tidal gauge stations in the Mekong River Delta (Fig. 1) were used to compare the results from the LISST-measurements with the tidal induced hydrodynamics. The zero water-level is referred to the Vietnamese national tidal datum in Hon Dau, northern Vietnam. It is the national reference datum not correlated to the mean sea level of the data base provided by the Permanent Service for Mean Sea level (PSMSL).

Two surveys lasting 25 hours each were performed on mooring stations in 12 m (mooring 1) and 26 m (mooring 2) water depth and located 3.2 km apart on the subaqueous delta slope (Fig. 1). During the moorings, LISST-profile was measured every hour and water velocity and direction were recorded continuously by an Acoustic Doppler Current Profiler (RDI Broadband ADCP at 1200 kHz). The ADCP measures the current velocity (in m/s) and direction (in °Mag) in the entire water column, except the upper 1.5 m due to the physical length of the ADCP and the blanking range and the near bottom layer (1 m above the sea bed).

4 Results

4.1 Spatial Distribution of the Suspended Sediment

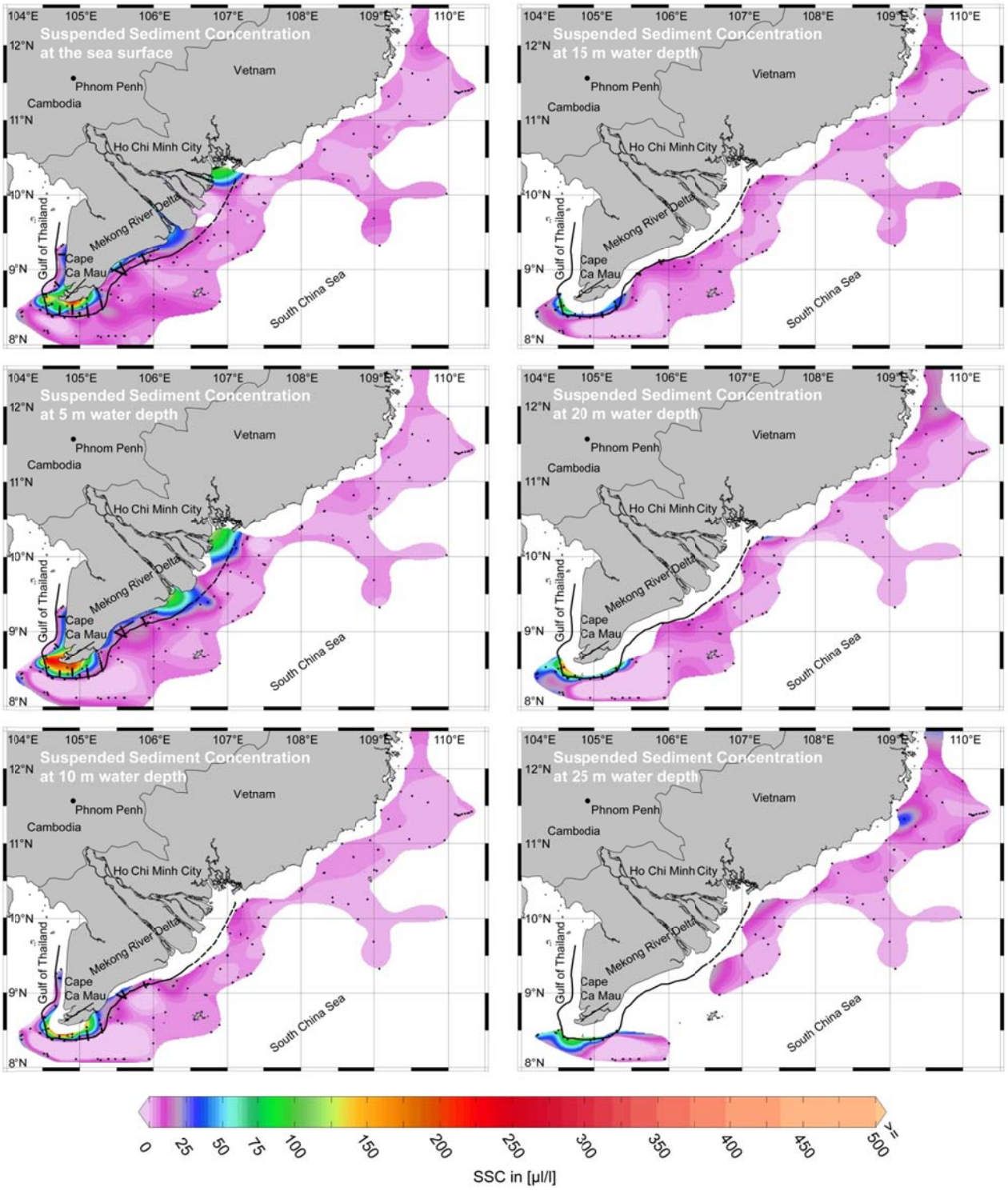

Fig. 2 Spatial distribution of suspended sediment concentrations ranging from the sea surface to 25 m water depth (5m intervals).

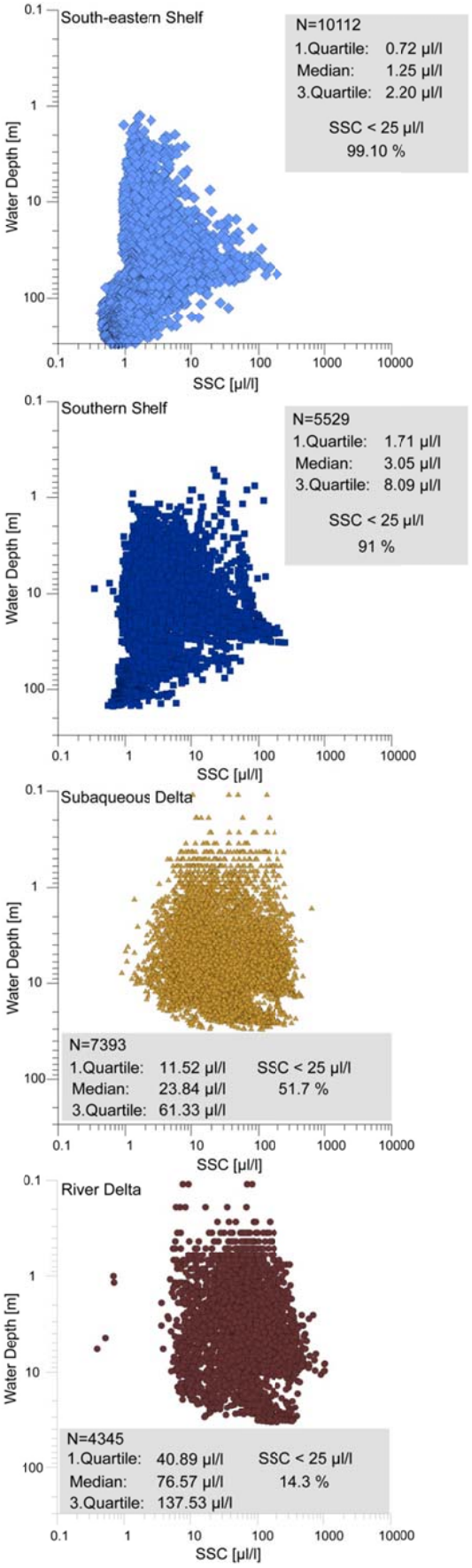

Apparently, the higher SSCs prevail within the subaqueous Mekong Delta and its river branches (Figs. 2) including a clear tendency with decreasing SSCs from the river branches into the subaqueous Mekong delta (Fig. 3). In the area of the subaqueous Mekong Delta the SSCs vary between 11 µl/l and 61 µl/l (1st and 3rd quartile) with a median of the SSC at 23 µl/l (Fig. 3). Higher SSCs of more than 100 µl/l amount 20 % and 65 % of them are less than 5 m above the sea bed (Fig. 2).

The isosurface map (Fig. 2) at the sea surface shows concentrations greater than 100 µl/l of suspended sediment around the river branches and close to the coast (Fig. 2). In the transition of the Bassac river branches and Cape Ca Mau just a thin band of increased SSCs extend in proximity to the coastline. In contrast, increased SSCs greater 100 µl/l are observed in the whole subaqueous delta region around Ca Mau Cape (Fig. 2).

The isosurface maps at 20 and 25 m water depth (Fig. 2) show suspended sediment concentration higher 25 µl/l around Ca Mau Peninsula both in the subaqueous Mekong delta and the adjacent shelf. The SSCs increase up to 257 µl/l in the transitional regions between shelf and subaqueous Mekong delta area (Fig. 2).

Fig. 3 Distribution of suspended sediment concentrations over water depth for each of the four sub-areas in Fig. 1. with descriptive statistics and number of LISST measurements (N).

The south-eastern and southern Vietnamese shelves show significantly lower SSCs in comparison to the rivers and the subaqueous Mekong Delta (Figs. 2 and 3). From the south-eastern and southern shelf only 4 % of all samples exceed 25 µl/l of SSC (Fig. 3). In both areas a gradient in SSC with the increasing water depth until 30 m can be seen (Fig. 3). In the shelf regions 86 % of the SSCs higher 25 µl/l occur mostly in water depth greater than 10 m. The south-eastern shelf shows the lowest particle concentrations of all investigated regions. Here, 99 % of all measured SSCs are lower than 25 µl/l followed by the southern shelf with nearly 91 % (Fig. 3). 67 % of the stations showing higher SSCs in the southern shelf are predominantly closer than 10 km to the subaqueous Mekong delta.

4.2 Hydro- and sediment dynamics during tidal cycles

The LISST-measurements at the two mooring stations reveal similar distribution pattern of SSCs in the water column and over time. At both stations the lower water layers ($D_{ratio} \geq 0.5$) have higher median values (Table 1). However, Mooring 2 has a 1.7 times higher SSC than Mooring 1 (Table 1). Obviously the SSCs are not uniformly distributed in the water column over time. Their increase is coupled with tidal current velocity, e.g. between 5 am and 10 am the suspension loads rise up into the upper water column (Fig. 4a, 4b, 4d).

Table 1 Descriptive statistics of the suspended sediment concentration is shown for both mooring stations over 25 hours. The water column is subdivided into two domains after the D_{ratio} (see methods). D_{ratio}- values smaller than 0.5 belong to the upper; water column and vice versa.

	Suspended Particle Concentration in [µl/l] over the entire water column			
	Mooring 1 (12 m water depth)		Mooring 2 (26 m water depth)	
	$D_{ratio} < 0.5$	$D_{ratio} > 0.5$	$D_{ratio} < 0.5$	$D_{ratio} > 0.5$
Mean	25	55	36	96
Median	22	41	31	69
1st Quartile	18	24	23	47
3rd Quartile	30	68	43	116

and flow directions over depth and time. The ebb phase at mooring 2 has the highest tidal current velocities at the bottom with more than 0.6 m/s (Fig. 4 d, 4e). Nevertheless, at mooring 1 high tidal velocity of up to 0.5 m/s are reached (Fig. 4 d, 4e). Water-level variations and tidal-current directions are not in phase (Fig. 4b, 4c). Apparently at mooring 1 the transition from flood current direction (western direction) to the ebb current direction (eastern direction) near the sea bed needs approximately 3 hours (Fig. 4c) from 10 pm to 1 am. In contrast, at Mooring 1 the current direction from ebb to flood phase (11 am) changes rapidly (Fig. 4d). Mooring 2 shows similar pattern to mooring 1, but the time interval of the change from flood to ebb phase is approximately 1 hour near the bottom. In comparison to the alignment of the coastline and the delta base, the tidal currents run nearly coastal parallel.

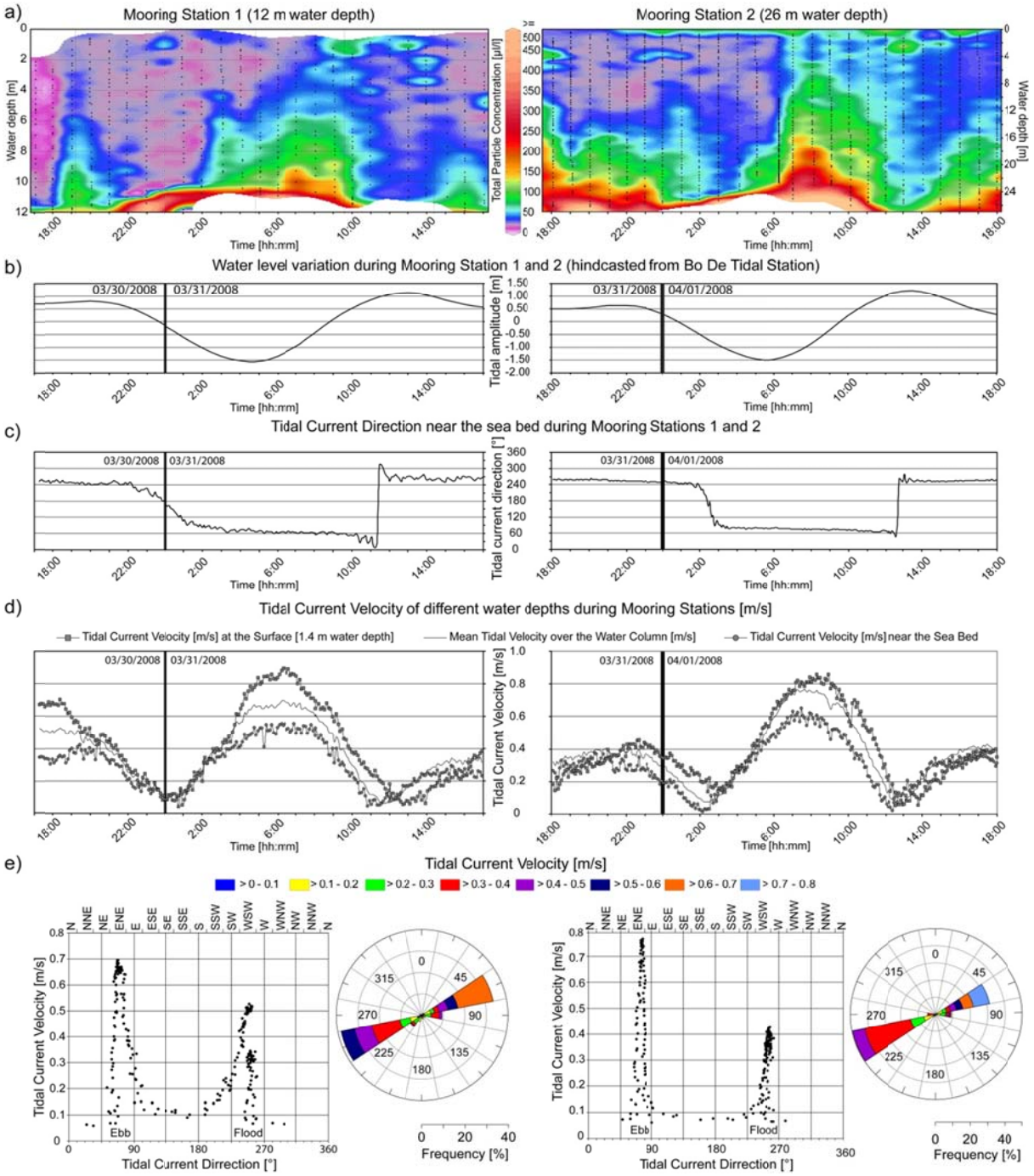

Fig. 4 Two mooring stations along the delta slope present the distribution of suspended sediment concentration over water depth and time (a), water level variations (b), and tidal current data: direction (c, e) and velocity (d).

Near-bottom current velocities and near-bed SSCs show similar pattern (Fig. 5). Their trends are slightly shifted in time. However, on average the SSCs are in phase with the tidal current velocity.

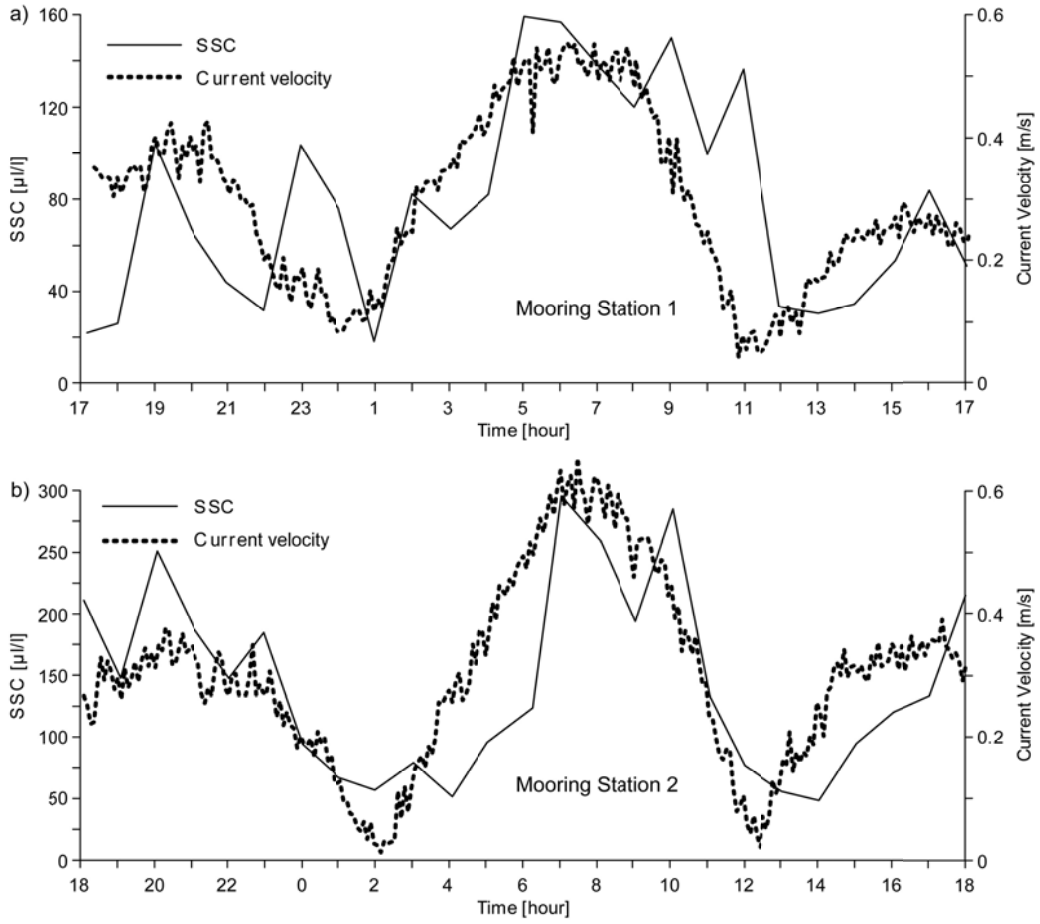

Fig. 5 Bottom tidal currents and average suspended sediment concentration (SSC) near the sea bed ($D_{ratio} \geq 0.8$) over time.

4.3 Transects of SSC within the subaqueous Mekong Delta

In addition to the isosurface maps (Fig. 2), more detailed vertical distributions of suspension load are presented along intra-day transects (Fig. 6). Section A and B (Fig. 6) show mainly similar pattern in the distribution of SSCs in the water column and across the delta slope. Close to the coast high suspended load is shown over the whole water column (Fig. 6 Section A and B). In general it can be observed that with increasing distance to the coastline the suspended particle concentrations in the water column drop below 25 µl/l. Exceptions are near the sea bed and close to the surface, where SSCs higher than 25 µl/l occur.

Section C (Fig. 6) differs from the previous transects in SSCs. Concentrations of suspended sediment higher than 25 µl/l occur close to the coast, near the sea surface between the channels and close to the sea bed along the delta slope (Fig. 6 Section C). The southern flanks of the channels have also increased SSCs. Section D (Fig. 6) shows in shallow waters (up to 10 m) SSCs higher than 25 µl/l over the entire water column. Along the delta slope SSCs higher than

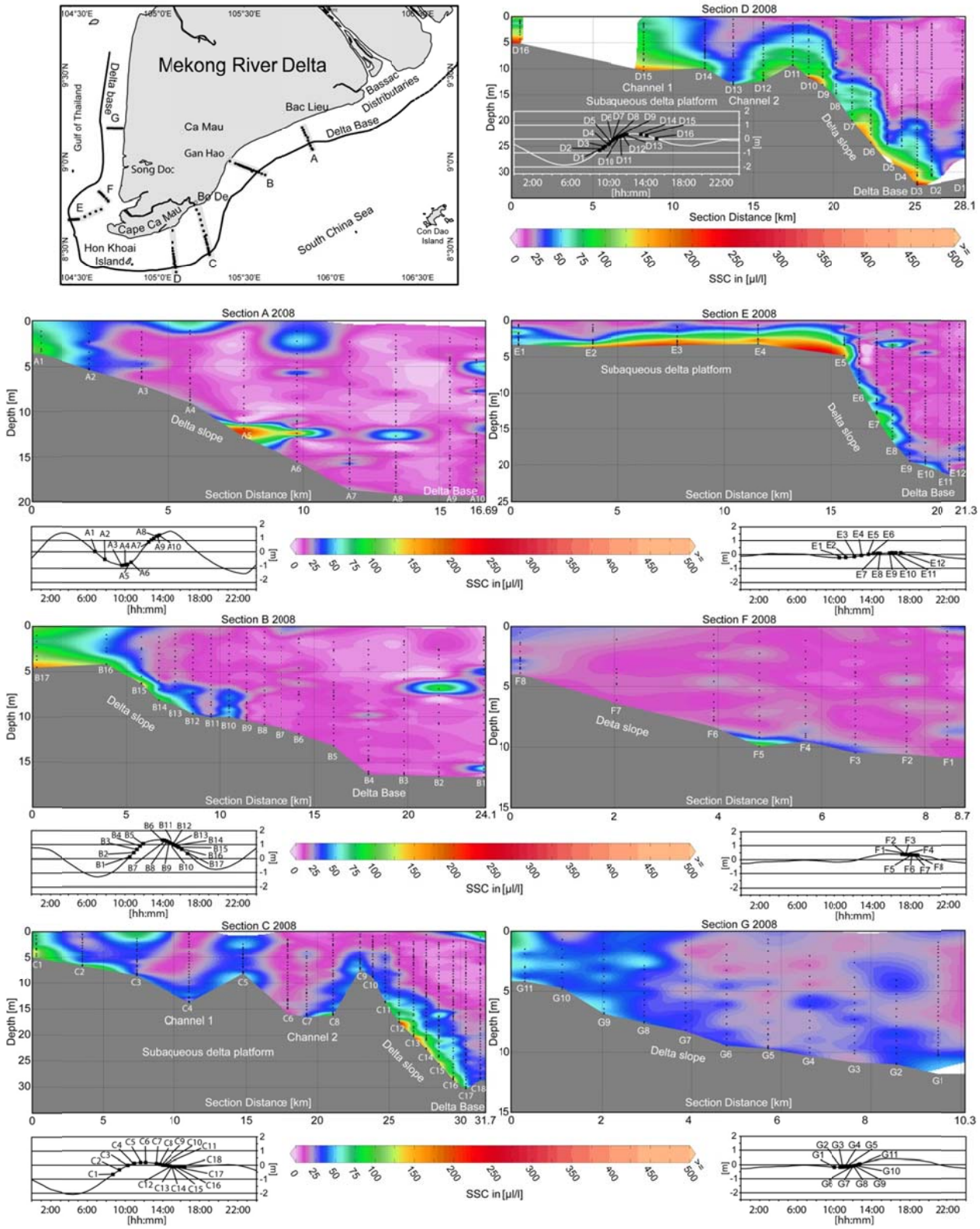

Fig. 6 Coastal normal transects of the inter-monsoon season in 2008 show the vertical distribution of SSC within the subaqueous Mekong Delta. Respective sampling times are marked in the inserted water-level curves.

25 µl/l can be observed until 10 m above the sea bed. Increased SSCs greater 25 µl/l also occur near the sea bed in the transition from the delta slope to the shelf.

Similar pattern of SSCs, but less developed can be seen in Section E (Fig. 6). Especially, in the very shallow water (lower than 3 m) of the subaqueous delta platform SSCs higher than 25 µl/l occur close to the sea bed. The upper water column ($D_{ratio} \leq 0.5$) has an average suspended sediment concentration of 13 µl/l.

Section F (Fig. 6) shows complete water body with SSCs lower 25 µl/l, except at the nearest station to the shore. However the suspended sediment concentrations exceed not 50 µl/l.

Section G (Fig. 6) has at near shore station SSCs until 75 µl/l and a decreasing trend to coastal distal stations. There is also apparent that the SSCs close to the sea bed are higher opposite to the sea surface SSCs.

5 Discussion and Conclusion

5.1 Distribution of Suspended Sediment

During the inter-monsoon period the suspended sediment is mainly distributed in the river branches and the adjacent subaqueous Mekong delta (Figs. 2 and 3). There, increasing SSCs near the seabed and in proximity to the coast are common. However, also on the adjacent shelf near Ca Mau Cape elevated SSCs occur close to the sea bed (Fig. 2 and Fig. 6 section D and E).

In the subaqueous delta region 50 % of all measured SSCs are greater than 23 µl/l, and the median of the SSC in the Mekong branches is nearly 76 µl/l (Fig. 3). The offshore region is beyond the delta base significantly depleted in suspended sediments higher than 25 µl/l. Additionally, a decreasing trend of SSCs from the Mekong River branches towards the shelf can be seen. We conclude that the suspended sediment delivery from the subaqueous Mekong delta on the adjacent shelf is very low during the inter-monsoon season.

5.2 Tidal influence on suspended sediment

Wave and tides commonly affect suspended sediment distribution. For instance, wave generated resuspension of sediments occurs widely in the subaqueous Changjiang River delta (Yangtze River), particularly in shallow water down to the boundary of wave influence (Wang, et al. 2005).

In the southern Mekong River Delta wave influence is negligible due to calm weather conditions during the inter-monsoon season. Especially, during the mooring period the wind speed does not exceed 3 Beaufort.

In contrast, during the summer and winter monsoon season high wind speeds prevail and trigger higher waves. In the river mouth region significant wave heights reach more than two meters (Tamura et al., 2010) and increase the wave-impact. Recently, no data about the wave influence in the subaqueous Mekong delta exist and hence, no relation between waves and its influences to sediment resuspension can be provided.

Good correlation of tidal current phases with the increasing SSC, as observed during moorings, implies that tidal currents cause the sediment resuspension. In the Jiaozhou Bay (Shandong Peninsula, China) similar correlation is observed (Yuan et al., 2008). Wang et al. (2005) interpreted sedimentary records from transition between Changjiang River subaqueous delta and continental shelf as effect of strong tidal currents in the East China Sea, particularly in deeper water at the transition of the subaqueous delta and the adjacent shelf.

Tidal currents cause sediment resuspension and transport in the subaqueous Yellow River Delta in alongshore direction (Wright et al., 1990). Wiseman et al. (1986) hypothesised that due to the coastal parallel tidal ellipses around the Yellow River Delta, tidal currents carry the sediment particle in onshore direction according to Stokes drift. It means that the particles follow the oscillating currents of the tidal ellipses, and driven by tidal asymmetry a net-transport in the dominant direction takes place (Fig. 7).

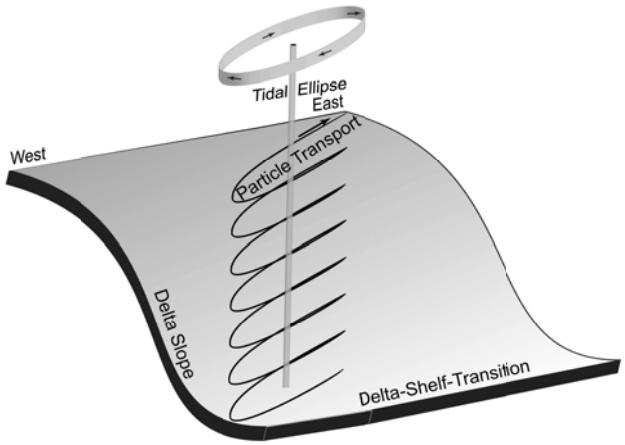

Fig. 7 Scheme of particle transport along the delta slope of the subaqueous Mekong delta due to tidal current induced reworking.

Shore-parallel tidal currents at the coast of Northern France transport sediment alongshore in dependence of their direction (Héquette et al., 2008). In addition wind blowing in the same direction can reinforce or decrease the tidal current energy depending on the prevailing direction. Similar influences of wind induced currents and wave impact under monsoonal conditions may change the sediment dynamics in the subaqueous Mekong delta.

In the case of the southern subaqueous Mekong delta the tidal current ellipses of the dominant M_2-tidal constituent extend in NE-SW-direction (Zu et al., 2008) and correlate with the tidal current direction of the mooring stations (Fig. 4). Accordingly, resuspended particles are accelerated in north-eastern direction during ebb phase. Around low water from ebb to flood phase the velocity vector turns fast to southwest (Fig. 4c) and suspended particles are accelerated in that direction. The turn from flood to ebb phase needs up to 3 hours (Fig. 4c). It leads to an asymmetry of the tidal ellipses and longer time interval of particle movement in northern direction occur due to the longer shift from ebb to flood phase. As a result of ebb phase dominance with higher current velocities particles are transported over a longer distance relatively to the flood phase with lower current velocities. Greater tidal ellipses in proximity to the coast cause faster particle movement (Wiseman et al., 1986). Further offshore tidal ellipses are smaller and hence lower acceleration occurs. Considering the subaqueous delta extension in the southern region of approximately east to west (Fig. 1) and the prevailing particle delivery into north-eastern direction during ebb phase, a tidal current induced net transport of resuspended sediment is caused into the subaqueous Mekong delta (Fig. 7).

5.3 Implications for understanding the fate of sediment dispersal

Wang et al. (2005) mention that the transition zone of the subaqueous Changjiang Delta is beyond the control of the deltaic processes, but rather under the strong shelf tidal regime of the East China Sea that reach a current top velocity of 0.46 m/s. The near bottom tidal current top velocity at Mooring 1 and Mooring 2 exceed this value significantly (Mean/Max tidal currents at mooring 1 = 0.3/0.66 m/s and mooring 2 = 0.37/0.78 m/s). The moorings were carried out under neap tide and calm wind conditions. Hence, stronger near bottom tidal currents can be assumed due to high tidal energy condition during spring tide.

Tidal processes in the subaqueous Mekong delta have a significant influence in sediment resuspension and its transport direction (Fig. 4 and 5). The tidal current in the southern region causes a net sediment transport directed into the subaqueous delta region with north-eastern direction due to ebb current dominance. It involves, as pointed out by the isosurface maps (Fig.

2), low cross-shore sediment transport during the inter-monsoon season. Increased SSCs occur only in the southern shelf region off Ca Mau Cape, where strong tidal currents can rework the sediment in deeper water (Fig. 2 isosurface map of 20 and 25 m water depth) supported by mooring 2 in 26 m water depth.

In front of the main river branches tidal currents have also a coast-parallel direction (Hung and Dien 2006). In this region only few data of SSCs exist from the river mouth (Wolanski et al., 1996; Wolanski et al., 1998), the subaqueous Mekong delta and the adjacent shelf (Anikiyev et al. 1986). However, no comprehensive data exist regarding the significant influence of wave, tide and river processes to the sediment dynamic in cross-shelf and along-shore direction over the annual seasons. Numerical models predict a plume of higher salinity (Hordoir et al., 2006) and field investigations fixed a hypopycnal plume by Radium isotopes (Chen et al., 2010) and lower salinities as well (Voss et al., 2006; Grosse et al. 2010). However, the formation of a hypo- or hyperpycnal sediment plume offshore the subaqueous delta is neither supported by our measurements nor evidenced in the open shelf which is remarkably depleted in modern sediments (Unverricht et al., 2013). In addition, the shelf sediments primarily consist of sand in front of the Mekong river branches (Kubicki, 2008).

Acknowledgements

The cruises were supported by research grant STA-401 10/2 of the German Research Foundation and through scientific cooperation with the Vietnamese Academy of Science and Technology (VAST) and the Ministry of Science and Technology (MOST), Vietnam.

The scientific experience in shallow water processes of Klaus Schwarzer (Sedimentology, University of Kiel) enriched all cruises significantly. We are thankful for his participation. Gratitude is owed to Thorben Amman (University of Hamburg, Germany), Robert Jagodziński (Adam Mickiewicz University, Poznan Poland), Klaus Ricklefs (FTZ Büsum, Germany), Bui Ngoc Chung (University of Science, Ho Chin Minh City, Vietnam) and Nguyen Trung Thanh (IMGG, Hanoi, Vietnam) for their manpower and scientific support during the cruises in 2006 or 2007. Thanks also to the fishermen who supported the cruises in 2007 and 2008. The project would not have been feasible without their endurance and willingness.

Chapter V

Alongshore sand-ridges and erosional channels in the subaqueous Mekong Delta, southern Vietnam

Daniel Unverricht[1], Christoph Heinrich[1], Thanh Cong Ngyuen[1,2], Karl Stattegger[1]

[1]*Institute of Geosciences – Department of Sedimentology, Christian-Albrechts-University of Kiel, Germany*

[2] *Department of Oceanology, Meteorology and Hydrology, University of Sciences, Ho Chi Minh City, Vietnam*

To be submitted to Continental Shelf Research

Abstract

Mega-deltas like the Mekong River delta differ in shape and sedimentary pattern in dependence on the interplay of river, tide and wave forces. Specific hydro- and morphodynamic conditions in the subaqueous part of the Mekong River Delta generate a sand-ridge-system combined with erosional channels, which is unique in subaqueous delta formations.

This large-scale morphological feature extends along the delta front, in particular, the delta slope and subaqueous delta platform of the Mekong River Delta. A system consisting of two sand ridges and two erosional channels (termed sand-ridge-channel-system (SRCS)) covers at least an area of 1971 km^2 and extends in minimum 128 km along the coast. Three different areas west of the Bassac river mouth, the largest and western-most Mekong distributary, were distinguished according to their morphology. The eastern area, where the channel-ridge formation begins, stretches along the delta slope and inner shelf platform southwest of the Bassac river mouth with slightly concave and erosional features. The central area covers the southern part of the subaqueous delta platform with a pronounced sand-ridge and erosional channel morphology. Hydroacoustic cross-sections of the SRCS reveal an asymmetric shape including steeper ridge flanks facing into offshore direction. The channel troughs incise up to 18.2 m b.s.l. and 10.5 from the ridge top at the shallow subaqueous delta platform, respectively. At the western part of the central area, the sand ridges pinch out while the two channels merge into one and form a giant scour of up to 33 m water depth within the subaqueous delta platform of generally less than 7.7 m water depth. In the western area, the channel gets shallower and vanishes along the south-western most subaqueous delta platform around Ca Mau Cape.

Headland retreat and sediment transport from erosive areas of the Mekong river delta coast are the source to form the sand-ridges and coastal subparallel tidal currents maintain and stabilize them. In contrast, tide and wind-driven currents cut the erosional channels, which act as fine sediment conveyor to the distal part of the delta front that is 200 km apart of the next main distributary. The SRCS represents a new morphological feature in the subaqueous deltaic environment and is a relevant indicator of delta instability and coastal erosion in subaqueous deltas.

1 Introduction

River deltas belong to the larges morphological features that are shaped by sediment- and hydro- dynamic processes at the interface between fluvial and shallow marine environments. Especially in large deltas, the physical forcing processes change in space and time (e.g. Po-delta (Correggiari et al., 2005), Danube-delta (Giosan et al., 2006), Mekong-delta (Unverricht et al., 2013)). It leads to different morphological features within the delta complex depending on the dominating hydrodynamic factors and the sedimentary composition (Orton and Reading, 1993). Therefore, the classification scheme for river deltas take their prevailing influence factors into account (Orton and Reading, 1993) and the pattern and nature of sediment accumulation (Walsh and Nittrouer, 2009), respectively.

Conceptual (Orton and Reading, 1993, Dalrymple and Choi, 2007) and numerical models (Edmonds and Slingerland, 2010, Edmonds et al., 2011) for delta evolution support that sediment dispersal is delivered via bed load and suspended sediment. The material gets deposited within the river mouth area or is transported further to deposition sites on the inner shelf (Wright and Nittrouer, 1995; Tamura et al., 2010, 2012b; Szczuciński et al., 2013). In a prograding delta system, high sediment accumulation rates result in a lateral succession of subaqueous delta platform, delta slope and prodelta environment forming a clinoform as large-scale sedimentary structures (Walsh and Nittrouer, 2009). Sediment pathways on the inner shelf are either coastal parallel or in across shelf directed. In both cases, the sediment gets sorted during transport with decreasing grain sizes away from the river mouth.

Both cases are shown in the subaqueous Mekong River Delta (MRD) (Unverricht et al., 2013). Beginning at the Bassac River mouth, the main distributary of the MRD, multiple variation of the subaqueous delta morphology occurs into south-western direction. The MRD consists of two prograding regions at the Bassac river mouth and near Ca Mau Cape that are connected by an area of a delta non-typical morphological feature. Sand enriched ridges combined with channels form an alternating and alongshore extending system (Fig. 1) that is partly incised into the subaqueous delta. The knowledge about the formation and development of these sedimentary features contributes the understanding of the younger evolution of the Mekong delta system in its particularly case.

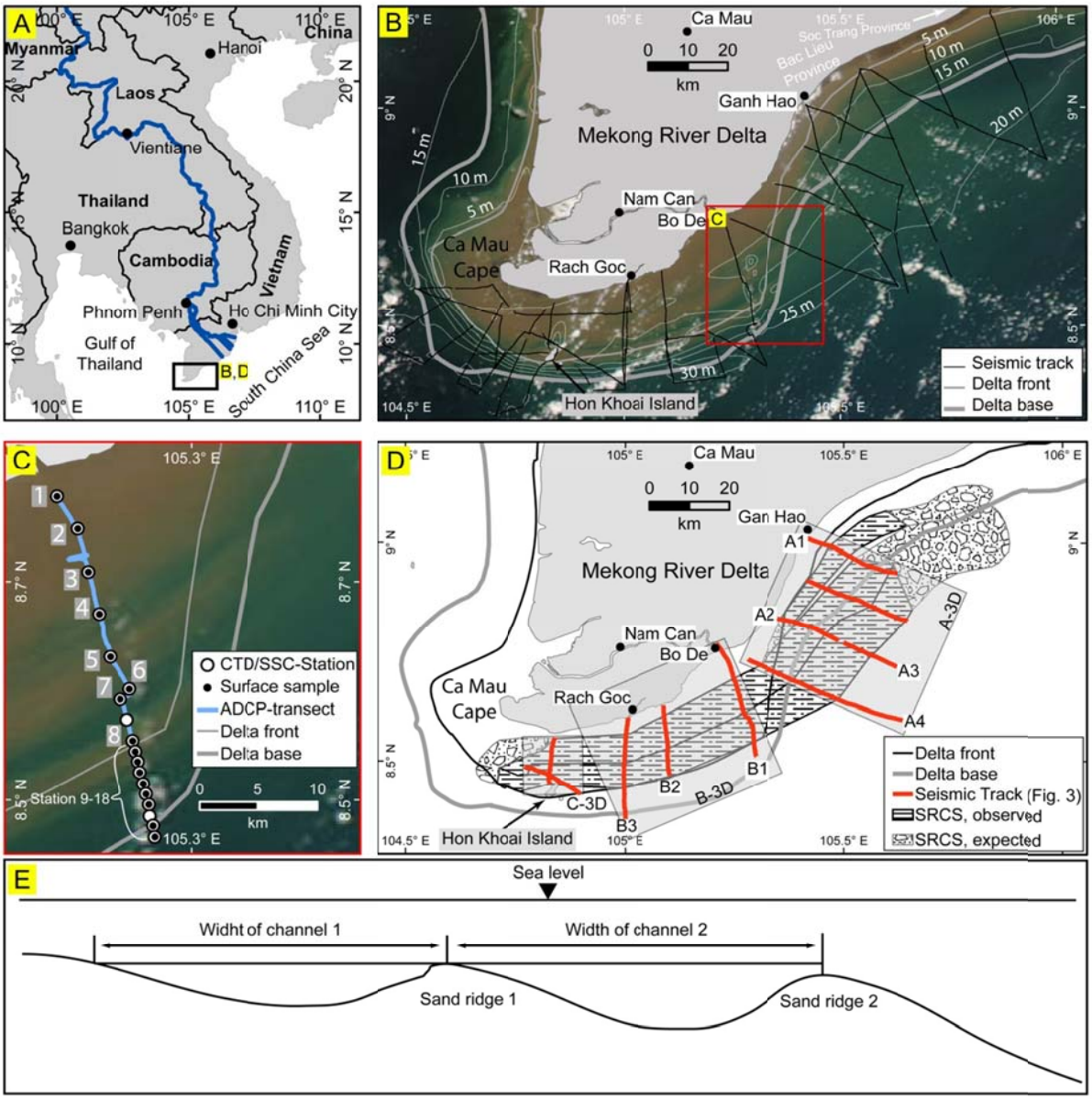

Fig. 1. A) provides the location of the research area in South-East-Asia and the Mekong River course. B) presents the seismic track lines, bathymetry contours and the spatial dimension of the subaqueous Mekong delta covered by a satellite image in optical range of the research area (recorded 22.08.2008 by MODIS/NASA). C) presents the key-cross-section off Bo De including the same satellite image combined with locations of an ADCP-profile, surface-samples- and CTD/SSC-stations crossing the subaqueous Mekong delta. D) provides seismic track lines shown in Fig. 3 and the interpolated spatial extension of the sand-ridge-channel-system. Here, sand-ridge-channel-system is abbreviated as SRCS. E) describes the estimation of the channel width including the top of the sand ridges.

This article provides (1) new insights into the subaqueous Mekong River Delta morphology; and (2) combines hydro-acoustic, sediment- and hydro-dynamic data to interpret sediment transport and morpho-dynamic processes in a prograding delta environment.

2 Regional Settings

The origin of the Mekong River lies in the Tibetan mountains. On its 4,800 km long way, the Mekong River passes six countries before draining via eight distributaries into the South-China-Sea. The river delta is mainly supplied with sediments from the two major distributaries Bassac and Mekong. The delta plain covers an area of approximately 62,520 km^2 between Phnom Penh in the Cambodian lowlands and the southeast Vietnam (Nguyen et al., 2000). Anthropogenic interventions in the Mekong basin like damming (Kummu and Varis, 2007) increases permanently and lead to coastal erosion (Cat et al., 2006; Nguyen, 2012).

The tidal regime along the Mekong River Delta is complex. The semi-diurnal to mixed meso-tidal system (Nguyen et al., 2000; Nguyen, 2012) with tidal ranges up to 2.5-3.8 m prevails in the South China Sea. In contrast, micro-diurnal tides and with tidal ranges of around 0.5 to 1.0 m can be found in the Gulf of Thailand (Nguyen, 2012). The harmonic M2- and K1-tidal-constituents are the most dominant constituents (Fang et al., 1999; Zu et al., 2008) in the South China Sea and generally propagate along the southern Vietnam coastline from northeast to southwest. In the subaqueous Mekong Delta, the tidal ellipses of the dominant tidal constituents with its according currents extend in alongshore direction (Hung and Dien, 2006; Fang et al., 1999; Unverricht et al., 2014). During neap-tide bottom currents of 0.6 m/s at the most southern delta slope were observed (Unverricht et al. 2014).

The East Asian Monsoon climate causes strong seasonal variations in the wind system (Hordoir et al., 2006; Mitsuguchi et al., 2008; Xue et al., 2011). The winter monsoon winds from November to early March come from north-easterly direction, whereas south-westerly winds dominate during the summer monsoon (May to September). In the Mekong River delta region southwest of the Bassac River, wind speeds and directions are more heterogeneous and do not exceed 6 m/s (Unverricht et al., 2014). Wind speeds between 20 and 30 m/s can be achieved under stormy conditions (Institute of Strategy and Policy on natural resources and environment (ISPONRE) 2009).

The East Asian Monsoon climate is driving the water circulation in the South China Sea. The offshore region of the Mekong River Delta is influenced by the western coastal current. During the winter monsoonal season dominates currents into south-western directions, whereas north-easterly currents prevail in the summer monsoon season (Fang et al., 1998).

Recently, two distinct areas of the Mekong River delta are prograding into the open shelf. First, the region of the major distributaries with surface sediments tending from well sorted fine

sand at proximal to moderate sorted clayey silt at distal locations (Unverricht et al., 2013). The progradation rate at the river mouth region is 16 m/yr (Xue et al., 2010). In contrast, the prograding Ca Mau Cape, which is situated more than 200 km southwest of the major distributaries, reaches 24 m/yr (Xue et al., 2010) caused by high sediment accumulation rates of up to 10 cm/yr (Xue et al., 2010; Unverricht et al., 2013). Both regions are intersected by an area of mainly decreasing sand content, except along two ridges of well sorted sand, which are discussed in this article. The subaqueous delta in the south-western region around Ca Mau Cape (Fig. 1) and the Gulf of Thailand is dominated by silt with clay percentages of up to 20 Vol% (Unverricht et al., 2013). During low energy conditions in the inter-monsoon season (March to May), sediment transport along the subaqueous Mekong delta is dominated by sediment resuspension due to coastal subparallel tidal currents (Unverricht et al., 2014). Model results show a north-eastward directed transport during the summer monsoon and a south-westward transport during the winter monsoon season (Xue et al., 2012a). However, most of the sediment is captured in the subaqueous Mekong delta and the sediment delivery to the open shelf is strongly limited (Xue et al., 2010, 2012a; Szczuciński et al., 2013, Unverricht et al., 2014).

3 Material and Methods

Surveys in 2007 and 2008 were carried out to gather information about sediment- and hydro-dynamics along the subaqueous Mekong Delta west of the Bassac river mouth. CTD-transects (Fig. 4) coupled with measurements of suspended sediment were performed along high-resolution seismic profiles (Fig. 3). The suspend sediment concentration (SSC) was estimated using a Seapoint turbidity meter to detect the backscattered light from the suspended particles. The sensor transmits infrared light at 880 nm wavelength and the detected backscattered light intensity are given in Formazine Turbidity Units (FTU). For calibration issues, water samples were taken 1 m above the seabed and filtered using glass fibre filters of 0.7

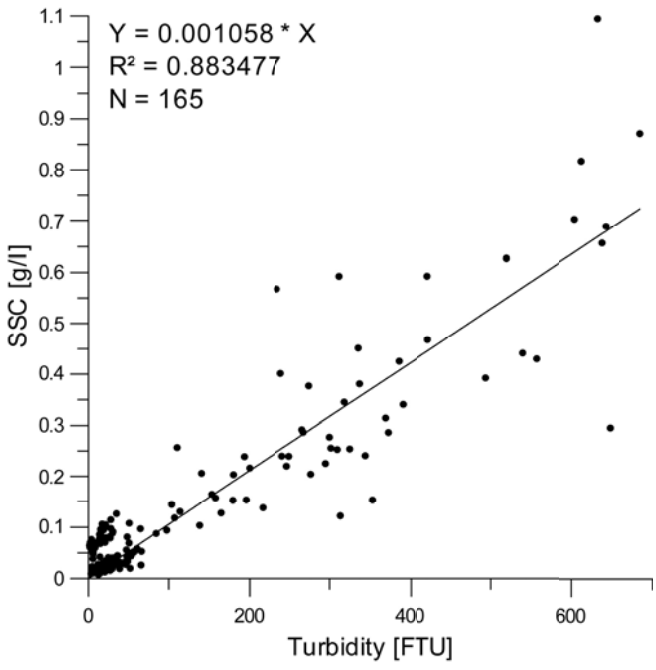

Fig. 2 Correlation plot of suspended sediment concentration and in situ measured turbidity.

µm pore density (Whatman GF Cat No 1822-047) and a vacuum pump at 300 mbar. Filters were dried at 100 °C and weighted. A regression model translates the measured FTU values into suspended sediment concentrations for all turbidity data (Fig. 2).

The sound velocity in sea water was calculated using the equation of the UNESCO from 1981 (UNESCO 1981) with measured CTD data. Estimated water depths in seismic profiles are based on the average value of 1540 m/s (± 5.01 m/s STD) during our campaign.

High resolution seismic profiles were recorded with the low-voltage C-boom-system working with a dominating frequency of 1.760 kHz and the high-voltage EG&G Uniboom-system with a dominant frequency of 3.5 kHz. Postprocessing includes band pass filtering using different software (C-View, NWC) and data were converted into SEGY-format. SEGY-files were imported into The SMT Kingdom Suite®-software for visualization and interpretation. Tidal offsets were not considered with the postprocessing due to no available tidal gauge stations further offshore. Tidal gauges in the River mouth regions are not representative for offshore surveys, because the tidal amplitudes decrease from the coast to the inner shelf.

Additionally, current velocities and flow directions were measured along sampling transects using an Acoustic Doppler Current Profiler (RDI Broadband ADCP at 1200 kHz). Positioning were carried out using a normal GPS-receiver.

4 Results

Subaqueous delta architecture west of the Bassac river mouth and Ca Mau Cape region is dominated by a morpho-dynamic system of channels and ridges composed of sand (see 4.3). Covering an area of 1971 km² and extending 128 km along the shore, the sand-ridge-channel-system (SRCS) can be subdivided into three subareas (eastern, central and western area) according to shape and sediment distribution.

4.1 Seismic stratigraphy and seabed morphology

4.1.1 Eastern area

Seismic data of the eastern area, located in front of Ganh Hao Fig. 1D) and approximately 120 km southwest of the Bassac-River mouth reveal complex sub-bottom architecture. High amplitude reflectors in hydro-acoustic profiles mark the sequence below the delta base (Fig. 3 A1, A-3D). Channel-like structures incise into downlapping reflectors and the channel infill of the lower subsequence shows draped features, whereas the upper subsequence has onlapping

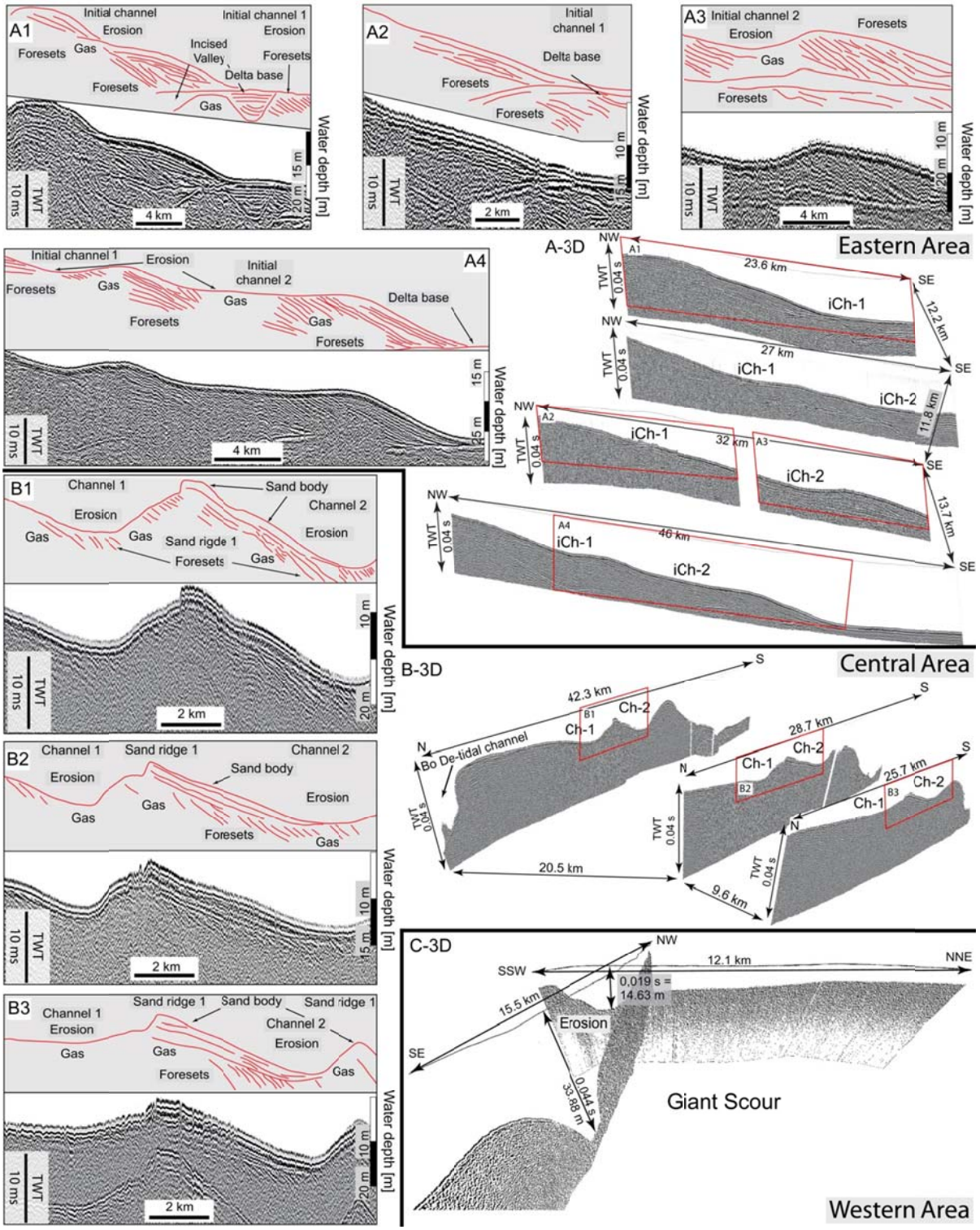

Fig. 3 Seismic data with colored interpretation (mark as grey background) is presented here. Spatial reference is given in Fig. 1D. A composition of characteristic forests, erosion and sand body structures are indicating a complex Sand-Ridge-Channel-System along the research area. Also a giant scour in the southern area is present. Sections A1-A4 are selected insets of 3D-curtain view A-3D as B1-B3 are insets of B-3D. Vertical scale is given as well as in two way travel time (TWT) and absolute water depth in meter. (iCh-# = initial Channel; Ch-# = Channel)

reflector pattern (Fig. 3 A1). The toplap surface of this sequence joins the bottom reflection At the delta base and forms the seabed of the open shelf between 15 and 17 m water depth (Fig. 3 A1-3, A-3D). The undulated seabed at the open shelf combined with the foreset pattern joining the seabed show an erosional truncation (Fig. 3 A1-3, A-3D).

Strong bottom reflection occurs, additionally, along the delta slope between 10 and 15 m water depth. Two subsequences of downlap reflector pattern terminate below the bottom reflector and show seaward inclined foresets (Fig. 3 A1). Between 5 and 10 m water depth occurs a sequence that forms the upper delta slope and the outer delta platform. Incident reflectors, mainly masked by gas, show further foreset pattern and terminate downlap to the foreset sequence below (Fig. 3A1).

The transition between the initial area and central area of the SRCS feature strong bottom reflectors. In seismic profiles, foresets, partly masked by gas, characterize the terraced clinoform and its toplap surface forms an unconformity with the seabed (Fig. 3 A4).

The recent delta base forms the central initial channel 1 (iCH-1) characterized as slightly concave shape (Fig. 3 A1) by a width of 8.2 km on average ($1\sigma \pm 725$ m). The initial channel 1 beginning at water depths of 17 m (Fig. 3 A1) becomes shallower until 15 m water depth at the end of the initial channel region (Fig. 3 A4).

The initial channel 2 (iCh-2) is located on the inner shelf platform outside the delta (Fig. 3 D) as slightly inclined and wide depression (Fig. 3 A3, A3-D). Channel-widths of 10862 m on average ($1\sigma \pm 1078$ m) are reached (Fig. 3 A3). In seismic sections, iCh-2 incise into the foreset-structures of the open shelf (Fig. 3 A3, A4) at water depths between 17 m and 18 m.

Offshore of Ganh Hao (Fig. 3 B), a small initial channel occurs at water depths shallower than 10 m (Fig. 3 A1-2). However, it vanished into western direction and cannot be observed in the other seismic profiles.

4.1.2 Central area

Extending at least 60 km coastal parallel (Fig. 3D), the central area of the SRCS has a pronounced morphology compared to the eastern area including its very slightly concave shape, which is embedded into the delta slope and inner shelf. Seismic profiles at the subaqueous delta platform show downlapping reflectors (foresets), which terminate with the bottom reflector at the area of two depressions. However, the downlapping reflectors are mainly masked by gas and show mainly the seismic structure of the clinoform near the seabed. In the area of two ridges, the

truncated foresets are covered by slightly inclined seismic reflectors (Fig. 3 B1-3, B-3D), whereas the upper most reflector of high amplitudes forms the sea bottom.

From sediment grab samples consisting of fine and very fine sand Fig. 3C), the ridges are interpreted as sand bodies (Fig. 3 B1-3) and due to their elongated shore-parallel extension as sand ridges. The two sand-ridges are asymmetric with steeper slopes at the southern flank (Fig. 3 B1-3, B-3D).

The depressions at the subaqueous delta platform are interpreted as erosional channels due to erosional truncations of seaward dipping foresets. Channel 1 (Ch-1) and channel 2 (Ch-2) separate the two sand-ridges, where sand-ridge 2 forms the top of the delta slope (Fig. 3 B1-3).

Channel widths of 7531 m on average ($1\sigma \pm 870$ m) are observed at channel 1 (Ch-1), which reaches incisions of up to 14.3 m b.s.l and 6.6 m from the ridge top in the transition to the easterly-channel-system SE of Bo De, respectively (Fig. 1 B and Fig. 3 B1). Into western direction, the central channel depth decreases to 9.3 m b.s.l. and 2.9 m from ridge top close to Hon Khoai Island (Fig. 1D, Fig. 3 B1-3).

The second channel (Ch-2) is 6023 m wide on average ($1\sigma \pm 1079$ m). In the central channel trough SE of Bo De, water depths of 18.2 m are observed (Fig. 3 B1) and the incision amounts 10.5 m from the ridge top, respectively. Similar to Ch-1, channel depths of Ch-2 decreases continuously up to 12.8 m b.s.l. into western direction until Hon Khoai Island. There, Ch-2 cut 6.4 m into the subaqueous delta platform beginning from the ridge top (Fig. 3 B3).

4.1.3 Western area and local depression

Although the delta platform bathymetry becomes shallower into western direction, north of Hon Khoai Island water depths increase abruptly within 3.8 km from 7.7 m to more than 33 m (Fig. 3 C-3D) and form a local depression that extends approximately 4.5 km in north-south and 12 km in southeast-northwest direction (estimated relative to 7.5 m b.s.l.). Gas is masking the seismic reflectors excepting the bottom reflector (Fig. 3 C-3D). The deepest part exceeding 33 m water depth has an east-west extension of approximately 350 m. Inclination is steeper to the southeast, whereas the western and northern flanks are more flattened (Fig. 3 C-3D). Both sand-ridges merge into the depression and pinch out in western direction as single flat depression until the delta front of Ca Mau Peninsula (Fig. 1 D).

4.2 Hydro-dynamic conditions

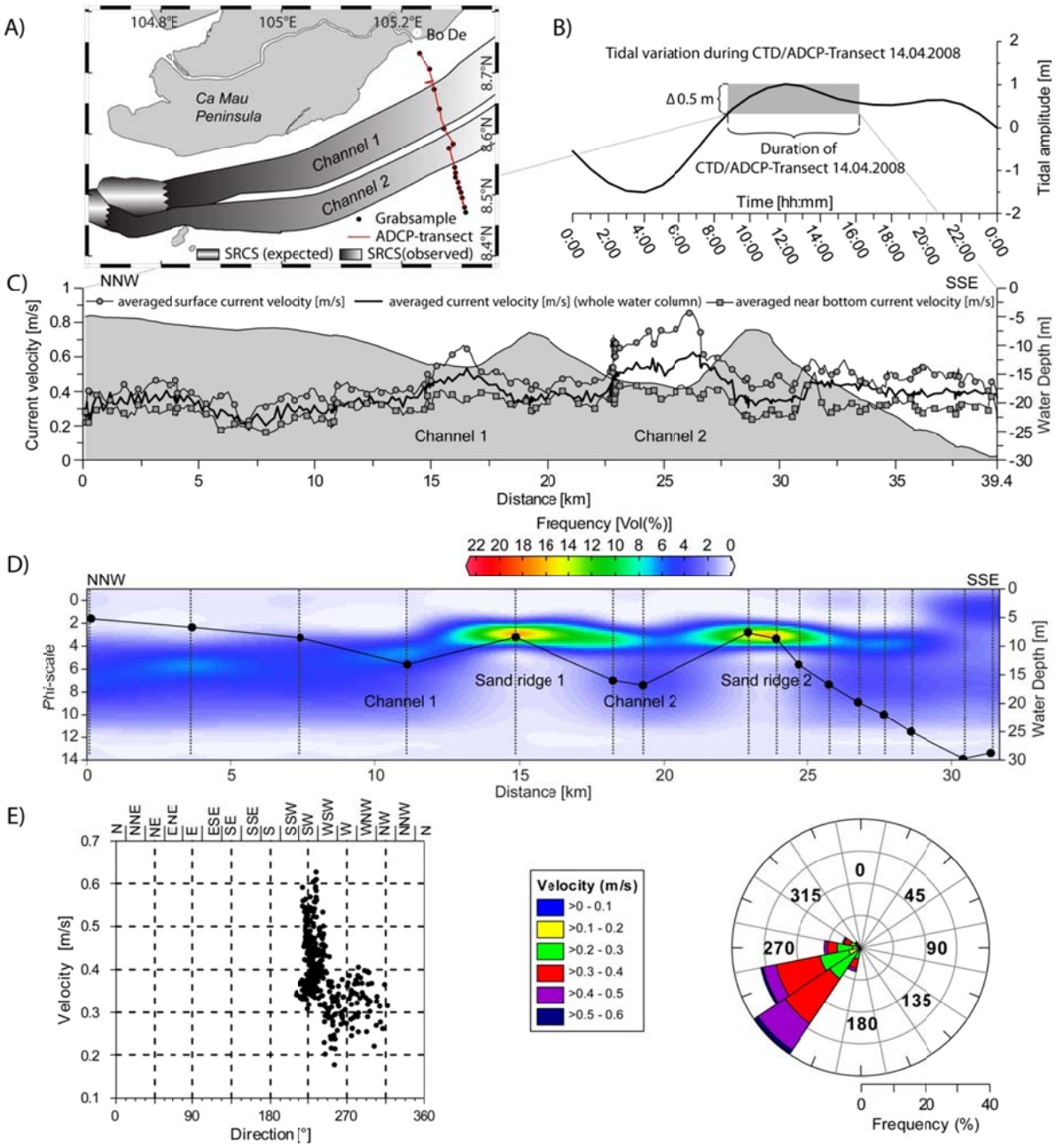

Fig. 4. A) Map of the subaqueous Mekong delta including the key-cross-section B) Water level variation recorded at Bo De station including the survey time (grey box) during flood phase. C) Averaged current velocities are shown at 1.4 m b.s.l, over the entire water column and 1 m above the seabed (morphology in grey as background). D) Grain size distribution of grab samples along the ADCP-transect (sample depth is indicated by black dots) (modified after Unverricht et al. 2013). E) provides dominant current direction in degrees and current velocities as absolute values and cumulative frequencies per direction.

The flow regime of the subaqueous Mekong is influenced by two different current types – tidal and wind driven currents. During our field campaigns, wind induced currents are negligible, because 81 % of the wind speed were below 8 m/s (< 5Bft) with main wind directions from east and south (annual wind speed recorded at Bac Lieu by the Southern

Regional Hydro-Meteorological Center (SRHMC, Vietnam)). During measurements of the ADCP-transect in Fig. 4 the wind speed did not exceeds 4 m/s and the south-eastern wind direction did not coincide with water current directions (opposite direction) recorded during flood phase condition (Fig. 4 B).

Currents from south-western direction were measured along the transect (Fig. 4 E). Near surface currents (1.5 m b.s.l.) reach velocities of up to 0.85 m/s (0.49 m/s on average, 1σ ±0.12 m/s), while near bottom currents (1 m above seabed) range between 0.16 m/s and 0.51 m/s (0.32 m/s on average, 1σ ±0.06 m/s). In both channels, higher current velocities occur near the sea surface and lower currents close to the seabed. Near surface currents in channel Ch-1 reach highest velocities of 0.66 m/s (0.47 m/s on average, 1σ ±0.07 m/s) close to its southern channel flank (Fig. 4 C). The same pattern is observed in channel Ch-2 with 0.85 m/s (0.6 m/s on average, 1σ ±0.1 m/s). Near the seabed, average currents of 0.34 m/s (min/max velocity = 0.26/0.40 m/s in maximum) were measured in channel Ch-1 and 0.36 m/s (min/max velocity = 0.23/0.44 m/s) in channel Ch-2. In comparison to the channels, the sand-ridge areas do not show significantly lower current velocities near the seabed. In the region of sand-ridge 1, the average currents near the seabed reach 0.34 m/s (min/max velocity = 0.26/0.40 in maximum) and at sand-ridge 2 average velocities of 0.30 m/s (min/max = 0.23/0.42 m/s) were measured (Fig. 4 C). In contrast to the channels, lower near surface currents (1.5 m b.s.l.) were observed at sand-ridge 1 with average velocities of 0.45 m/s (min/max velocities = 0.39/0.52 m/s) and 0.47m m/s (min/max velocities = 0.40/0.60 m/s) along sand-ridge 2.

4.3 Distribution of sand

As presented in (Unverricht et al., 2013), subfractions of fine and very fine sand dominate the subaqueous Mekong delta. Concerning the source of the sand-ridges, it is necessary to consider a detailed analysis of the sand fraction.

Starting at the Bassac River mouth, sand content, which consists of mainly fine and very fine sand, decreases alongshore in southwest direction from 79% to less than 20% until the Ganh Hao region approximately 95 km southwest of the Bassac River (Fig. 5 section 1).

Sand content below 20% occurs additionally at the cross-shore section 2 (Fig. 5), approximately 60 km west of the Bassac River mouth. Fine and very fine sand prevail along the section until the transition to the outer shelf, where coarse and medium sand dominate.

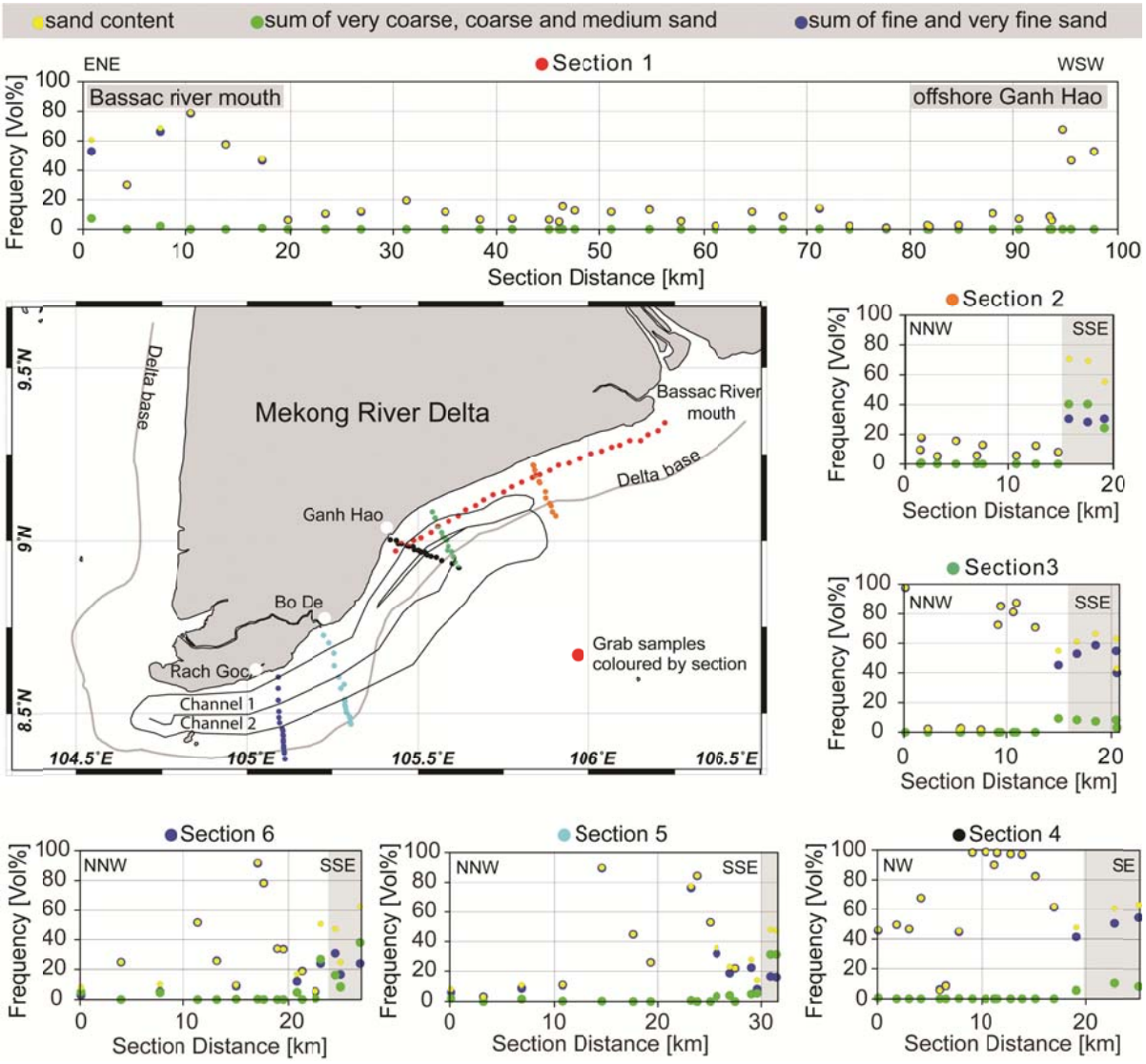

Fig. 5 The map shows surface samples taken at alongshore and cross-shore sections (1-6) in the subaqueous Mekong Delta. Sand content is provided including additionally percentages of combined subfractions ((very coarse, coarse and medium sand) and (fine and very fine sand)). The area of the SRCS is lineated as well as the delta base. Grey rectangle in the section boxes marks the section area that covers the open shelf.

Increasing sand content was found offshore Ganh Hao City (Fig. 5 section 1, 3 and 4). Sand contents of more than 80% are reached across the subaqueous delta approximately 10 km offshore (Fig. 5 section 3 and 4). Fine and very fine sand dominate, but the amount of coarse and medium sand increases at the transition to the open shelf.

At the sand-ridges, fine and very fine sand with percentages between 84 and 92 % are observed (Fig. 5 section 5 and 6). At the delta slope, the amount of fine and very fine sand decrease below 20%. Medium and coarse sand are negligible at the sand ridges (percentages < 1 %), but at the in transition to the open shelf increase their percentage (Fig. 5section 5 and 6).

4.4 Suspended sediment

This study provide detailed information on the vertical distribution of suspended sediment compared with temperature and salinity along the key cross-section of Bo De in addition to bathymetric, seismic, hydro-dynamic and grain size data presented above (Fig. 1 C, Fig. 3B; B3D, Fig. 4 and Fig. 5 Section 5). (Unverricht et al., 2014) present suspended sediment distribution under low energy conditions for the entire subaqueous Mekong Delta.

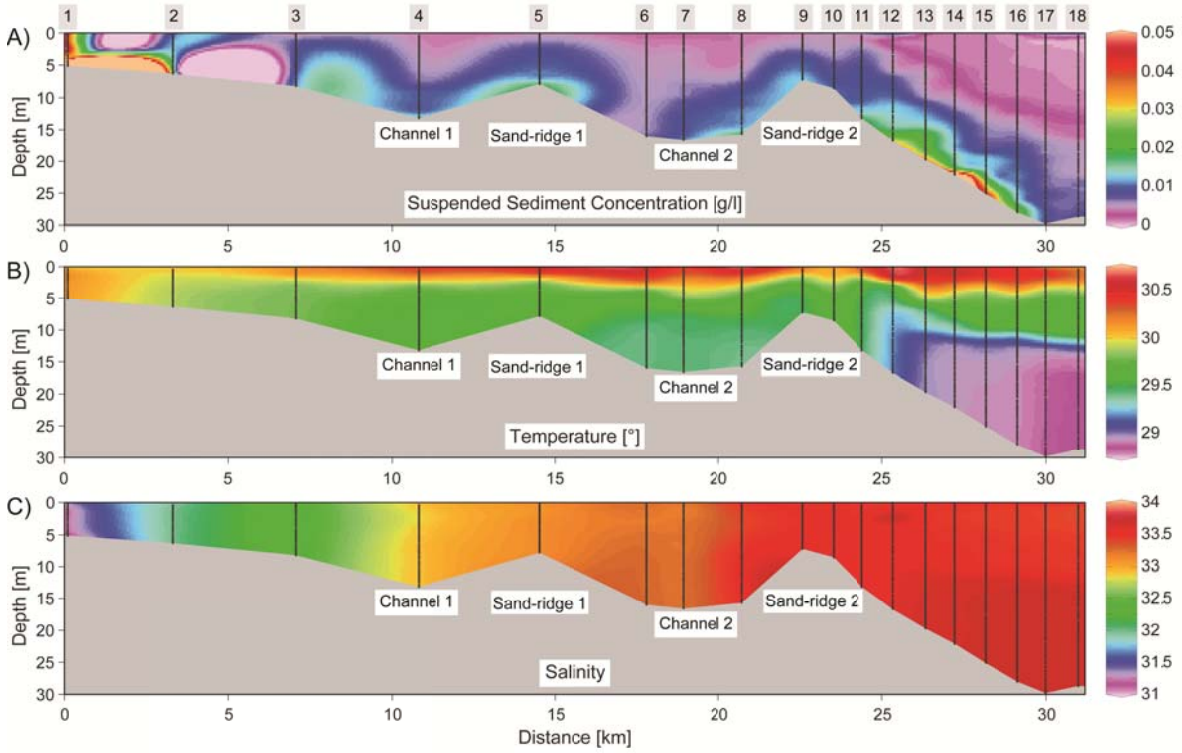

Fig. 6 CTD/SSC-Profile (Fig. 1C, Fig. 4) orientated perpendicular to the SRCS structure. Vertical distribution of suspended sediment concentration (Fig. 6A), temperature (Fig. 6B) and salinity (Fig. 6C) are given here. Black lines mark CTD/SSC-stations (Fig. 1C).

The spatial distribution of suspended sediment concentrations (SSC) along the key cross-section (Fig. 1C) varies vertically and horizontally in shore-normal direction (Fig. 6A). SSCs greater 30 mg/l occur close to the shoreline (CTD/SSC-station 1, Fig. 6A) in water depths lower 5 m and also near the seabed along the delta slope (CTD/SSC-station 14-15;Fig. 6A). At the sea surface, SSCs (0-2 m b.s.l.) range between 0.4 mg/l and 47 mg/l (5.5 mg/l on average, 1σ ±8 mg/l). Particularly low SSCs of 4.7 mg/l on average (1σ ± 1.2 mg/l; min/max= 2.7/7.5 mg/l) are measured near the sea surface of the channels.

SSCs up to 2.5 m above the seabed reach values of 137 mg/l by 18.6 mg/l on average (1σ ±16.9 mg/l). Sampling stations in the channel areas have SSCs of 10.6 mg/l on average (1σ ±2.9 mg/l; min/max =5.3/19.1 mg/l) close to the seabed (≤ 2.5 m above the seabed). Particularly, channel 1 (CTD/SSC-station 4, Fig. 6A) shows lower SSCs of 7.1 mg/l on average (1σ ± 3.2 mg/l, min/max= 4.0/19.1 mg/l) and in the central channel 2 the SSCs range between 2.7 mg/l and 7.0 mg/l (4.9 mg/l on average, 1σ ±0.6 mg/l) (CTD/SSC-station 6, Fig. 6A).

The low suspended sediment concentrations of the upper water column at CTD/SSC-station 4 and 6 (Fig. 6A) indicate a correlation with lower turbid water of the satellite image of Fig. 1C. These two areas of lower turbidity follow the central region of both channels until Hon Khoai-island. To the west, one area of lower turbid water is evident and located at the same region as the western area of the SRCS (Fig. 1 B).

Water temperatures along the CTD transect (Fig. 6 B) are stratified. In the surface layer (< 2 m b.s.l.) vary the temperatures between 29.81°C and 30.73 °C (30.27 °C on average, 1σ ±0.2 °C). The water body below shows slightly lower temperatures ranging between 29.39 °C and 30.28 °C (29.65°C on average, 1σ ±0.19°C) at the subaqueous delta platform (CTD/SSC-station 11, Fig. 6B). At the shelf transition, underneath the surface layer occurs a water mass with temperatures of 28.94°C on average (1σ ±0.08°C; min/max = 28.84/29.22°C).

The salinity values of the surface layer (< 2 m b.s.l.) vary from 31.21 to 33.8 (33.09 on average, 1σ ±0.61), whereas generally increasing salinity values into offshore direction are observed (Fig. 6 C). In the southern South China Sea, full marine conditions are reached at salinities exceeding 33.5 (Grosse et al. 2010), which are observed in offshore direction beginning at the region of ridge 2 (Fig. 6 C).

5 Discussion

Directional currents like tide induced currents in shallow marine environments could generate elongated morphological features (Dyer and Huntley, 1999; Héquette et al., 2008; Garel, 2010) governed either by erosion or deposition. In the case of the subaqueous Mekong delta occurs both, channelized depressions (erosional feature) and sand ridges (depositional feature) extending subparallel to the coast (Fig. 3). However, due to their spatial neighbourhood it is obviously to argue that they have a similar temporal origin. The arrangement into three subareas implies that local hydro- and sediment dynamic conditions origin have to be considered in the interpretation of the development of the SRCS.

5.1 Sediment Source

The accumulation of large scale sand bodies leads to the question of the available source of the large sand volumes, because the next Mekong distributary (Bassac River) is located 90 km apart from the sand ridges (Fig. 1D). Furthermore, sand content decreases below 20 percent in the subaqueous Mekong delta southwest of the Bassac River indicating a reduction in sand supply in direction to the sand ridges (Fig. 5 section 1).

Offshore sediment surface samples close to the smaller tidal channel at Bo De and Rach Goc (Fig. 1B) have sand contents below 20 percent as well (Fig. 5 section 5 and 6). The erosional character at the Bo De key section (most eastern transect in Fig. 3 B3D) and stiff clay at the tidal inlet (Heinrich, 2009) implies in addition no source of sandy material.

Sand transport from the inner shelf into the subaqueous delta by wave action is eligible. However, surface sediments from sand ridge 2 (top of the delta slope) until the open shelf decrease continuously in sand content (Fig. 4C; Fig. 5 section 5 and 6) contradicting a landward sand transport. In addition, sands of the inner shelf are enriched in coarse and medium fractions (Fig. 5 section 5 and 6), which do not occur at the sand ridges.

Surface sediments of the central channel troughs (Fig. 4C) consist of mud to sandy mud (Unverricht et al., 2013; Fig. 5 section 5 and 6). As proven by channel incision, erosion in the channel troughs is probable, but secondary as source of sand.

The south-western part of the subaqueous delta around Ca Mau Cape can be excluded as a sand source because it consists mainly of muddy sediments (Xue et al., 2012b; Unverricht et al., 2013). Therefore, we conclude that the main source of sandy material must be located between the main distributaries in the NE and the beginning of the SRCS.

This area suffers severely erosion of mangrove forests and sandy tidal flats extending from Soc Trang and Bac Lieu provinces (Fig. 1 B) near the Bassac river mouth until Bo De since the last decades (Cat et al., 2006; Pham and Furukawa, 2007; Joffre, 2010; Albers et al., 2011; Pham, 2011; Nguyen, 2012; Schmitt et al., 2013). Coastal sediments of the Soc Trang province contain high sand portions up to 70 % (Pham, 2011) and provide a suitable sediment source to nourish the sand ridges.

In the Ganh Hao region erosion occurs along both mangrove coast (Cat et al., 2006; Pham and Furukawa, 2007) and delta slope of the eastern area, where channel 1 begins (Fig. 3 A1). Up to 20 cm thick surface sediment at the delta slope (Unverricht et al., 2013) mainly comprise well sorted fine and very fine sand (Fig. 5 section 3 and 4) coinciding with grain size composition of the sand ridges. After Cat et al. (2006) coastal erosion at the Ganh Hao region mainly occurs during NE monsoonal winds (October until March) reaching speeds of 10-24 m/s (data from 1999-2008 of the Southern Regional Hydro-Meteorological Center (SRHMC, Vietnam)) and indicating a (Cat et al., 2006) net-sediment transport in SW-direction to the sand ridges due to wind driven currents.

5.2 Morpho- and sediment dynamic processes

The Ganh Hao region presents the eastern area of the sand-ridge-channel-system in the subaqueous Mekong delta. Undulations, subparallel aligned to the delta slope, show an erosional truncation of foreset pattern below the surface layer (Fig. 3 A1-A3). This implies that initial morphological channelization may be caused by NE monsoonal erosive currents. Coastal subparallel currents (Xue et al., 2012a) provoke alongshore sediment drift, but prevent offshore sand transport. Taken into account that wind driven currents during the north-eastern winter monsoon prevail (Ta et al., 2005), sediment transport is directed to the sand ridge region in the SW.

The ridge top consists of a sand body (Fig. 4 C) covering truncated foresets (Fig. 3 B1-3). Ridges and troughs do have a channeling effect leading to heterogeneous current velocities along the transects (Fig. 4B). As consequence, sediment sorting occurs (Fig. 4 C) due to gradients in current velocity, supporting sand deposition along the ridges. Although, the velocity gradient is observable only near the sea surface (Fig. 1 B) in the inter-monsoon season it may increase by wind-driven currents during the winter monsoon season. Suspended sediment is

observed especially along the sand-ridges and especially at the out flank of sand ridge 2 (Fig. 6A). Similar trend is documented by (Unverricht et al., 2014) along the delta slope close to Hon Khoai Island and indicates tidally induced sediment resuspension.

Several studies about sand ridges in different tidal environments and different scale (Mid Atlantic Bight (Swift, 1975), German Bight (Antia et al., 1995) and Southern North Sea (Garel, 2010)) provide information on convergences of sediment fluxes along sand ridges, which are induced by flood current dominance on one ridge flank and ebb current dominance on the other side. Therefore, tidal currents play the primary role in sand ridge maintenance and stabilisation (Antia et al., 1995, Dyer and Huntley, 1999). Héquette et al. (2008) stated that wave-induced oscillatory movement can cause additionally sediment agitation and remobilization, but sediment transport is dominated by the mean flow consisting of tidal and wind induced currents. In the subaqueous Mekong delta, sediment resuspension due to tidal currents can occur without wind and wave influences (Unverricht et al., 2014). This indicates that wave and wind driven particle fluxes can additionally amplify sediment transport, especially in the subaqueous Mekong delta.

Dyer and Huntley (1999) classify sand ridges in dependence of their location and source of sand. The subclass of alternating ridges has its origin in shoreline retreat as sand source. Initially, sand built ridge-systems close to headlands depend on the availability of sand supply. Aided by shoreface erosion sand ridges move further away from the source and run subparallel to dominant current directions. Headland associated banner banks arise as result which are modified either by tidal or storm forcing (Swift, 1975; Dyer and Huntley, 1999). In comparison with the morpho-, sediment- and hydro-dynamic conditions of the study site, the SRCS can be described as alternating ridge-system. The retrograding coastline between Ganh Hao and Bo De (Fig. 1B) forms a local headland including flow directions changing from NNE-SSW to NE-SW. The currents support the idea of a net-transport into south-western direction to nourish the sand ridges with sediment from the erosion sites offshore Ganh Hao and the coast of Bac Lieu and Soc Trang provinces (Fig. 1 B). Furthermore, the coastline around Bo De (Fig. 1 B/D), which is just opposite of the SRCS of a distance of 10 km, is also under erosion (Nguyen 2012). It causes coastline retreat including relative offshore migration of the sand ridges.

(Dyer and Huntley, 1999; Garel, 2010) provide studies along sand ridges of similar dimensions and describe deflection angles between ridge crests and prevailing tidal currents between 7-15° and 15-25°, respectively. Along transect B1, west-southwest directed tidal

current (241° on average) during flood phase crosses the ridge crests in an angle of 32 degrees, which extends in southwest direction (209° on average), representing a comparable deflection angle like the examples of the mentioned studies before. Compared to the upper water column higher SSC occur close to the seabed around the sand ridges (Fig. 6 A) and indicate resuspension. Similar patterns are described in the area along the southern delta slope (Unverricht et al., 2014) and sand ridge 2, respectively.

5.3 Coastal erosion –delta front instabilities

In the last decades, worldwide increasing dam constructions (Syvitski et al., 2005b, 2009; Walling, 2006; Syvitski and Saito, 2007; Ran et al., 2013) lead to sediment reduction to coastal waters and hence, diminishing delta progradation and erosion (Bi et al. in press, Yang et al. 2011), respectively.

Particularly at the erosion sites at Ganh Hao and the Bac Lieu province (Fig. 1 B) close to the Bassac river mouth, 93.7% of the eroded beaches consist of sand (Cat et al., 2006).

In the Yangtze River, 50% decrease of sediment supply is attributed to enhanced sand mining at the mid-lower Yangtze and less sediment supply of the Hanjiang River after building the Danjiangkou Reservoir (Chen et al., 2005).

Increasing dam constructions in the entire Mekong basin (Kummu et al., 2010) combined with sand mining (Kummu et al., 2008) will increase the erosion of sandy coasts in deltaic environments with consequences for morphological changes (Wang et al., 2011). The delta front instabilities at the subaqueous Mekong delta, shown as truncated foreset pattern with the sea bottom (Fig. 3), high amounts of fine and very fine sand (Fig. 5) and an upper sandy layer above a hiatus along the delta slope (Unverricht et al., 2013), respectively, are indicators for subaqueous delta erosion.

6 Conclusion and outlook

The subaqueous Mekong delta architecture shows a complex pattern. Between two pronounced delta clinoforms at the Bassac river mouth and around Ca Mau Cape that lying approximately 200 km apart (Xue et al., 2010; Unverricht et al., 2013) a sand-ridge-system combined with erosional channels (SRCS) exists (Fig. 1 and Fig. 3). This large-scale morphological feature extending over at least 128 km is unique in deltaic realms. The SRCS is subdivided by shape and sediment distribution into three areas. The eastern area when the SRCS initiates, is embedded along the delta slope and at the transition to the inner shelf platform.

Truncated foresets cut by the bottom reflector indicate erosional activity (Fig. 3 A1-3). In particular, delta slope regions are covered by a sand layer up to 20 cm thick (Unverricht et al., 2013). The shape of the SRCS is smooth with slightly concavity along the delta slope and inner shelf platform (Fig. 3 A1-3, A3-D).

In contrast, the central area is characterized by two prominent sand ridges, which are accompanied by two erosional channels. The channels incised down to 18 m b.s.l. into the southern subaqueous delta platform and 10.5 m from the ridge top respectively. Seismic profiles crossing the central area reveal an asymmetric shape of the sand-ridge-channel-system, whereas the steeper flanks are inclined to the south. Coastal tidal currents cross the crest of the sand ridges at an angle of 32° on average and lead to ridge maintenance and stabilization (Swift, 1975; Dyer and Huntley, 1999). Presumably, the ridges are fed by different sand sources due to erosion and sediment resuspension in both the shore and subaqueous Mekong delta.

In the transition of the central and western area, where the SRCS terminate, the erosional channels merge into a local depression that reaches north of Hon Khoai Island water depth of 33 m (Fig. 1B). The asymmetric depression with a steeper flank to the east is interpreted as giant scour. West of the scour, the SRCS runs out as single shallow and wide channel at the second delta front around Ca Mau Cape. With regard to the delta progradation around Ca Mau Cape, the sand-ridge-channel-system serves as sediment conveyor. Tide and wind-driven currents initiate and maintain the net-sediment transport path until Ca Mau Cape.

This sand-ridge-channel-system can be classified by its shape and hydrodynamic conditions as tidal sand ridge massif, especially as alternating ridge complex (after Swift, 1975; Dyer and Huntley, 1999). However, a detailed analysis of severely variability in sediment-, morpho- and hydro-dynamics over a longer period is required together with the adaption of numerical models and must be included into future studies.

Coastal erosion is a particular issue in recent delta environments. Dam constructions (reservoirs) and sand mining reduces the sediment supply to coastal areas (Syvitski and Saito, 2007; Kummu et al., 2008, 2010), groundwater extraction and river embankments leads to accelerated subsidence (Syvitski et al., 2009) and mangrove deforestation destroy the natural coastal protection (Nguyen et al., 2013). Many studies include only the onshore area into erosional studies, although sediment reduction also destabilizes the delta front and hence the delta progradation. In particular cases like the Yellow river (Bi et al., in press) and Yangtze (Chen et al., 2005; Yang et al., 2011) it leads to strong coastal erosion and delta retreat.

The initially deterioration of the subaqueous delta environment is observed in this study, which documents erosional pattern along the wide extending delta front of the Mekong River delta. These erosional patterns may occur also in other deltaic realms and therefore, we recommend incorporating the subaqueous delta areas into future investigation about coastal erosion.

Acknowledgements

The cruises were supported by a research grant of the German Research Foundation (STA-401 10/2) and through scientific cooperation with the Vietnamese Academy of Science and Technology (VAST) and the Ministry of Science and Technology (MOST), Vietnam.

The scientific experience in shallow water processes of Klaus Schwarzer (Sedimentology, University of Kiel) enriched all cruises significantly. We are thankful for his participation and time-consuming engagement.

Special thanks to the Vietnamese fishermen who have supported us with their knowledge about the local waters and as talented chefs. The project would not have been feasible without their endurance and willingness.

General Acknowledgements

Before I wish to thank all the scientific involved persons I would like to thank my girlfriend Sarah Kasten. Without her strength and endurance to give me a wonderful home and place for recovering and also pieces of advice or concerns this thesis will never be finished! I have to apologize to her for being rarely available in the last years.

I would like to express the immense gratitude to Prof. Karl Stattegger to initiate this thesis, supervising and supporting me over this long period. Furthermore, I wish to thank him for proof-reading the articles and insightful discussions and experiences at several cruises, joint conferences and field trips.

Special thanks to Prof. Sebastian Krastel for his co-supervision, especially in the support of hydro acoustic procedures.

Nguyen Cong Thanh and Bui Viet Dung I wish to thank for supporting me during the cruises on the Vietnamese fisher boats, their logistical organization in Vietnam, good discussions about the Mekong delta and especially Thanh for writing the data conversion-scripts for ocean data view. You introduce me also into the Vietnamese culture, especially the food, which was not very appropriate for me at the beginning. We met us as strangers and went as friends.

Same, same but different – I would like to thank Christoph “The White Daddy” Heinrich. You gave me your help, insightful debates and friendship during the cruise in 2008 until the end of the thesis. I hope this will be continued and therefore, a special wine is waiting for you!

Witold Szczuciński and Robert Jagodziński deserve special recognition for their support at the cruises in 2006 and 2007 and during the several visits in Poznan. Especially Witold I wish to thank for guiding me through the large valley of the first manuscript and the nightly long discussions of our skype sessions.

My special thanks go to my student worker Mischa Schönke, the best Hiwi ever, for his endurance in grain size analysis and other technical task, which had to be performed.

Our Technicians Eric Steen and Helmut Beese I would express my gratitude for their ideas and constructions to handle all measurement tools on the Vietnamese fisher boats.

Many thanks to Philip Held for the nice tool to calculate the sound velocities from CTD-data and of course the nice kite sessions, which we could enjoy together. I would like to thank also Jan Scholten of his advice for the Pb210-method and the good discussions about freshwater and Peter Feldens for writing the NWC-script.

Angela Trumpf deserves particularly a big thank-you for supporting me during the never ending grain size measurements and the tasks in the laboratory.

The cruise on the Vietnamese fisher boats never happened without the support of the Vietnamese scientists and helpers, escpecially the Captains Cai and An, the scientists Thuyen Xuan Le and Phung Van Phach and my German colleagues Klaus Schwarzer and Klaus Rickleffs - many thanks to you.

Moreover, I'm grateful to all the group members for the nice working atmosphere, especially during the coffee breaks. Moreover, many thanks to my office mate Agata Szczygielski for her tolerance towards the sometimes crowded office. I would like to improve that.

Not to forget, many thanks to Ms. Reinhardt of the Radiology at the "Prüner Gang" to spend many afternoons with us for scanning X-rays instead of bones.

I wish also thank to the laboratory assistants in the Geography Ms. Bock, Ms Berger and in the Geosciences Ms Inge Dold, Ms Petra Fiedler and Ms Petra Kluge. This and other thesis would never have taken place without your support, especially in developing the method of the grain size analysis!

At the end, but extending with particular thanks, I would like to address my family, especially my parents Christel and Dietmar Unverricht. You supported me over the long period of my study and PhD. I never forget this and hope to give a lot back of them as well.

References

Agrawal, Y.C., Pottsmith, H.C., 2000. Instruments for particle size and settling velocity observations in sediment transport. Marine Geology 168: 89–114.

Albers, T., Lieberman, N. v., San, D.C., Schmidt, K., 2011. Current and erosion survey in the coastal zone of Soc Trang province, Vietnam. 26–30.

Anikiev, V.V., Shumilin, E.N., Dudarev, O.V., Botsul, A.I., Zakharova, P.V., Kolesov, G.M., Sapozhnikov, D.Y., Smith, R., 2004. Spatial Variability in the Distribution of Lithological Characteristics and Chemical Elements in the Bottom Sediments of the South China Sea near the Mekong and Saigon River Deltas. Geochemistry International 42: 1301–1318.

Anikiyev, V.V., Zaytsev, O.V., Hieu, T.T., Savil'Yeva II, Starodubtsev, Y.G., Shumilin, Y.N., 1986. Variation in the Space-time Distribution of Suspended Matter in the Coastal Zone of the Mekong River. Okeanologiya 26: 259–266.

Antia, E.E., Flemming, B.W., Wefer, G., 1995. Calm-weather spring and neap tidal current characteristics on a shoreface-connected ridge complex in the German Bight (southern north Sea). Geo-Marine Letters 15: 30–36.

Appleby, P.G., Oldfield, F., 1978. The calculation of lead-210 dates assuming a constant rate of supply of unsupported 210Pb to the sediment. CATENA 5: 1–8.

Bhattacharya, J.P., Giosan, L., 2003. Wave-influenced deltas: geomorphological implications for facies reconstruction. Sedimentology 50: 187–210.

Bi, N., Wang, H., Yang, Z., in press. Recent changes in the erosion–accretion patterns of the active Huanghe (Yellow River) delta lobe caused by human activities. Continental Shelf Research .

Blott, S.J., Pye, K., 2001. GRADISTAT: a grain size distribution and statistics package for the analysis of unconsolidated sediments. Earth Surface Processes and Landforms 26: 1237–1248.

Bowers, D.G., Braithwaite, K.M., Nimmo-Smith, W.A.M., Graham, G.W., 2009. Light scattering by particles suspended in the sea: The role of particle size and density. Continental Shelf Research 29: 1748–1755.

Cat, N.N., Tien, P.H., Sam, D.D., Binh, N.N., 2006. Status of coastal erosion of Vietnam and proposed measures for protection. Proceedings of the Regional Technical Workshop, Khao Lak, Thailand, 28–31 August 2006.

Chen, W., Liu, Q., Huh, C.-A., Dai, M., Miao, Y.-C., 2010. Signature of the Mekong River plume in the western South China Sea revealed by radium isotopes. Journal of Geophysical Research 115: .

Chen, X., Zhang, E., Mu, H., Zong, Y., 2005. A Preliminary Analysis of Human Impacts on Sediment Discharges from the Yangtze, China, into the Sea. Journal of Coastal Research 213: 515–521.

Correggiari, A., Cattaneo, A., Trincardi, F., 2005. The modern Po Delta system: Lobe switching and asymmetric prodelta growth. Marine Geology 222–223: 49–74.

Crockett, J.S., Nittrouer, C.A., 2004. The sandy inner shelf as a repository for muddy sediment: an example from Northern California. Continental Shelf Research 24: 55–73.

Dalrymple, R.W., Choi, K., 2007. Morphologic and facies trends through the fluvial-marine transition in tide-dominated depositional systems: A schematic framework for environmental and sequence-stratigraphic interpretation. Earth-Science Reviews 81: 135–174.

Dean, W.E., 1974. Determination of carbonate and organic matter in calcareous sediments and sedimentary rocks by loss on ignition; comparison with other methods. Journal of Sedimentary Research 44: 242–248.

Duc, D.M., Nhuan, M.T., Ngoi, C.V., Nghi, T., Tien, D.M., van Weering, T.C.E., van den Bergh, G.D., 2007. Sediment distribution and transport at the nearshore zone of the Red River delta, Northern Vietnam. Journal of Asian Earth Sciences 29: 558–565.

Dyer, K.R., Huntley, D.A., 1999. The origin, classification and modelling of sand banks and ridges. Continental Shelf Research 19: 1285–1330.

Edmonds, D.A., Shaw, J.B., Mohrig, D., 2011. Topset-dominated deltas: A new model for river delta stratigraphy. Geology 39: 1175–1178.

Edmonds, D.A., Slingerland, R.L., 2010. Significant effect of sediment cohesion on delta morphology. Nature Geoscience 3: 105–109.

Ericson, J.P., Vörösmarty, C.J., Dingman, S.L., Ward, L.G., Meybeck, M., 2006. Effective sea-level rise and deltas: Causes of change and human dimension implications. Global and Planetary Change 50: 63–82.

Fang, G., Kwok, Y.-K., Yu, K., Zhu, Y., 1999. Numerical simulation of principal tidal constituents in the South China Sea, Gulf of Tonkin and Gulf of Thailand. Continental Shelf Research 19: 845–869.

Fang, W., Guo, Z., Huang, Y., 1998. Observational study of the circulation in the southern South China Sea. Chinese Science Bulletin 43: 898–905.

Flynn, W.W., 1968. The determination of low levels of polonium-210 in environmental materials. Analytica Chimica Acta 43: 221–227.

Gagliano, S.M., McIntire, W.G., 1968. Reports on the Mekong River Delta. 144.

Galloway, W.E., 1975. Process framework for describing the morphologic and stratigraphic evolution of deltaic depositional systems. Broussard, M.L. (Ed.), Deltas, Models for Exploration Houston Geological Society. p. 87–98.

Garel, E., 2010. Tidally-averaged Currents and Bedload Transport over the Kwinte Bank, Southern North Sea. Journal of Coastal Research 87–94.

Giosan, L., Donnelly, J.P., Constantinescu, S., Filip, F., Ovejanu, I., Vespremeanu-Stroe, A., Vespremeanu, E., Duller, G.A.T., 2006. Young Danube delta documents stable Black

Sea level since the middle Holocene: Morphodynamic, paleogeographic, and archaeological implications. Geology 34: 757.

Gordon, 1996. Acoustic Doppler Current Profiler - Principles of Operation - A Practical Primer. 1–57.

Grosse, J., Bombar, D., Doan, H.N., Nguyen, L.N., Voss, M. 2010., The Mekong River plume fuels nitrogen fixation and determines phytoplankton species distribution in the South China Sea during low and high discharge season. Limnology and Oceanography 55: 1668–1680.

Grossmann, E.E., Stevens, A., Gelfenbaum, G., Curran, C., 2007. Nearshore Circulation and Water-Column Properties in the Skagit River Delta, Northern Puget Sound, Washington - Juvenile Chinook salmon habitat availability in the Swinomish Channel. 97.

Hanebuth, T.J.J., Proske, U., Saito, Y., Nguyen, V.L., Ta, T.K.O., 2012. Early growth stage of a large delta — Transformation from estuarine-platform to deltaic-progradational conditions (the northeastern Mekong River Delta, Vietnam). Sedimentary Geology 261–262: 108–119.

Harris, P.T., Hughes, M.G., Baker, E.K., Dalrymple, R.W., Keene, J.B., 2004. Sediment transport in distributary channels and its export to the pro-deltaic environment in a tidally dominated delta: Fly River, Papua New Guinea. Continental Shelf Research 24: 2431–2454.

Heinrich, C., 2009. Hydro- und Sedimentdynamik in Tidekanälen der Ca Mau Halbinsel (Südvietnam). Christian-Albrechts-Universität of Kiel.

Heiri, O., Lotter, A.F., Lemcke, G., 2001. Loss on ignition as a method for estimating organic and carbonate content in sediments: reproducibility and comparability of results. Journal of Paleolimnology 25: 101–110.

Héquette, A., Hemdane, Y., Anthony, E.J., 2008. Sediment transport under wave and current combined flows on a tide-dominated shoreface, northern coast of France. Marine Geology 249: 226–242.

Hoitink, A.J.F., Hoekstra, P., 2005. Observations of suspended sediment from ADCP and OBS measurements in a mud-dominated environment. Coastal Engineering 52: 103–118.

Hordoir, R., Nguyen, K.D., Polcher, J., 2006. Simulating tropical river plumes, a set of parametrizations based on macroscale data: A test case in the Mekong Delta region. Journal of Geophysical Research 111: .

Hung, N.M., Dien, D.C., 2006. Coupled circulation, wave modeling in the Dinh An estuary for studying of the navigational access channel migration.

Institute of Strategy and Policy on natural resources and environment (ISPONRE)., 2009. Vietnam Assessment Report on Climate Change. 127.

Jagodziński, R., 2005. Petrography and geochemistry of surface sediments from Sunda and Vietnamese shelves (South China Sea). Adam Mickiewicz University.

Joffre, O., 2010. Management of Natural Resources in the Coastal Zone of Soc Trang Province-Mangrove Dynamics in Soc Trang Province 1889 - 1965. Deutsche Gesellschaft für Internationale Zusammenarbeit (GIZ) .

Käkönen, M., 2008. Mekong Delta at the Crossroads: More Control or Adaptation? AMBIO: A Journal of the Human Environment 37: 205–212.

Kostaschuk, R., Best, J., Villard, P., Peakall, J., Franklin, M., 2005. Measuring flow velocity and sediment transport with an acoustic Doppler current profiler. Geomorphology 68: 25–37.

Kubicki, A., 2008. Large and very large subaqueous dunes on the continental shelf off southern Vietnam, South China Sea. Geo-Marine Letters 28: 229–238.

Kummu, M., Lu, X.X., Rasphone, A., Sarkkula, J., Koponen, J., 2008. Riverbank changes along the Mekong River: Remote sensing detection in the Vientiane-Nong Khai area. Quaternary International 186: 100–112.

Kummu, M., Lu, X.X., Wang, J.J., Varis, O., 2010. Basin-wide sediment trapping efficiency of emerging reservoirs along the Mekong. Geomorphology 119: 181–197.

Kummu, M., Varis, O., 2007. Sediment-related impacts due to upstream reservoir trapping, the Lower Mekong River. Geomorphology 85: 275–293.

Le, T.V.H., Nguyen, H.N., Wolanski, E., Tran, T.C., Haruyama, S., 2007. The combined impact on the flooding in Vietnam's Mekong River delta of local man-made structures, sea level rise, and dams upstream in the river catchment. Estuarine, Coastal and Shelf Science 71: 110–116.

Leslie, C., Hancock, G.J., 2008. Estimating the date corresponding to the horizon of the first detection of 137Cs and 239+240Pu in sediment cores. Journal of Environmental Radioactivity 99: 483–490.

Liu, J.P., Xue, Z., Ross, K., Wang, H.J., Yang, Z.S., Li, A.C., Gao, S., 2009. Fate of sediments delivered to the sea by Asian large rivers: Long-distance transport and formation of remote alongshore clinothems. Sedimentary Record 7: 4–9.

Van Maren, D.S., Hoekstra, P., 2004. Seasonal variation of hydrodynamics and sediment dynamics in a shallow subtropical estuary: the Ba Lat River, Vietnam. Estuarine, Coastal and Shelf Science 60: 529–540.

McKee, B.A., Nittrouer, C.A., DeMaster, D.J., 1983. Concepts of sediment deposition and accumulation applied to the continental shelf near the mouth of the Yangtze River. Geology 11: 631 –633.

Mekong River Commission., 2005. Overview of the Hydrology of the Mekong Basin. 0–73.

Mekong River Commission., 2009. Adaptation to climate change in the countries of the Lower Mekong Basin: regional synthesis report. 112.

Mikkelsen, O.A., Hill, P.S., Milligan, T.G., Chant, R.J., 2005. In situ particle size distributions and volume concentrations from a LISST-100 laser particle sizer and a digital floc camera. Continental Shelf Research 25: 1959–1978.

Mikkelsen, O.A., Pejrup, M., 2000. In situ particle size spectra and density of particle aggregates in a dredging plume. Marine Geology 170: 443–459.

Mikkelsen, O.A., Pejrup, M., 2001. The use of a LISST-100 laser particle sizer for in-situ estimates of floc size, density and settling velocity. Geo-Marine Letters 20: 187–195.

Mikkelsen, O.A., 2002a. Examples of spatial and temporal variations of some fine-grained suspended particle characteristics in two Danish coastal water bodies. Oceanologica Acta 25: 39–49.

Mikkelsen, O.A., 2002b. Variation in the projected surface area of suspended particles: Implications for remote sensing assessment of TSM. Remote Sensing of Environment 79: 23–29.

Milliman, J.D., Meade, R.H., 1983. World-Wide Delivery of River Sediment to the Oceans. The Journal of Geology 91: 1–21.

Milliman, J.D., Ren, M.E., 1995. River flux to the sea: impact of human intervention on river systems and adjacent coastal areas. Impact on Coastal Habitation CRC Press. p. 57–83.

Mitsuguchi, T., Dang, P.X., Kitagawa, H., Uchida, T., Shibata, Y., 2008. Coral Sr/Ca and Mg/Ca records in Con Dao Island off the Mekong Delta: Assessment of their potential for monitoring ENSO and East Asian monsoon. Global and Planetary Change 63: 341–352.

MRC., 2010. Mekong River Comission -State of the Basin Report 2010. .

Mueller, D.S., Wagner, C.R., 2006. Application of the Loop Method for Correcting Acoustic Doppler Current Profiler Discharge Measurements Biased by Sediment Transport. 18.

Neill, C.F., Allison MA. 2005. Subaqueous deltaic formation on the Atchafalaya Shelf, Louisiana. Marine Geology 214: 411–430.

Nguyen, C.T., 2012. Processes and factors controlling and affecting the retreat of mangrove shorelines in South Vietnam. Christian-Albrechts-Universität zu of Kiel.

Nguyen, H.-H., McAlpine, C., Pullar, D., Johansen, K., Duke, N.C., 2013. The relationship of spatial–temporal changes in fringe mangrove extent and adjacent land-use: Case study of Kien Giang coast, Vietnam. Ocean & Coastal Management 76: 12–22.

Nguyen, V.L., Ta, T.K.O., Tateishi, M., 2000. Late Holocene depositional environments and coastal evolution of the Mekong River Delta, Southern Vietnam. Journal of Asian Earth Sciences 18: 427–439.

Nittrouer, C., DeMaster, D., McKee, B., 1984. Fine-scale stratigraphy in proximal and distal deposits of sediment dispersal systems in the East China Sea. Marine Geology 61: 13–24.

Nittrouer, C.A., Austin, J.A., Field, M.E., Kravitz, J.H., Syvitski, J.P.M., Wiberg, P.L., 2009. Writing a Rosetta Stone: Insights into Continental-Margin Sedimentary Processes and Strata. Blackwell Publishing Ltd.

Nittrouer, C.A., Sternberg, R.W., Carpenter, R., Bennett, J.T., 1979. The use of Pb-210 geochronology as a sedimentological tool: Application to the Washington continental shelf. Marine Geology 31: 297–316.

Orton, G.J., Reading, H.G., 1993. Variability of deltaic processes in terms of sediment supply, with particular emphasis on grain size. Sedimentology 40: 475–512.

Pham, T.T., 2011. Mangroves of Soc Trang 1965 - 2007. Deutsche Gesellschaft für Internationale Zusammenarbeit (GIZ) 70.

Pham, T.T.H., Furukawa, M., 2007. Impact of sea level rise on coastal zone of Vietnam. Bulletin of the Faculty of Science, University of Ryukyus 84: 45–59.

Postma, G., Kleinhans, M.G., Meijer, P.T., Eggenhuisen, J.T., 2008. Sediment transport in analogue flume models compared with real-world sedimentary systems: a new look at scaling evolution of sedimentary systems in a flume. Sedimentology 55: 1541–1557.

Proske, U., Hanebuth, T.J.J., Gröger, J., Diệm, B.P., 2011. Late Holocene sedimentary and environmental development of the northern Mekong River Delta, Vietnam. Quaternary International 230: 57–66.

Ran, L., Lu, X.X., Xin, Z., Yang, X., 2013. Cumulative sediment trapping by reservoirs in large river basins: A case study of the Yellow River basin. Global and Planetary Change 100: 308–319.

Robbins, J.A., Edgington, D.N., Kemp, A.L.W., 1978. Comparative 210Pb, 137Cs, and pollen geochronologies of sediments from Lakes Ontario and Erie. Quaternary Research 10: 256–278.

Robbins, J.A., Edgington, D.N., 1975. Determination of recent sedimentation rates in Lake Michigan using Pb-210 and Cs-137. Geochimica et Cosmochimica Acta 39: 285–304.

Saito, Y., Yang, Z., Hori, K., 2001. The Huanghe (Yellow River) and Changjiang (Yangtze River) deltas: a review on their characteristics, evolution and sediment discharge during the Holocene. Geomorphology 41: 219–231.

Sakamoto, T., Van Nguyen, N., Kotera, A., Ohno, H., Ishitsuka, N., Yokozawa, M., 2007. Detecting temporal changes in the extent of annual flooding within the Cambodia and the Vietnamese Mekong Delta from MODIS time-series imagery. Remote Sensing of Environment 109: 295–313.

Santisteban, J.I., Mediavilla, R., López-Pamo, E., Dabrio, C.J., Zapata, M.B.R., García, M.J.G., Castaño, S., Martínez-Alfaro, P.E., 2004. Loss on ignition: a qualitative or quantitative method for organic matter and carbonate mineral content in sediments? Journal of Paleolimnology 32: 287–299.

Schimanski, A., Stattegger, K., 2005. Deglacial and Holocene evolution of the Vietnam shelf: stratigraphy, sediments and sea-level change. Marine Geology 214: 365–387.

Schlitzer, R., 2011. Ocean Data View. Alfred Wegener Institut.

Schmitt, K., Albers, T., Pham, T.T., Dinh, S.C., 2013. Site-specific and integrated adaptation to climate change in the coastal mangrove zone of Soc Trang Province, Viet Nam. Journal of Coastal Conservation 1–14.

Seapoint Sensors, Inc., 2013. Seapoint Turbidity Meter - User Manual. .

Shi, J.Z., 2010. Tidal resuspension and transport processes of fine sediment within the river plume in the partially-mixed Changjiang River estuary, China: A personal perspective. Geomorphology 121: 133–151.

Simpson, M., 2001. Discharge Measurements Using a Broad-Band Acoustic Doppler Current Profiler. 134.

Snidvongs, A., Teng, S.-K., 2006. Mekong River - GIWA Regional assessment 55, UNEP. 75.

Swift, D.J.P., 1975. Tidal sand ridges and shoal-retreat massifs. Marine Geology 18: 105–133.

Syvitski, J.P.M., Kettner, A.J., Correggiari, A., Nelson, B.W., 2005a. Distributary channels and their impact on sediment dispersal. Marine Geology 222-223: 75–94.

Syvitski, J.P.M., Kettner, A.J., Overeem, I., Hutton, E.W.H., Hannon, M.T., Brakenridge, G.R., Day, J., Vorosmarty, C., Saito, Y., Giosan, L., Nicholls, R.J., 2009. Sinking deltas due to human activities. Nature Geoscience 2: 681–686.

Syvitski, J.P.M., Saito, Y., 2007. Morphodynamics of deltas under the influence of humans. Global and Planetary Change 57: 261–282.

Syvitski, J.P.M., Vörösmarty, C.J., Kettner, A.J., Green, P., 2005b. Impact of Humans on the Flux of Terrestrial Sediment to the Global Coastal Ocean. Science 308: 376 –380.

Szczuciński, W., Jagodziński, R., Hanebuth, T.J.J., Stattegger, K., Wetzel, A., Mitręga, M., Unverricht, D., Van Phach, P. 2013. Modern sedimentation and sediment dispersal pattern on the continental shelf off the Mekong River delta, South China Sea. Global and Planetary Change .

Szczuciński, W., Stattegger, K., Scholten, J., 2009. Modern sediments and sediment accumulation rates on the narrow shelf off central Vietnam, South China Sea. Geo-Marine Letters 29: 47–59.

Ta, T.K.O, Van Nguyen, L., Tateishi, M., Kobayashi, I., Saito, Y., 2005. Holocene delta evolution and depositional models of the Mekong River Delta, southern Vietnam. SEPM 453–466.

Ta, T.K.O., Nguyen, V.L., Tateishi, M., Kobayashi, I., Saito, Y., Nakamura, T., 2002a. Sediment facies and Late Holocene progradation of the Mekong River Delta in Bentre Province, southern Vietnam: an example of evolution from a tide-dominated to a tide- and wave-dominated delta. Sedimentary Geology 152: 313–325.

Ta, T.K.O., Nguyen, V.L., Tateishi, M., Kobayashi, I., Tanabe, S., Saito, Y., 2002b. Holocene delta evolution and sediment discharge of the Mekong River, southern Vietnam. Quaternary Science Reviews 21: 1807–1819.

Tamura, T., Horaguchi, K., Saito, Y., Nguyen, V.L., Tateishi, M., Ta, T.K.O., Nanayama, F., Watanabe, K., 2010. Monsoon-influenced variations in morphology and sediment of a mesotidal beach on the Mekong River delta coast. Geomorphology 116: 11–23.

Tamura, T., Saito, Y., Bateman, M.D., Nguyen, V.L., Ta, T.K.O., Matsumoto, D., 2012a. Luminescence dating of beach ridges for characterizing multi-decadal to centennial deltaic shoreline changes during Late Holocene, Mekong River delta. Marine Geology 326–328: 140–153.

Tamura, T., Saito, Y., Nguyen, V.L., Ta, T.K.O., Bateman, M.D., Matsumoto, D., Yamashita, S., 2012b. Origin and evolution of interdistributary delta plains; insights from Mekong River delta. Geology 40: 303–306.

Tamura, T., Saito, Y., Sieng, S., Ben, B., Kong, M., Sim, I., Choup, S., Akiba, F., 2009. Initiation of the Mekong River delta at 8 ka: evidence from the sedimentary succession in the Cambodian lowland. Quaternary Science Reviews 28: 327–344.

UNESCO., 1981. Background papers and supporting data on the Practical Salinity Scale 1978. UNESCO technical papers in marine science 37: 141.

Unverricht, D., Nguyen, T.C., Heinrich, C., Szczuciński, W., Lahajnar, N., Stattegger, K., 2014. Suspended sediment dynamics during the inter-monsoon season in the subaqueous Mekong Delta and adjacent shelf, southern Vietnam. Journal of Asian Earth Sciences 79, Part A: 509–519.

Unverricht, D., Szczuciński, W., Stattegger, K., Jagodziński, R., Le, X.T., Kwong, L.L.W., 2013. Modern sedimentation and morphology of the subaqueous Mekong Delta, Southern Vietnam. Global and Planetary Change .

Vörösmarty, C.J., Meybeck, M., Fekete, B., Sharma, K., Green, P., Syvitski, J.P.M., 2003. Anthropogenic sediment retention: major global impact from registered river impoundments. Global and Planetary Change 39: 169–190.

Voss, M., Bombar, D., Loick, N., Dippner, J.W., 2006. Riverine influence on nitrogen fixation in the upwelling region off Vietnam, South China Sea. Geophysical Research Letters 33:

Walling, D.E., 2006. Human impact on land–ocean sediment transfer by the world's rivers. Geomorphology 79: 192–216.

Walsh, J.P., Nittrouer, C.A., Palinkas, C.M., Ogston, A.S., Sternberg, R.W., Brunskill, G.J., 2004. Clinoform mechanics in the Gulf of Papua, New Guinea. Continental Shelf Research 24: 2487–2510.

Walsh, J.P., Nittrouer, C.A., 2009. Understanding fine-grained river-sediment dispersal on continental margins. Marine Geology 263: 34–45.

Wang, H., Saito, Y., Zhang, Y., Bi, N., Sun, X., Yang, Z., 2011. Recent changes of sediment flux to the western Pacific Ocean from major rivers in East and Southeast Asia. Earth-Science Reviews 108: 80–100.

Wang, Z., Saito, Y., Hori, K., Kitamura, A., Chen, Z., 2005. Yangtze offshore, China: highly laminated sediments from the transition zone between subaqueous delta and the continental shelf. Estuarine, Coastal and Shelf Science 62: 161–168.

Wendong, F., Zhongxin, G., Yuting, H., 1998. Observational study of the circulation in the southern South China Sea. Chinese Science Bulletin 43: 898–905.

Wiseman, W.J., Fan, Y.-B., Bornhold, B.D., Keller, G.H., Su, Z.-Q., Prior, D.B., Yu, Z.-X., Wright, L.D., Wang, F.-Q., Qian, Q.-Y., 1986. Suspended sediment advection by tidal currents off the Huanghe (Yellow River) delta. Geo-Marine Letters 6: 107–113.

Wolanski, E., Ngoc Huan, N., Trong Dao, L., Huu Nhan, N., Ngoc Thuy, N., 1996. Fine-sediment Dynamics in the Mekong River Estuary, Vietnam. Estuarine, Coastal and Shelf Science 43: 565–582.

Wolanski, E., Nhan, N.H., Spagnol, S., 1998. Sediment Dynamics during Low Flow Conditions in the Mekong River Estuary, Vietnam. Journal of Coastal Research 14: 472–482.

Wright, L.D., Nittrouer, C.A., 1995. Dispersal of River Sediments in Coastal Seas: Six Contrasting Cases. Estuaries 18: 494–508.

Wright, L.D., Wiseman, Jr. W.J., Yang, Z.-S., Bornhold, B.D., Keller, G.H., Prior, D.B., Suhayda, J.N., 1990. Processes of marine dispersal and deposition of suspended silts off the modern mouth of the Huanghe (Yellow River). Continental Shelf Research 10: 1–40.

Xue, Z., He, R., Liu, J.P., Warner, J.C., 2012a. Modeling transport and deposition of the Mekong River sediment. Continental Shelf Research 37: 66–78.

Xue, Z., Liu, J.P., DeMaster, D., Van Nguyen, L., Ta, T.KO., 2010. Late Holocene Evolution of the Mekong Subaqueous Delta, Southern Vietnam. Marine Geology 269: 46–60.

Xue, Z., Liu, J.P., Ge, Q., 2011. Changes in hydrology and sediment delivery of the Mekong River in the last 50 years: connection to damming, monsoon, and ENSO. Earth Surface Processes and Landforms 36: 296–308.

Xue, Z., Liu, J.P., DeMaster, D., Leithold, E.L., Wan, S., Ge, Q., Nguyen, V.L., Ta, T.K.O., 2012b. Sedimentary processes on the Mekong subaqueous delta: Clay mineral and geochemical analysis. Journal of Asian Earth Sciences .

Yang, S.L., Milliman, J.D., Li, P., Xu, K., 2011. 50,000 dams later: Erosion of the Yangtze River and its delta. Global and Planetary Change 75: 14–20.

Yuan, Y., Wei, H., Zhao, L., Jiang, W., 2008. Observations of sediment resuspension and settling off the mouth of Jiaozhou Bay, Yellow Sea. Continental Shelf Research 28: 2630–2643.

Zhen, X.L., Dong, X.X., Berne, S., Kui, Y.W., Marsset, T., Yu, X.T., Bourillet, J.F., 1998. Tidal deposition systems of China's continental shelf, with special reference to the eastern Bohai Sea. Marine Geology 145: 225–253.

Zu, T., Gan, J., Erofeeva, S.Y., 2008. Numerical study of the tide and tidal dynamics in the South China Sea. Deep Sea Research Part I: Oceanographic Research Papers 55: 137–154.